CHAPTER 1

INTRODUCTION

1.1 Background

The reaction turbines are widely used in various power projects. Turbines are the main part of various power plants. Its cost varies 15-35% of the total cost of power plant. During operation of turbine various types of contaminants are comes into contact with the turbine walls and blades. These contaminants create corrosion, erosion, deposition in turbines. The corrosion is basically a loss of turbine material due to various types of contaminants present in the working medium like steam, water or gas injection. Erosion is the loss of material due to the hard particle present in the stream. Degradation, failure of turbine components for turbine is depend on the various parameters like Mach number, Reynolds number, particle size, particle material etc. Particle having diameter less than 10µm is responsible for fouling because they do not have sufficient kinetic energy to cause erosion. This particle generally strikes and deposits on the blade surface, particles having diameter more than 10µm having less efficiency of sticking. Basically erosion is caused by the solid particles having large diameter, chances of erosion is mainly found in the leading edge and trailing edge of blade. Despite advancement in gas filtration systems, another issue is the formation of particles during combustion because of low grade fuel. The flow behavior of the turbine under injection of solid and liquid particles is analyze here. The model testing of turbines give overall performance of turbines based on global parameters but it is too expensive. This approach is time consuming. But the detailed analysis of the performance of turbine is important under off-design and overloading conditions for this Now-a-days computational fluid dynamics compliments experimental and theoretical approach by providing an alternate cost effective means of simulating real flow as it is much cheaper than experimental testing.

In the present project, the numerical flow simulation in reaction turbines has been carried out to study the effect of solid and liquid particles on profile loss coefficient at different inlet velocity conditions; Investigation on the effected length of blade due to particle injection has also been done.

CHAPTER 2

LITERATURE REVIEW

This chapter deals with theoretical background and the published research work that is related to the project work.

2.1 Theoretical background

Cascade is a row of blades representing the blade ring of a turbo machine. These blade can be arranged either in straight line or in annular form, These arrangements are called rectilinear cascade and annular cascade. In two dimensional flow we neglect the blade height to make our problem quite easy. In two dimensional flow, variations are occur only in pitch wise and stream wise directions only. The boundary layer growth on the suction and pressure sides of the blades in a real flow leads to the formation of low energy regions in the exit flow field. The velocity (c_2) and angle (direction α_2) profiles at the exit of a cascade with two-dimensional flow are shown in figure. In two-dimensional flow these profiles remain constant at all blade heights.

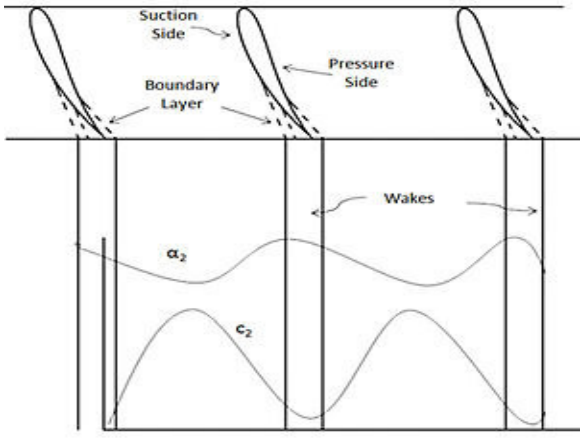

Figure 2.1: Two dimensional flow through a cascade

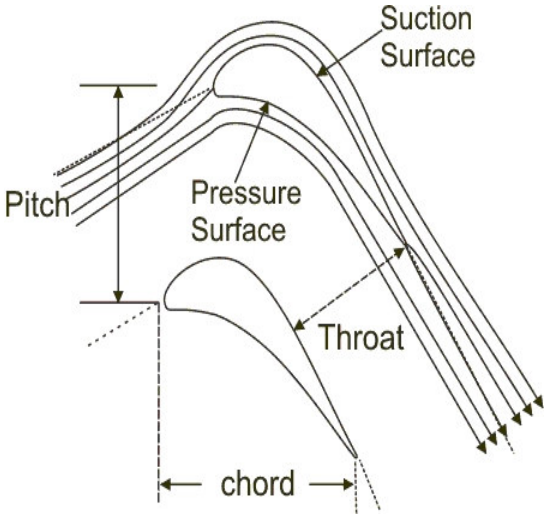

Figure 2.2: Flow through a turbine blade passage

Losses in cascade occur due to the growth and separation of boundary layers that takes place on the surface of the blades. Other losses occur due to the loss of stagnation pressure across the cascade and due to wasteful circulatory flows and the formation of shock waves.
Profile losses relates with the growth of boundary layer on the blade profile. Separation of the boundary layer occurs when the adverse pressure gradient on the surface becomes too steep and this increases the profile losses. The pattern of the boundary layer growth and its separation depends on the geometries of the blade and flow. Generally suction surface is more prone to boundary layer separation. The separation is also depends on other factors like degree of turbulence, incidence and Reynolds number. If the flow is supersonic in starting or becomes supersonic on the blade surface then the other losses are due to the formation of shock wave.

Some additional losses are due to the contamination present in the working fluid or due to the deposition of contamination. Blade surface and the turbine walls get damaged due to these contaminations. Blade strength and overall efficiency is also get reduced. These contaminations leads to the formation of trilogy "CDE" corrosion, deposition and erosion depending on the

working fluid, material used in the turbine and the other factors like mach number, particle size and Reynolds number. Any type of particle admission in the turbo machines is the main reason of principle damage and failure mechanism. Main interest is focus to enhance the durability of the machines that operates in environments where ingestion of solid particles, such as sand, dust, and dirt, cannot be avoided for operational or environmental condition reasons.

Erosion: Erosion is removal of material due to hard particles suspended in the working medium. More than 10µm diameter particles are responsible for corrosion. They have sufficient kinetic energy to strike on the surface. Chances of erosion increases with increase in particle diameter, density and working fluid velocity and decreases with blade size. This reduces turbine efficiency and also limits its capacity. Erosion at the high pressure end of a turbine is usually caused by solid particles present in the working medium. Erosion in the intermediate and low pressure blades is usually caused by the water. Main erosion damage was found at leading and trailing edges of the blade.

Deposition: Deposition is caused due to the particle having diameter less than micron. They do not have sufficient kinetic energy to create erosion. They create fouling in the turbines and easily stick with the blade surface.

Corrosion: Corrosion is the gradual destruction of material by chemical reaction. This means electrochemical oxidation of metals in reaction with an oxidant such as oxygen. Rusting, the formation of iron oxide is an example of electrochemical corrosion. Corrosion degrades the useful properties of material and structures including strength, appearance and permeability.
The following are some of the literature reviews of research under this topic:

Rainer kurz et al. [1] presented a detail of degradation mechanism and impact of components degradation on over all gas turbine performance. Proper maintenance and operating practices affects the level of performance degradation. They also explains the gas turbine mechanism and the factors affecting gas turbine performance like fouling, corrosion, abrasion, erosion and hot corrosion. In aero foils, any type of increased surface roughness may leads to increase friction losses and also change the shape of aerofoil geometries. They also discuss about the clearances of the machinery. Turbine section is subjected to very high temperature. Due to this temperature rise the inlet air properties are changed after entering to the turbine. A variety of problems are arises from the type and quality of fuel. They found the three major effect of degradation of turbine are increased tip clearances, changes in aero foil geometry and surface quality. Degradation is of recoverable and non recoverable type. Recovery by any means of washing like water washing, detergent online washing, detergent on crank washing they conclude that the pro active condition monitoring will allow the gas turbine operator to make intelligent service decisions based on the actual condition of the gas turbine. Maintenance and overhaul decisions are ultimately based on economic and safety considerations. Understanding performance degradation and factors that influence degradation can help in these decisions.

A Bolcs, O. Sari et al. [2] presented an experimental study on a gas turbine cascade which is operating under various conditions. For this they perform a experiment in the linear test facility

at the laboratoire de thermique applique et de turbomachines (LTT). The experiment is performed at various down stream flow velocities at three different inlet flow angles and they analyze the behavior at a nominal inlet incidence flow angle ($\beta=10^{o}$). The experimental set up is consists of five blades. The original blade is fabricated in aluminum with surface oxidation to prevent blade surface and the deposition profile is made up by using plastic cement coating on the pressure surface to make the print of the gas turbine blade which is removed after few thousand of running hours. Then the flow conditions are measured by wedge probe, the main objective of the original cascade design is the indirect method to validate the blade surface pressures, flow evaluation and its comparison with numerical simulation results. In the measurement of the blade with deposit it can be found that in gas turbines blade pressure surface is rough and uneven and the inter blade passage is reduced by 5% at the throat. Trailing edge thickness increases and its shape is modified. The effect is discussed for three different mach numbers and the flow angle is same. They shows that due to the more roughness of the deposit on the suction side the boundary will become turbulent and thicker to the leading edge of the blade and on the suction side there is no significant change in the boundary layer.

HP Hodson et al. [3] presented the effect of unsteady flow on the stagnation quantities at exit from the turbo machine blade row. Measurements of stagnation pressure at exit from a turbine cascade that is subjected to incoming wakes have been presented. The measured exit flow is characterized by the presence of large pitch wise variations in stagnation pressure in the "free-stream", some of which appears as an apparent loss of stagnation pressure towards the pressure side of the passage and some as an apparent gain near the suction side. Predictions and measurements of the unsteady flow field reveal fluctuations in stagnation pressure and stagnation temperature that are greater than the defects that occur in the wake at inlet to the blade row in question. The large stagnation temperature fluctuations are caused by large variations in dp/dt which are mostly associated with the suction side flow and are driven by the wake interaction. The flow field predictions of entropy show little evidence of non-uniformity outside the blade wakes which suggests that many of the stagnation pressure fluctuations are isentropic in origin and therefore related to variations in stagnation temperature. The observed time-mean non-

uniformity in stagnation pressure at cascade exit is a direct consequence of these unsteady processes. Though the fluctuations are relatively large, the time-mean change in stagnation pressure across the cascade is shown to be representative of the entropy generation within the blade row. The mixing loss associated with the unsteady flow field increases by a factor of two as the wake pass through the blade row but even at exit, this only amounts to about 0.25 percent of the exit dynamic pressure.

R.J Boyle et al. [4] presented the Measurements and Predictions of surface roughness effects on turbine vane aerodynamics. They measured the aerodynamic performance of a turbine vane in linear cascade. These measurements were conducted for exit-true chord Reynolds numbers between 150,000 and 1,800,000. They compare total pressure loss for smooth and rough vanes over a range of Reynolds and mach numbers for three turbulence levels. Prediction using algebraic and two-equations turbulence models are compared with data to determine an appropriate model to predict the effect of roughness on aerodynamic performance. The turbulence was low when no grid was present. The wide range of Reynolds numbers was chosen so that, at the lower Reynolds numbers the rough surfaces would be hydraulically smooth. The primary purpose of the tests was to provide data to verify CFD predictions of surface roughness effects on aerodynamic performance. Data comparisons are made using a two-dimensional Navier-Stokes analysis. Both two-equation and algebraic roughness turbulence models were used. A model is proposed to account for the increase in loss due to roughness as the Reynolds number increases.

L Weili, L Jinling et al. [5] presented numerical simulation of cavitation characteristics in pure water and solid-liquid two-phase flow in Kaplan turbine. The solid-liquid two-fluid model was adopted in the numerical simulation. Under the condition of two-phase flow with water and sand, the sand distribution on blade surface is non uniform. The sand concentration is small in the area near to hub, while it is big at the inlet. The concentration changes a little for the rest parts. Under the condition of two phase flow with water and sand, the sand distribution on blade surface is closely related with its diameter. The bigger the diameter is, then the more non-uniform the distribution becomes. So the main part of wear on blade changes with the diameter of sand. The

cavity volume fraction at blade pressure side or suction side in sediment flow is bigger than in clean flow and the combined action of sand wear and cavitations causes greater abrasion, which results to the decrease of efficiency cones.

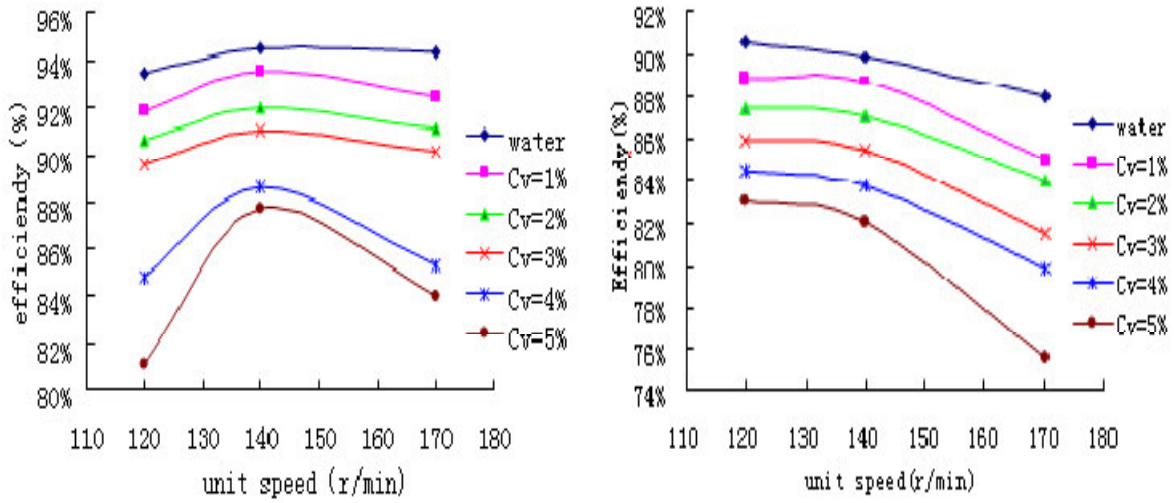

Figure 2.3: Efficiency with different sand volume fraction (sand diameter of 0.024mm)

(L Weili, L Jinling et al. 2010)

Sanjay Jain et al. [6] analyzed the performance and efficiency of Francis runner at four different operative points of guide vanes by using CFD and validate the same with model testing. The numerical simulations were carried out using two sets of boundary conditions viz. (i) pressure inlet and pressure outlet and (ii) mass flow inlet and pressure outlet. However, it was felt that second set of boundary conditions, i.e. mass flow at casing inlet and total pressure at draft tube outlet, were better suited for the CFD analysis of Francis turbine. The overall efficiency of turbine was predicted using CFD approach and compared with the model testing results obtained from the manufacturer and very good agreement was found.

P Drtina et al. [7] compared the experimental data and 3D Euler and 3D navier-stokes results for the flow in Francis runner, and also elaborates the state of the art for the prediction of performance of Francis turbine by numerical simulation.

Alok Mishra et al. [8] simulation has been carried out for design and part load conditions at three different opening points for Kaplan turbine. The optimization of runner blade angle has been provided the part load efficiency of Kaplan turbine. This paper present the CFD approach for prediction of efficiency of 100 kW capacity Kaplan turbine. The numerical simulations were carried out using commercial CFD package Fluent in ANSYS 14 software for the prediction of overall efficiency of Kaplan turbine. Standard k-ε turbulence model for single phase was used for the numerical simulation. The simulations were carried out for design condition and part load conditions with wicket gate openings at 75%, 65% and 55%. For each wicket gate opening four simulations were carried out by varying runner blade angle to optimize the efficiency. The efficiency of the Kaplan tubular. Turbine has been found to be maximum as 91% for design condition i.e. at rated discharge 7.03m^3/s and at rated head 1.5 m at 85% wicket gate opening.

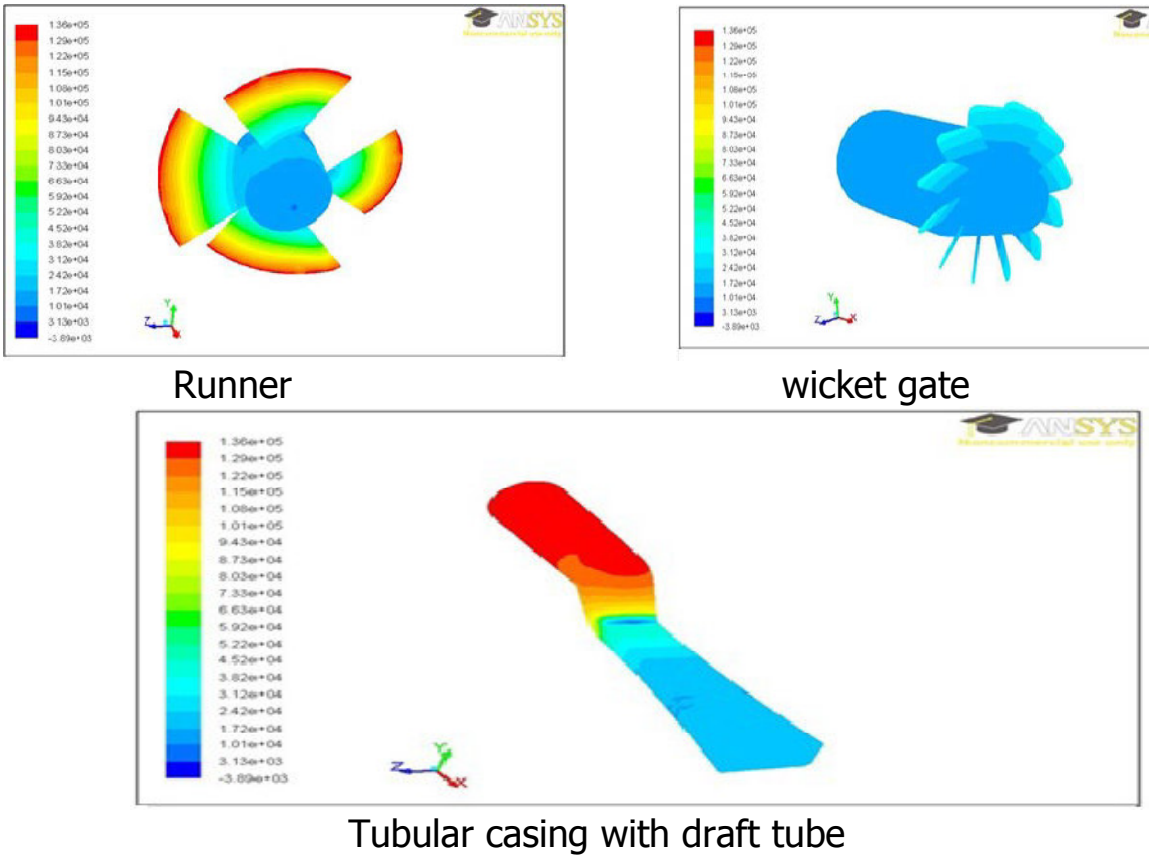

Figure 2.4 Contours of components of Kaplan turbine for design conditions (Mishra and saini et al.)

Harsh vats et al. [9] investigated the combined effect of cavitations and silt erosion of Francis turbine by using four different flow conditions namely pure water flow, cavitation flow, sedimentation flow and combined flow and then efficiency was calculated for each flow and their comparison was made by using fluent. It has been observed that the drop in efficiency was much higher in case of combined flow condition rather than the other two cases of cavitation flow and sediment flow. The affected zones of the runner blade were identified and the erosion rate has been found to be highest in the case of combined flow condition. CFD approach has been adopted to investigate the combined effect of cavitation and silt erosion on Francis turbine. Francis turbine rated head as 48 m and the rated discharge as 7.2 m3/s. The computational model comprising of 13 runner blades, 14 guide vanes and stay vanes, spiral casing and draft tube is considered. The geometric model was generated with the help of Pro-e and 'BladeGen' module of ANSYS. The final assembly of the computational model was meshed using the 'Mesh' module of ANSYS. The total number of elements obtained was around 2.6 millions. The flow in the hydro turbine was calculated in the stationary reference frame except that in runner where flow was calculated in the moving reference frame.

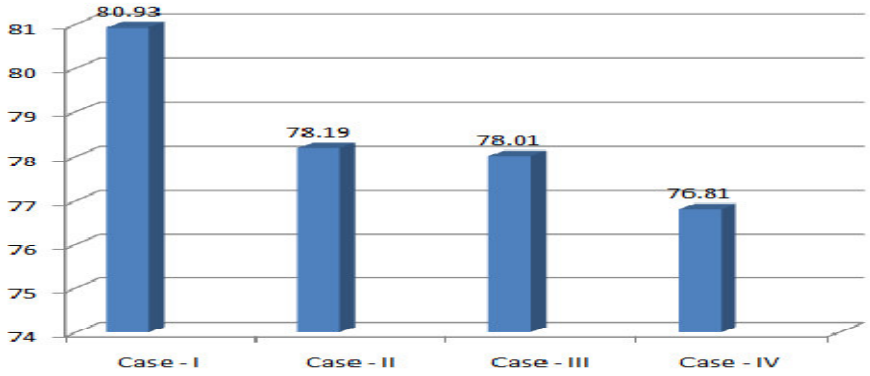

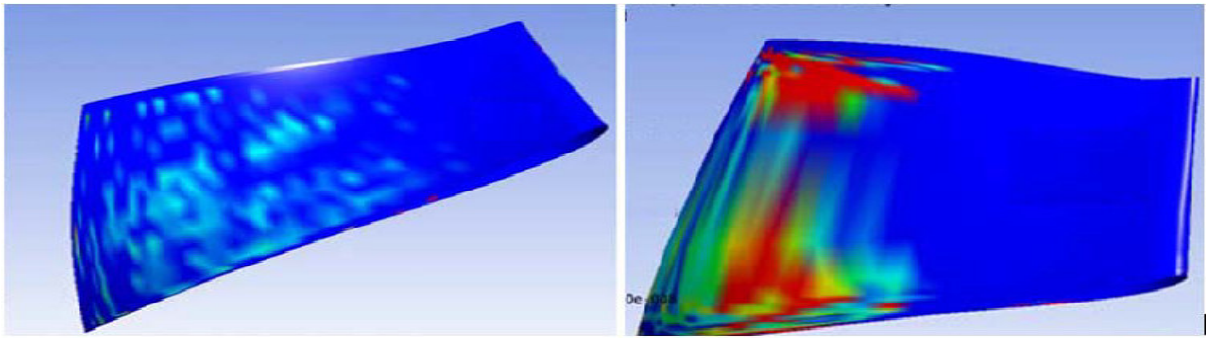

Figure 2.5: Percentage of silt erosion and their contours (Harsh vats and R.P. saini)

Shuhong LIU et al. [10] presented the numerical simulation with a cavitating model and mixture two-phase model by using fluent has been performed to unsteady turbulent flow in the entire passage of Kaplan turbine. And the results of this simulation the region and degree of cavitations occurrence in the turbine and also shows its performance. They use RNG k-ε turbulence model for the unsteady turbulent flow with the wall function near walls. The finite volume algorithms with the second order central difference for the source term and with the second order upstream differences for the convective term of the spatial discrete governing equations is used for the numerical simulation. In this work cavitation model is simulated by using pressure correction method derived from the SIMPLE algorithm and a finite volume discretization The results shows that the cavitation appears on the suction surface and the blade skirt rim of the runner while in the other parts, no any cavity is observed.

L Poudel et al. [11] presented that shape and size of the hard particles with their velocity plays a important role to decide the rate of erosion. They conducted this study by implementing computational tool to characterize the sediment particles with respect to their shape and size of hard particles on turbine material. Experimental studies of impact of different shapes and sizes of sediment particles on hydraulic turbine material have been conducted on two different test rigs methods. Twenty one different sediments shape samples and four different sand size ranges were studied to determine the effect of it on turbine components. Impact of sediment on turbine material is the loss of weight of material expressed in gram and the sediment size in micrometer.

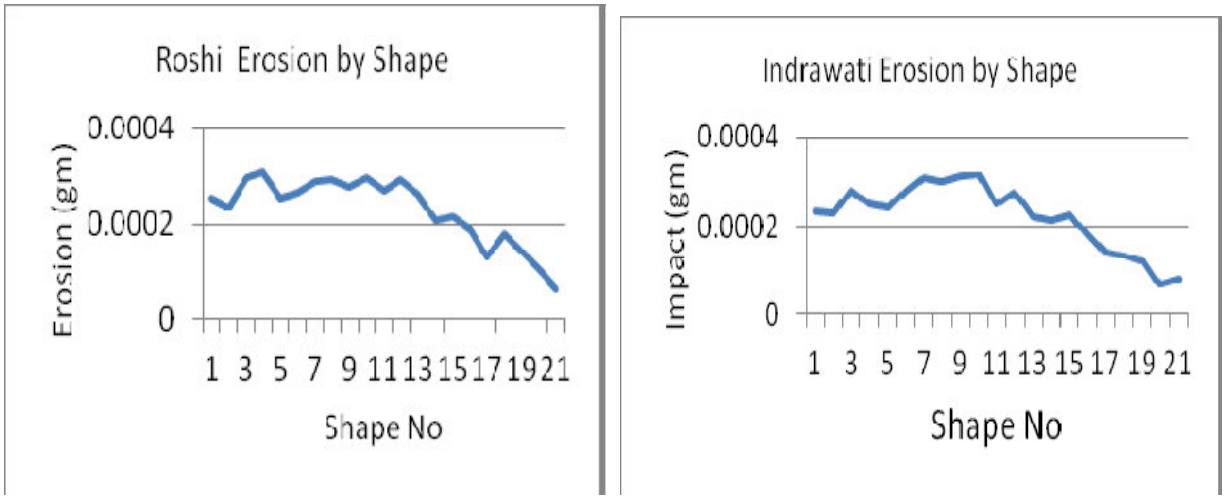

Figure 2.6: Sediment shape effect (L Poudel, B Thapa, B P Shrestha et al.)

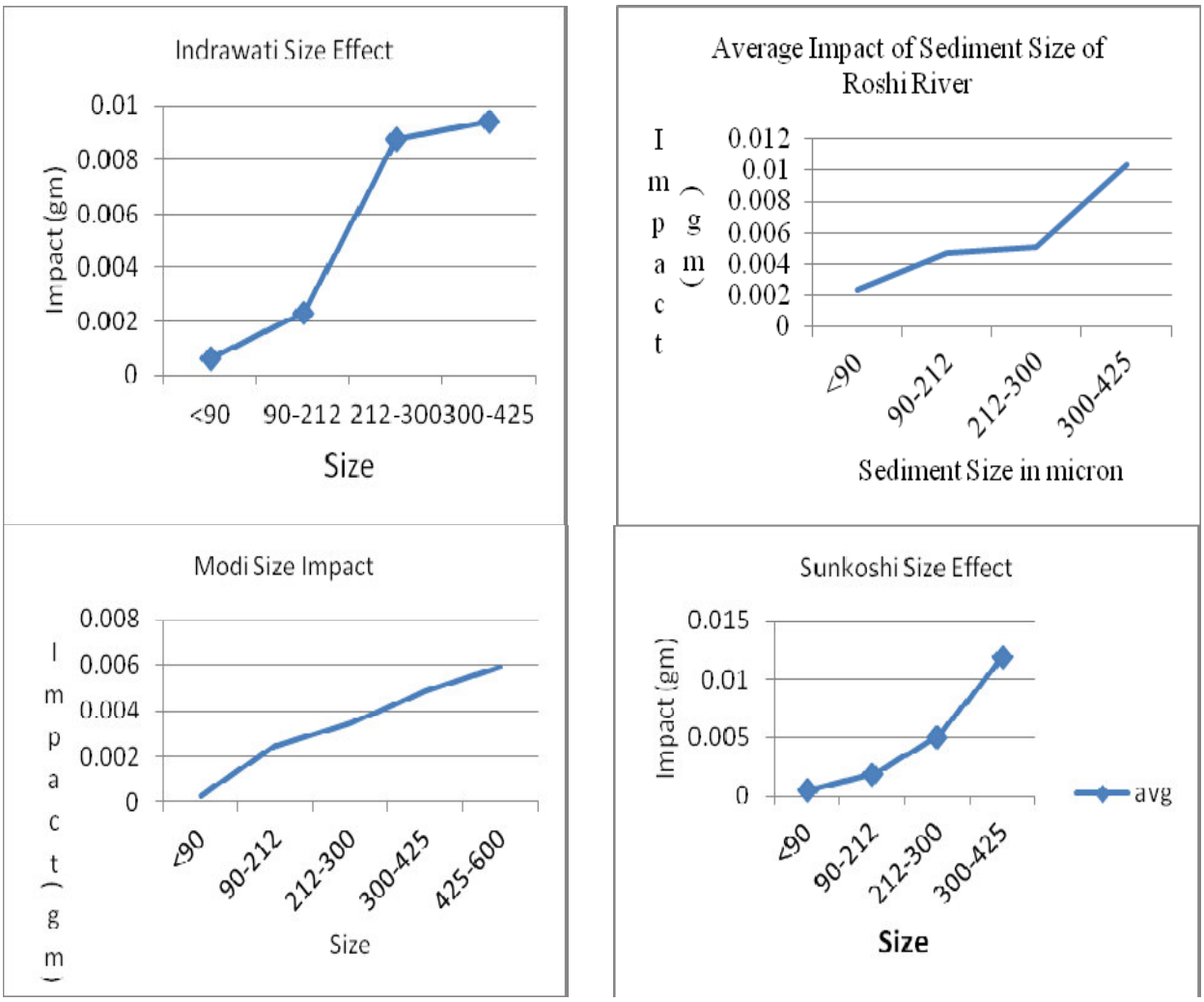

Figure 2.7 Size impact by sediment (L Poudel, B Thapa, B P Shrestha et al.)

Vinod Kumar Singoria et al. [12] presented the effect of surface roughness on secondary flow in a rectilinear turbine cascade. They apply roughness of 500µm on pressure and suction surface individually and in next case, on both surfaces to see the effect of it on secondary flow. For this they uses computational software gambit and fluent. After simulation they found that in smooth blade average loss is 14.7% and in case of a blade having both surface rough 27.7%. when roughness is applied on all the suction surfaces then loss is 24.7% and when the roughness is presents in pressure surfaces then it is 18.2%. and all these results are compared with the experimental results performed by Prof. samsher.

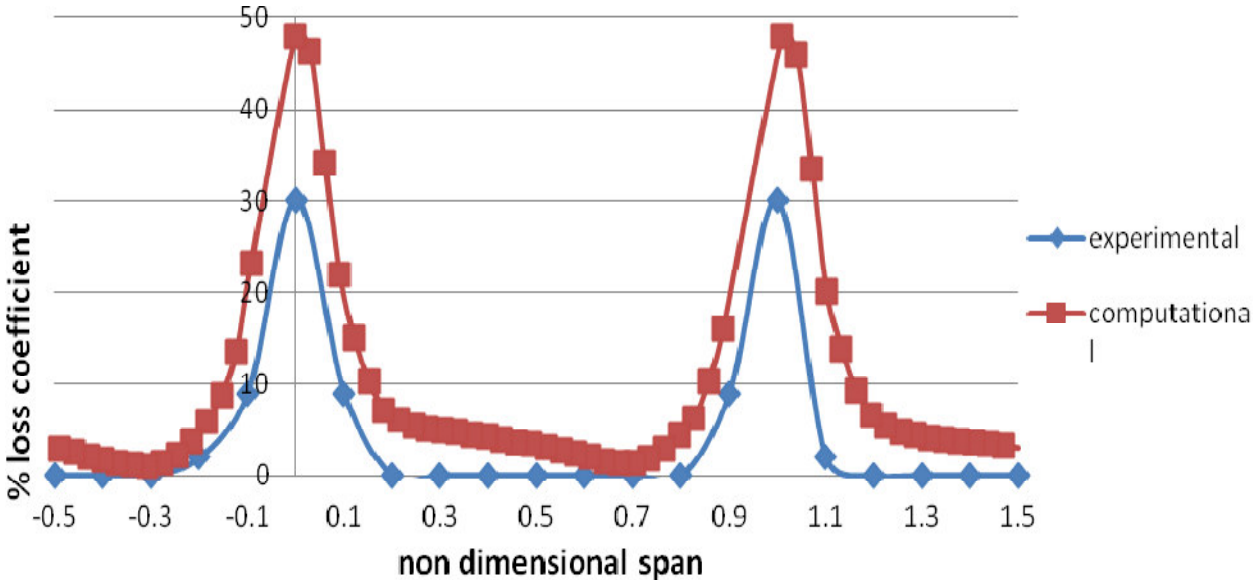

Figure 2.8: Validation of computational result with the experimental result obtained by Samsher (Vinod Kumar Singoria, Deepika Sharma and Samsher)

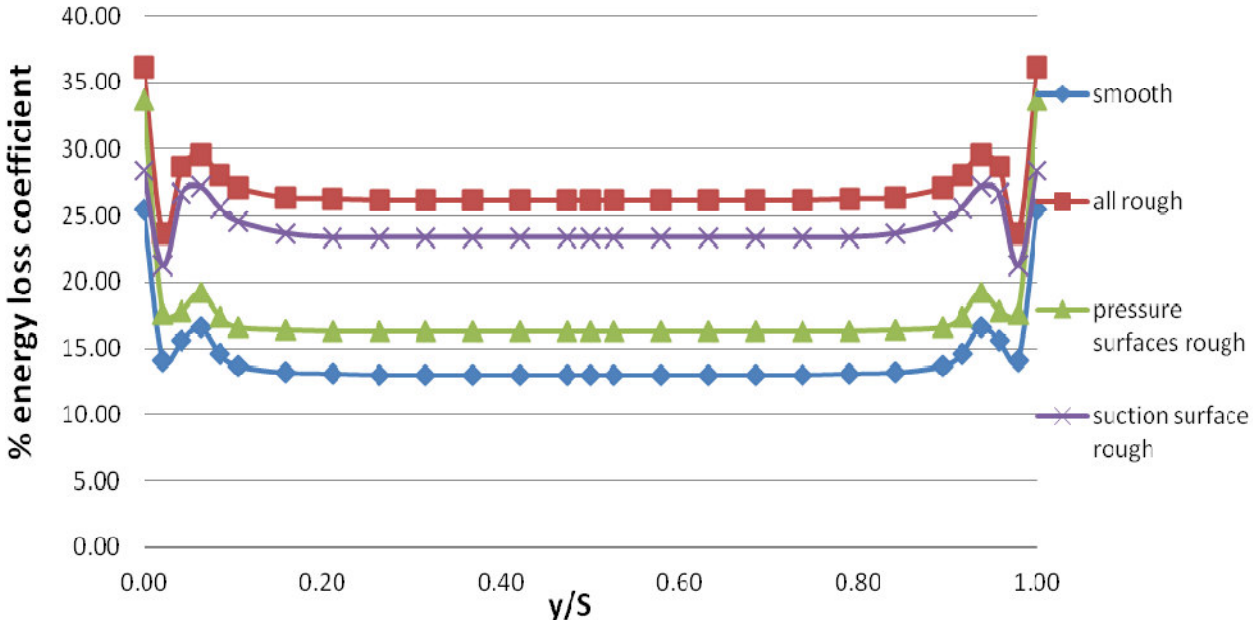

Figure 2.9: Comparison of secondary loss in a) smooth blades, b) all rough c) pressure surface rough d) suction surface rough. (Vinod Kumar Singoria, Deepika Sharma and Samsher)

2.2 Summary of literature review

After going through the literature review, It can be summarized that more of the work has been done in turbines rotor, stator and on turbines cascade. Many researchers work on the efficiency, sediment shape and size, mach number, blade angle, measurement of stagnation pressure, surface roughness, secondary losses, degradation of turbine life, cavitations characteristics. Reflection of light is not clear on effect of contamination content of turbine on profile loss. Therefore the work on the effect of some contaminants on profile loss coefficient of turbine and also analyze its effect on affected surface of blade has been carried out in this project.

2.3 Problem Statement

The main aim of this project is to use the computational software to check the effect of particles on profile loss coefficient. In turbines various types of impurities is also flowing with working fluid which damages the blades and also reduce the efficiency of turbine. The trilogy of "CDE" (Corrosion, Deposition, Erosion) is a result of injection of particles. Here injection of some steel, ash and water particles with diameter ranging 50µm to 300µm at different velocities ranging from 50m/s to 150m/s. In the model of cascade, designing is done in gambit software, modeling and simulation is done with the help of fluent software. The effect of particle injection on the turbine cascade performance is analyzed. With the help of results obtained by fluent the variation of profile loss coefficient for different inlet velocity conditions with particle injection are studied. The effected length of blade due to particle injection is also investigated out by using simulations.

2.4 Organization of report

The report has been organized in the following sequence. The report is divided into 6 chapters. Introduction of the project topic is given in Chapter-1. An overview of the related literature has been given in Chapter 2.

Description of governing equations used has been described in Chapter 3. Results followed by discussions are presented in Chapter 4. Conclusions are presented in Chapter 5. Future Scope of the present work is presented in Chapter-6. References are presented after Chapter 6, followed by appendices.

CHAPTER 3
METHODOLOGY

3.1 Computational fluid dynamics

CFD stands for computational fluid dynamics. It is a branch of continuum mechanics which deals with the numerical simulation of a fluid flow for various hydraulic machinery and heat transfer problems. CFD deals with approximate numerical solution of governing equations based on conservation law of physics namely mass, Momentum and energy conservation. The CFD solution includes conservation of governing equations for a continuum medium into a set of different algebraic equations using a process called discretization. Solution of discrete equations by using a computer to obtain a numerical solution with desired level of accuracy.

3.2 Need for CFD

CFD provides us to study the dynamics of flowing fluids. We can make a computational model that represents a system that we want to study. Therefore, CFD is a sophisticated computationally-based design and analysis technique. This process starts with converting the unsolvable governing equations to a solvable set of algebraic equations for a finite set of points within the space under considerations. By solving the equations, we get the values of temperature, pressure, turbulence at any point in the flow field. The conservation of mass momentum equation and continuity equation form a set of coupled non linear partial differential equations. It is not possible to solve these equations analytically for various problems. It is only possible with the help of CFD for different flow problems.

3.3 Equations for CFD

To analyze the fluid flow, the basic governing equations has to be solved. The equation that governs the flow includes:

1. Continuity equation (conservation of mass)
2. Navier stokes equation (conservation of momentum)
3. Energy equation (conservation of energy)

3.3.1 Continuity equation

The general continuity equation in tensor notation is expressed as:-

$$\frac{\partial \rho}{\partial t} + \frac{\partial}{\partial x_i}(\rho u_i) = S_m \tag{2.1}$$

The equation 2.1 is valid for both incompressible as well as compressible flow. If the flow in which the density of the fluid remains constant, then the continuity equation reduces to

$$\frac{\partial}{\partial x_i}(\rho u_i) = S_m \tag{2.2}$$

Where, ρ is the density of the fluid, $\frac{\partial}{\partial xi}$ is the divergent operator, u_i is the velocity vector of the fluid and S_m is the source term.

3.3.2 Momentum equation

The conservation of momentum in an inertial reference frame in Cartesian coordinate system is expressed as:-

$$\frac{\partial}{\partial t}(\rho u_i) + \frac{\partial}{\partial x_j}(\rho u_i u_j) = -\frac{\partial p}{\partial x_j} + \frac{\partial \tau_{ij}}{\partial x_j} + \rho g_i + F_i \tag{2.3}$$

Where p is the static pressure, ρg_i is the gravitational body force, F_i is the external body force and τ_{ij} is the stress tensor (which is expressed as below).

$$\tau_{ij} = \left[\mu \left(\frac{\partial u_i}{\partial x_j} + \frac{\partial u_j}{\partial x_i} \right) \right] - \frac{2}{3} \mu \frac{\partial u_i}{\partial x_j} \delta_{ij} \quad (2.4)$$

Where μ is the molecular viscosity and the second term on the right hand side is the effect of volume dilation and δ_{ij} is the Kronecker's delta.

The value of $\delta_{ij} = 0$ if, $i \neq j$

$= 1$ if, $i=j$.

3.3.3 Energy equation

The conservation of energy equation is expressed as:-

$$\frac{\partial}{\partial t}(\rho E) + \frac{\partial}{\partial x_i}(u_i(\rho E + p)) = \frac{\partial}{\partial x_i}\left(k_{eff} \frac{\partial T}{\partial x_i} - \sum_{j'} h_{j'} j_{j'} + u_j (\tau_{ij})_{eff}\right) + S_h \quad (2.5)$$

Where k_{eff} is the effective conductivity ($k+k_t$), where k_t is the turbulent thermal conductivity) and j_j' is the diffusion flux of species j'. The first three terms on the right hand side of energy equation represent energy transfer due to conduction, species diffusion and viscous dissipation respectively. S_h source term if any includes heat of chemical reaction.

The energy term 'E' is further expanded as

$$E = h - \frac{p}{\rho} + \frac{u_i^2}{2} \quad (2.6)$$

Where sensible enthalpy 'h' is defined as

For ideal gases

$$h = \sum_{j'} m_{j'} h_{j'} \tag{2.7}$$

And for incompressible flows

$$h = \sum_{j'} m_{j'} h_{j'} + \frac{p}{\rho} \tag{2.8}$$

$m_{j'}$ is the mass fraction of species j' and enthalpy $h_{j'}$ is expressed as

$$h_{j'} = \int_{T_{ref}}^{T} c_{p,j'} dT \tag{2.9}$$

In addition to the above three basic equations of flow, some other equations are also solved depending on the nature of flow phenomenon involved in the problem. For example, if swirling flow takes place in the flow domain, then axial and radial momentum conservation equations are to be solved, where the swirl velocity is included in the equation. Similarly, viscous heating (dissipation) is important for compressible flows, PDF model in energy equation for combustion process, energy source term for chemical reactions, Boussinesq model for natural convection etc. The numerical solution of the three basic equations of fluid flow gives a close approximation to the flow problem for a steady and laminar flow. Most of the flow occurring in nature and engineering applications is turbulent. So treatment for turbulence is required to have better solution to the problem.

3.4 Strategy of CFD

Broadly, the strategy of CFD is to replace the continuous problem domain with a discrete domain using a grid. In the continuous domain, each flow variable is defined at every point in the domain.

For instance, the pressure *p* in the continuous 1D domain can be given as

$p = p(x)$, $0 < x < 1$

In the discrete domain, each flow variable is defined only at the grid points. So, in the discrete domain shown below, the pressure would be defined only at the N grid points.

$p_i = p(x_i), \quad i = 1, 2, ..., N$

Continuous Domain Discrete Domain

$0 \leq x \leq 1$ $x_i = x_1, x_2, \ldots\ldots x_n$

In a CFD solution, one would directly solve for the relevant flow variables only at the grid points. The values at other locations are determined by interpolating the values at the grid points.

The governing partial differential equations and boundary conditions are defined in terms of the continuous variables p, ~V etc. One can approximate these in the discrete domain in terms of the discrete variables p_i, V etc. The discrete system is a large set of coupled, algebraic equations in the discrete variables. Setting up the discrete system and solving it (which is a matrix inversion problem) involves a very large number of repetitive calculations, a task we humans palm over to the digital computer.

3.5 Discretization of Equations

Whenever the linearization procedure is necessary, a iterative calculation procedure must be adopted, whereby the equations are successively re-linearized and solved until the solution to the original numerical form of the equations is attained. Each discretization scheme differs in the assumption of profile within a small volume considered and the way space is discretized. Once discretized, it leaves meshes that cover the domain and a set of algebraic equations for that control volume.

There are two ways to solve the set of algebraic equations obtained by discretization, direct method (i.e., those requiring no iteration) and iterative method. One of the direct methods is called the Tri-diagonal Matrix Algorithm (TDMA), which is very efficient but applicable only in 1-D applications because the direct method is usually involved with matrix inversion that may cause very expensive calculations in 2-D or 3-D problems. Alternatively, the iterative method

is widely accepted since it is stable and applies to 2-D and 3-D situations. It starts with guessed variables and uses the algebraic equations to get improved variables. It goes on until the difference between new values and the previous values is minor. Then the converged solution is acquired. Discretization is done by these methods:

1) FEM (finite element method)
2) FDM (finite difference method)
3) FVM (finite volume method)
4) Spectral element method
5) Boundary element method
6) Higher resolution discretization schemes

3.6 CFD Process

Any CFD process is divided into three categories namely pre processing, simulation and post processing.

3.6.1 Pre processing:

The pre-processing stage consists of:

- determining the equations to be solved (flow physics);
- specifying boundary conditions;
- generating a mesh.

It depends upon:

- The desired outputs of the simulation (e.g. force coefficients, heat transfer ...);
- The capabilities of the solver.

3.6.2 Simulation

The CFD solver does the flow calculations and produces the results. The equations are solved iteratively as a steady-state or transient. FLUENT, Flow wizard, FIDAP, and POLYFLOW are the four general – purpose rapid flow modeling tools. The FLUENT CFD code has extensive interactivity, so one can make changes to the analysis at any time during the process. This saves time and enables refining of designs more efficiently.

3.6.3 Post processing

Commercial packages routinely provide:

- plotting tools to visualize the flow;
- Analysis tools to extract and manipulate data.

Finally a postprocessor is used for the analysis and visualization of the resulting solution. It involves the organization and interpretation of the predicted flow data and the production of CFD images and animations. All of Fluent's software products include full post processing capabilities

3.7 Designing of Cascade

3.7.1 Description of Computational domain

This work is to analysis the effect of particle injection on profile loss coefficient of a rectilinear turbine cascade computationally using commercially available software fluent 6.3.26. The cascade profile consists of six blades with five flow channels with appropriate stagger angle, chord, pitch, inlet fluid flow angle, working medium is air. A two dimensional model was created in gambit. Various parameters are given below:

Table 3.1 Cascade dimensions and parameter

Parameters	**Profile 6030**
Cascade type	Rectilinear
Inlet cross section	95 x 99.7 mm^2
Type of test blade	Reaction type
Chord (mm), c	50
Pitch (mm), S	22
Blade stagger angle	70°
Inlet flow angle	65°
Number of blades	6
Number of channels	5
Working fluid	Air
Inlet air temperature	30°C

3.7.2 Basic Steps

First of all various co-ordinates of blade profile are plotted using vertex command in Gambit®. By using the edge command all the co-ordinates are joined to obtain a wireframe model. This gives us a blade of the turbine. Now rotate this blade at the stagger angle of 70°. Copy this profile 6 times to get the desired cascade and now adjust the cascade to the required inlet flow angle for the shock less entry of fluid.

Now the boundary types are defined. The inlet of the cascade is defined as velocity inlet and outlet as pressure outlet; all other boundaries are defined as wall. These boundary types will be used in Fluent to define the boundary conditions which is an important aspect of Fluent. This meshed 2-D geometry of cascade is saved and then exported to mesh which will be used read in fluent as case file. Grid checking and scaling of the model is done in fluent. K-epsilon realizable

viscous solver model is selected because of its added advantage. The various operating and boundary conditions are stated and the model is iterated to convergence.

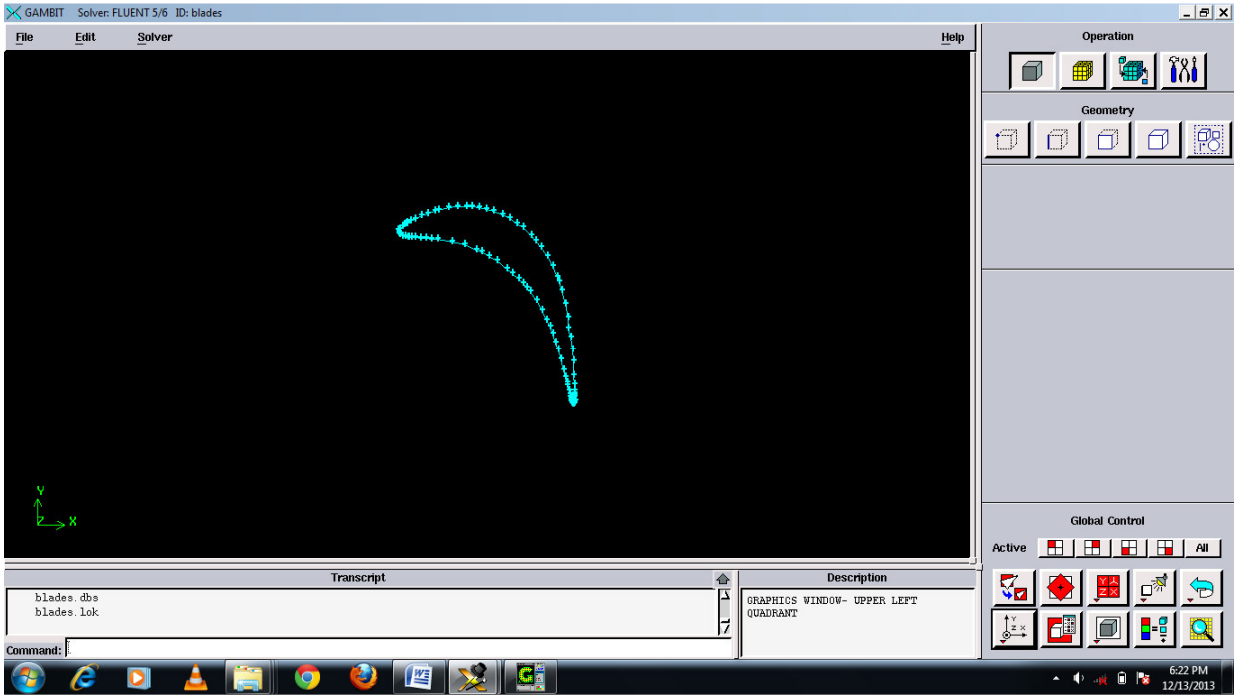

Figure 3.1: A Blade at Required Stagger Angle

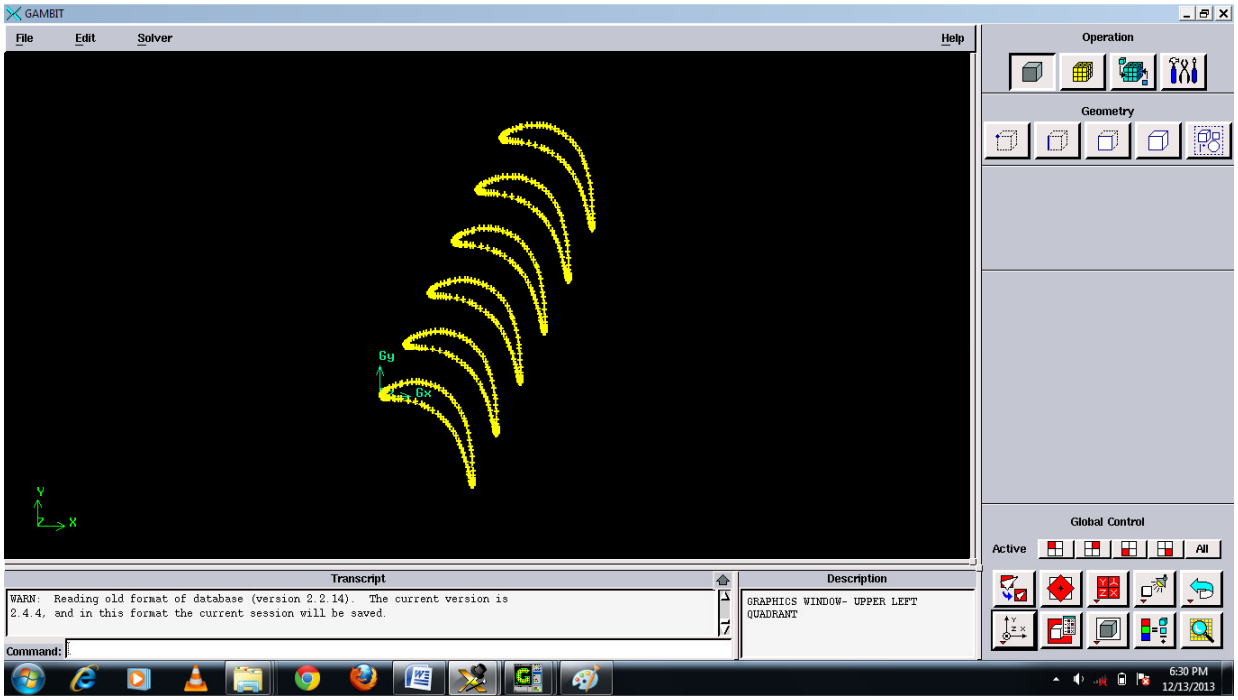

Figure 3.2: The Required Set of Blade

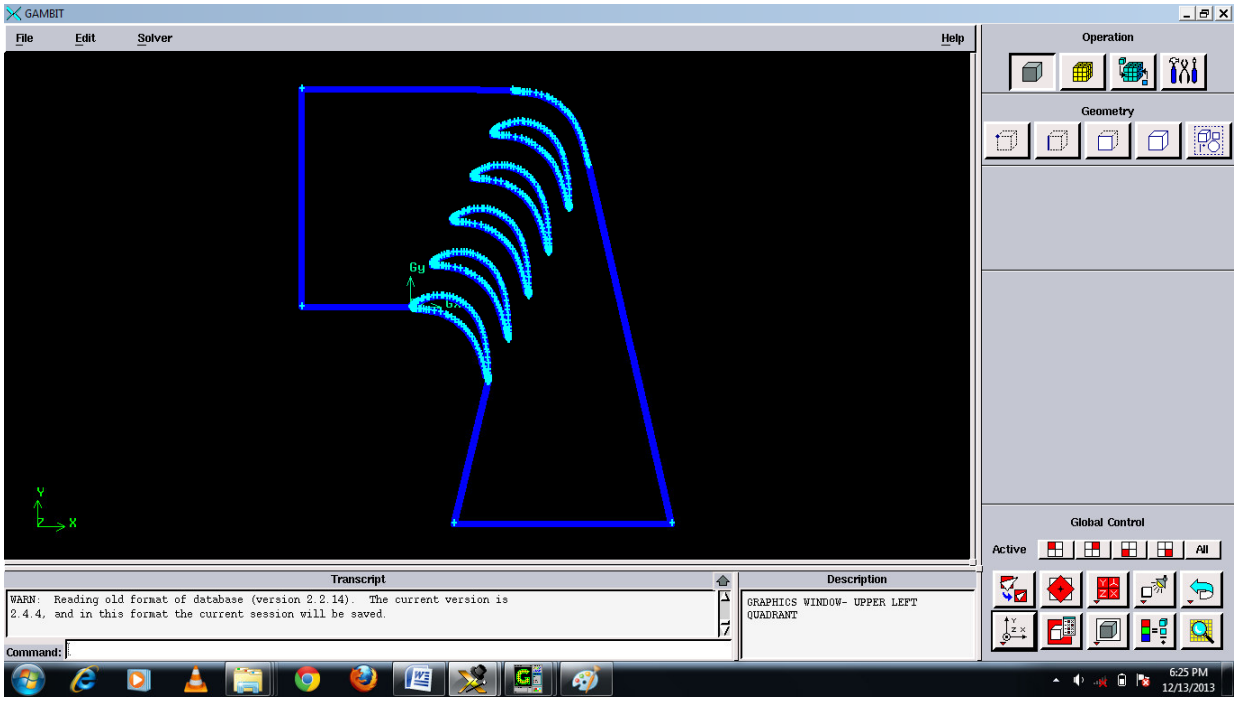

Figure 3.3: Designed Cascade

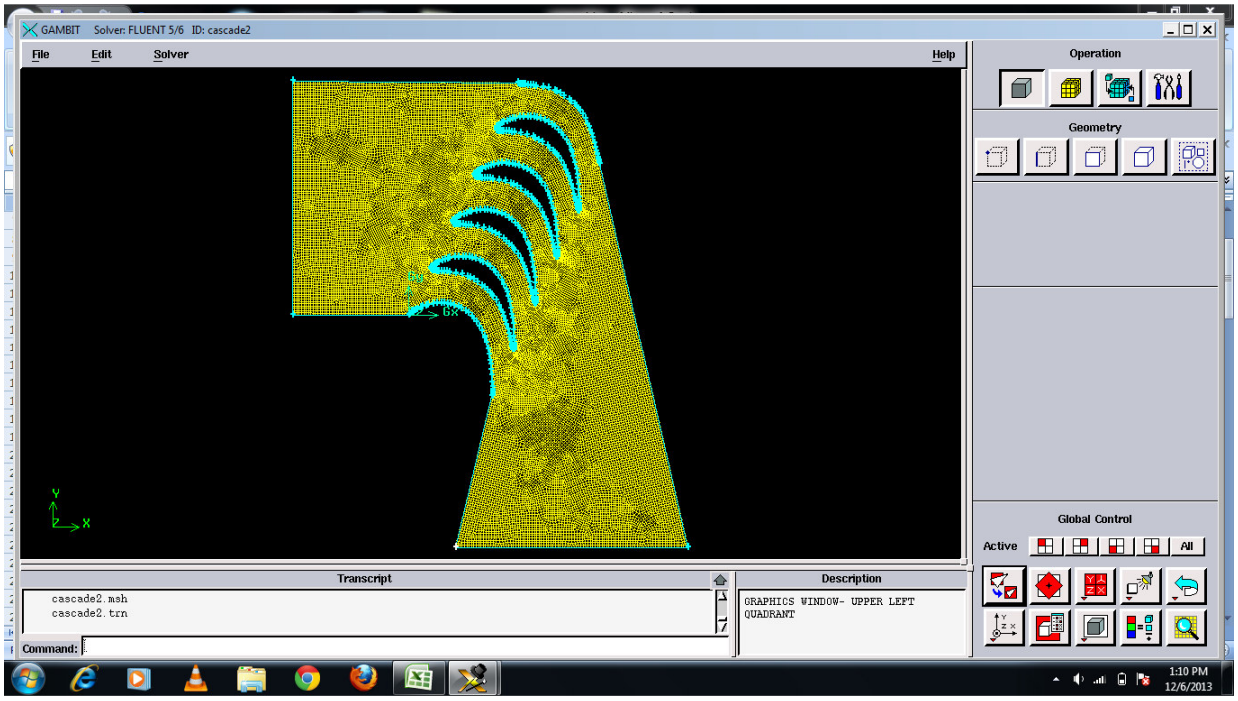

Figure 3.4: Meshing of fluid field

3.7.3 Fluent Simulation Procedure

After meshing, the mesh file is exported to fluent 6.3.26. Then checking, scaling and smoothening of the cascade grid is to be done. K-epsilon realizable viscous model is chosen because of its advantage and discrete phase model is used for particle injection. Injections are define here. The various operating and boundary conditions are defined. The pressure velocity compounding is SIMPLE. Discreatization is of second order upwind and the cascade is iterated to be convergence for different velocities from 50m/s to 150m/s and for different particle sizes from 50µm to 300µm.Simulations with ash, steel and water particles is carried out. The values of static pressure at outlet, total pressure at outlet and inlet are found. From these values we find out the value of profile loss coefficient. With the help of discrete phase model the effected length of blade due to particles hitting is find out.

Particle injection: The steel, Ash and Water particles at velocity 50m/s,100m/s, 150m/s with particles of diameter 50µm, 100µm, 200µm and 300µm is injected at above defined velocities. For this discrete phase model is used. Mass flow rate is 0.06 kg/s.

3.8 Profile Loss Calculations

The profile loss coefficient ξ_y is calculated by using the relation proposed by Dejc and Trojanovskij, expressed as

$$\xi_y = 1- \eta$$

Substituting the value of η in above equation, we have

$$\xi_y = 1- \frac{\left[1-\left[\frac{P_{01}-P_{02}}{P_{01}-P_2}\right]\left[1-\frac{P_2}{P_{01}}\right]\right]^{\frac{\gamma-1}{\gamma}} - \left[\frac{P_2}{P_{01}}\right]^{\frac{\gamma-1}{\gamma}}}{\left[1-\left[\frac{P_{2s}}{P_{01}}\right]^{\frac{\gamma-1}{\gamma}}\right]\left[1-\left[\frac{P_{01}-P_{02}}{P_{01}-P_2}\right]\left[1-\frac{P_2}{P_{01}}\right]\right]^{\frac{\gamma-1}{\gamma}}} \quad (2.10)$$

On simplification the above equation and putting value of $P_2 = P_{2s}$ (as both points are on same pressure line), equation is expressed as follows,

$$\xi_y = \left[\frac{P_{2s}}{P_{01}}\right]^{\frac{\gamma-1}{\gamma}} \frac{1-\left[1-\left[\frac{P_{01}-P_{02}}{P_{01}-P_{2s}}\right]\left[1-\frac{P_{2s}}{P_{01}}\right]\right]^{\frac{\gamma-1}{\gamma}}}{\left[1-\left[\frac{P_{2s}}{P_{01}}\right]^{\frac{\gamma-1}{\gamma}}\right]\left[1-\left[\frac{P_{01}-P_{02}}{P_{01}-P_{2s}}\right]\left[1-\frac{P_{2s}}{P_{01}}\right]\right]^{\frac{\gamma-1}{\gamma}}} \tag{2.11}$$

The effect of change of pitch distance on the profile loss is shown in Figure given below;

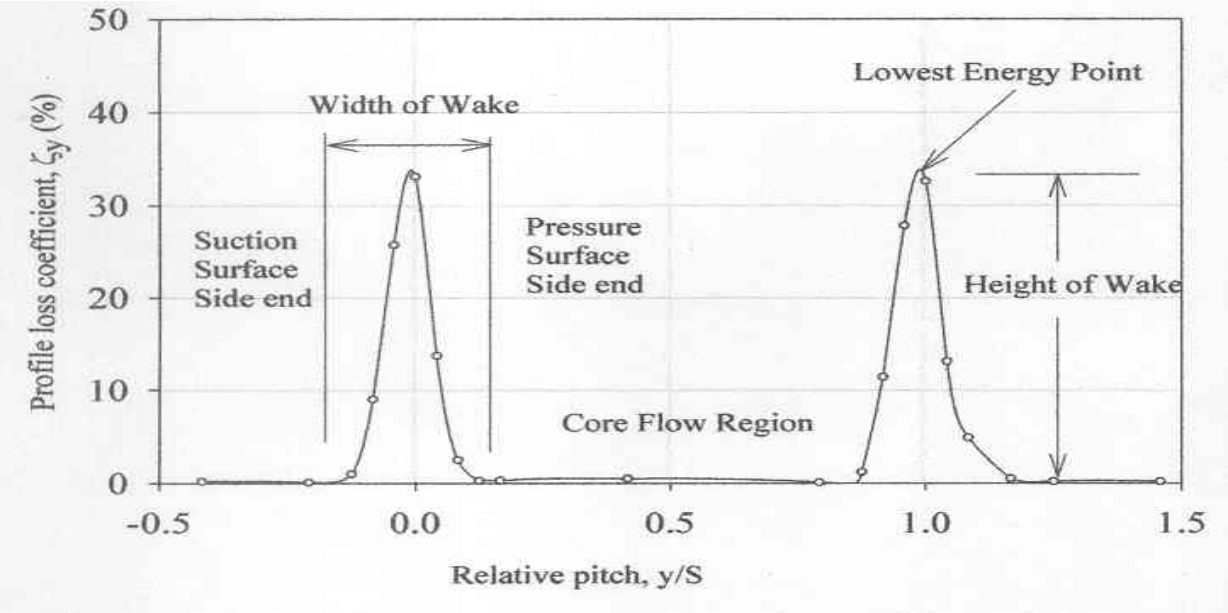

Figure 3.5: Profile loss coefficient versus relative pitch (Samsher)**.**

Where, P_{2s} is static pressure at outlet of cascade, P_{01} and P_{02} are the total pressures at the inlet and outlet of cascade respectively, γ is the ratio of specific heats for air.

CHAPTER 4

RESULTS AND DISCUSSION

The designing part is done in gambit as pre processor and the meshed file is analyzed in fluent as solver. The flow, velocity, pressure are analyzed at the appropriate location in fluent. The detail of boundary conditions is described in fluent. For the measurement of profile loss coefficient, a rake is drawn at inlet with coordinates (26, 99) and (-20, -0.14) by choosing rake option in fluent. Similarly a rake is drawn at outlet with coordinates (86.44, 43) and (25.18,-82) which is approx 15% of chord behind the cascade. The simulations in fluent are carried out on three different inlet velocity conditions with injection of particles of 50µm to 300µm to find out the change in profile loss coefficient and we also find out the portion of blade which is mainly affected by the particle hitting. In first cascade simulation is done on 50m/s velocity, in second and third cascade inlet velocity is 100m/s and the last one is at 150m/s velocity. The injection of ash, water and steel particles with diameter 50µm, 100µm, 200µm, 300µm are simulated at different velocities. The values of static pressure at outlet P2S, total pressure at inlet and outlet P01 and P02 are obtained and with the help of these values excel sheet is prepared to observe the effect of inlet velocity with steel particles injection on profile loss coefficient. The effected length of blade due to hitting of particles is also calculated.

4.1 Validation of data:

The profile loss coefficient is calculated with the help of the values obtained in fluent. Results are validated from the experimental and computational results shown by Prof. Samsher [2002] and Ms. Deepika [2012] M tech Scholar respectively. From the graph given below we checked the trend of graph. We also validate our results from the original turbine blade to check the area affected by the particle hitting. The images of original blade of turbine are shown below. There is a good agreement between the computational results, experimental results and original blade

affected area from particle hitting. Purpose of validation is that the numerical model or methodology used for simulation is reliable and can be further used for analysis and studies.

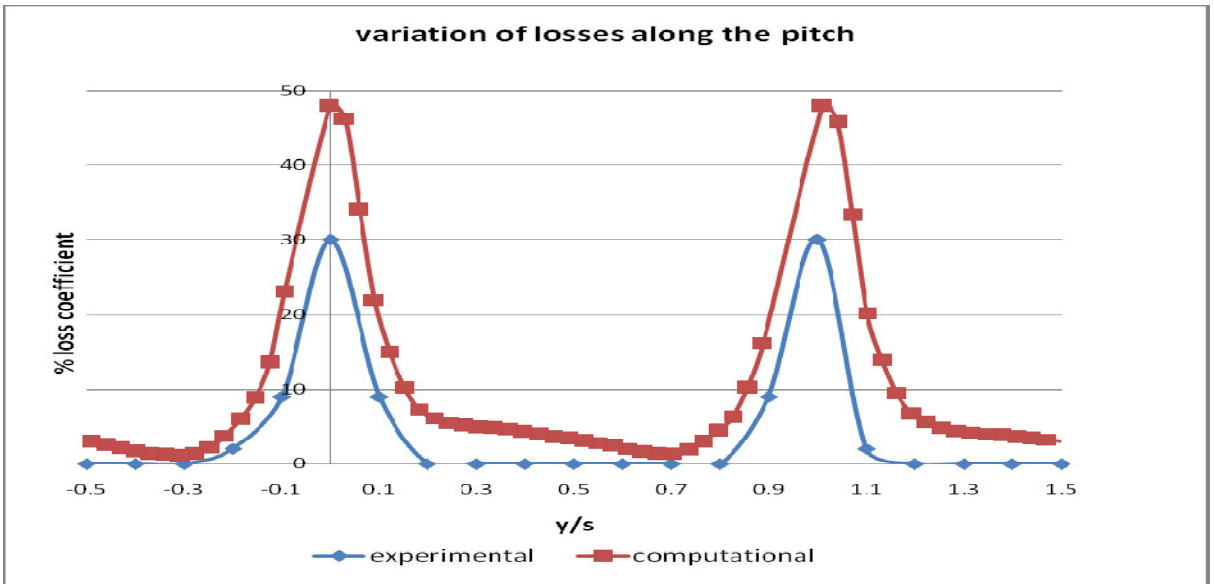

Figure 4.1: Comparison of computational results with experimental data on loss coefficient along the pitch.

Figure 4.2: leading edge and the suction surface of a turbine blade effected by the particles

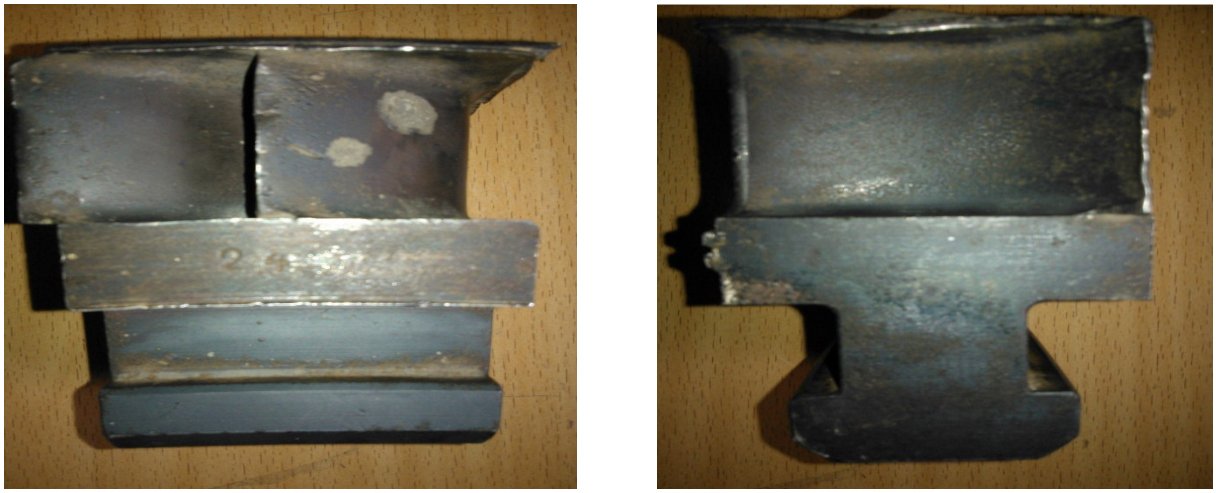

Figure 4.3: trailing edge and the pressure surface of a turbine blade effected by the particles

As seen in the figure of blade that leading edge and trailing edge of the blade is affected by the particles. The suction side is affected from starting to the mid of the blade from the particles. The particles having high inertia is strikes on the suction surface as it seen clearly and the particle having low value of inertia is not that much affected the blade by hitting and the chances of fouling is more with the low inertia particles as seen in the pressure side of the blade. The suction side is not effected from the mid to end as seen from the figure.

4.1.1 Analysis of data:

On the basis of readings obtained by the simulation of flow with the help of fluent, profile loss coefficient was calculated. The profile loss coefficient is calculated by using the relation proposed by Dejc and Trojanovskij (1973) as shown in equation below:

$$\xi_y = \left[\frac{P_{2s}}{P_{01}}\right]^{\frac{\gamma-1}{\gamma}} \frac{1-\left[1-\left[\frac{P_{01}-P_{02}}{P_{01}-P_{2s}}\right]\left[1-\frac{P_{2s}}{P_{01}}\right]\right]^{\frac{\gamma-1}{\gamma}}}{\left[1-\left[\frac{P_{2s}}{P_{01}}\right]^{\frac{\gamma-1}{\gamma}}\right]\left[1-\left[\frac{P_{01}-P_{02}}{P_{01}-P_{2s}}\right]\left[1-\frac{P_{2s}}{P_{01}}\right]\right]^{\frac{\gamma-1}{\gamma}}}$$

Here P_{01} and P_{02} are the total pressures at inlet and outlet, P_{2s} is the static pressure at outlet.

On the basis of above formulae, calculations is done in excel sheet for the evaluation of profile loss coefficient. Each data is taken in pitch wise position.

4.2 Computation of Profile loss:

4.2.1 For ash particles:

After validation of model and blade, the simulations are carried out for ash particles, As these particles are present as contaminants in gas turbine. The simulations are carried out for three different velocities 50m/s, 100m/s, 150m/s and ash particles of 50µm, 100µm, 200µm and 300µm diameter are injected into the turbine cascade. After simulation, profile loss is calculated for a blade span.

Contours of total pressure distribution at velocity 50m/s, 100m/s and 150m/s with ash particles of 50µm are shown below in figures. After entering the cascade section due to expansion the total pressure of the fluid is reduced. Boundary layer developed due to presence of eddies will creates low energy region at the exit of cascade field. Wake is formed due to these low energy regions and total pressure is reduced at the exit of the cascade as shown in total pressure contours of simulation. At some distance from the trailing edge, intermixing of flow is starts and wake is goes broader at the exit. It seen from the total pressure contours the pressure will goes decreasing with the increasing particle diameter. After increasing the velocity from 50m/s to 100m/s and 150m/s the total pressure increases for the turbine cascade. Different combination of velocities and particle size are shown in the form of graph to clearly understand the phenomenon. Similarly pressure distribution is seen for different µm size and the pattern of flow is same.

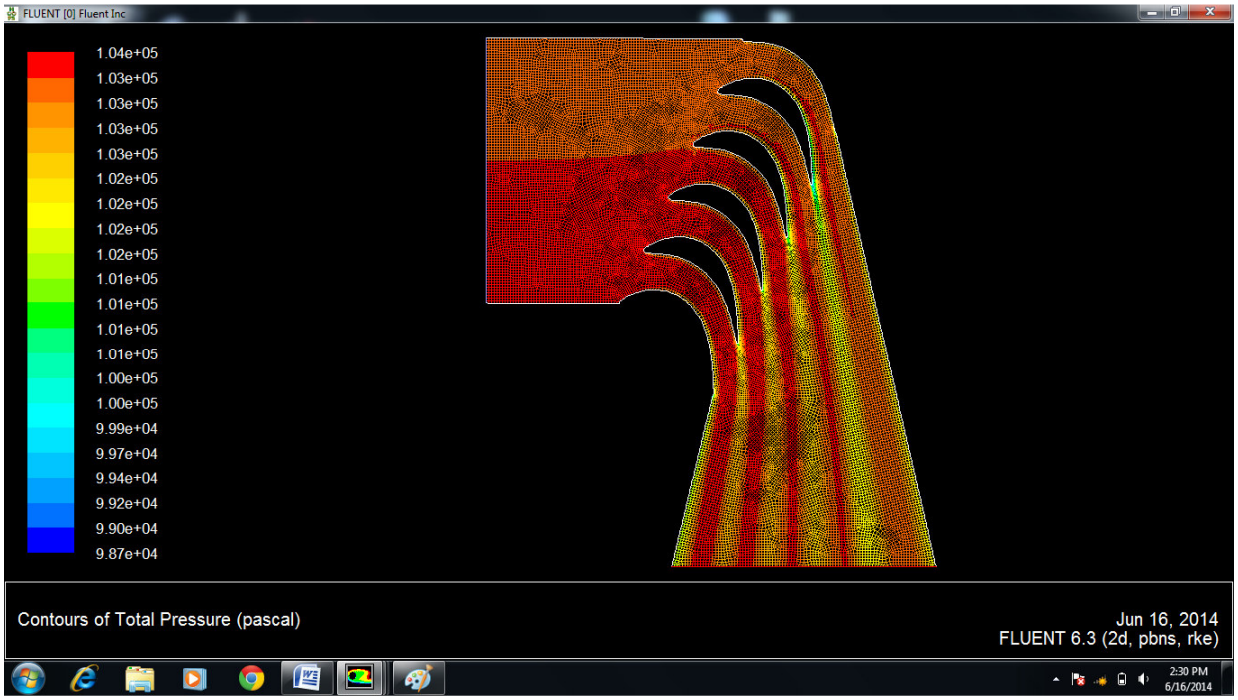

Figure 4.4: Contours of total pressure loss at velocity 50m/s with ash particles of 50µm

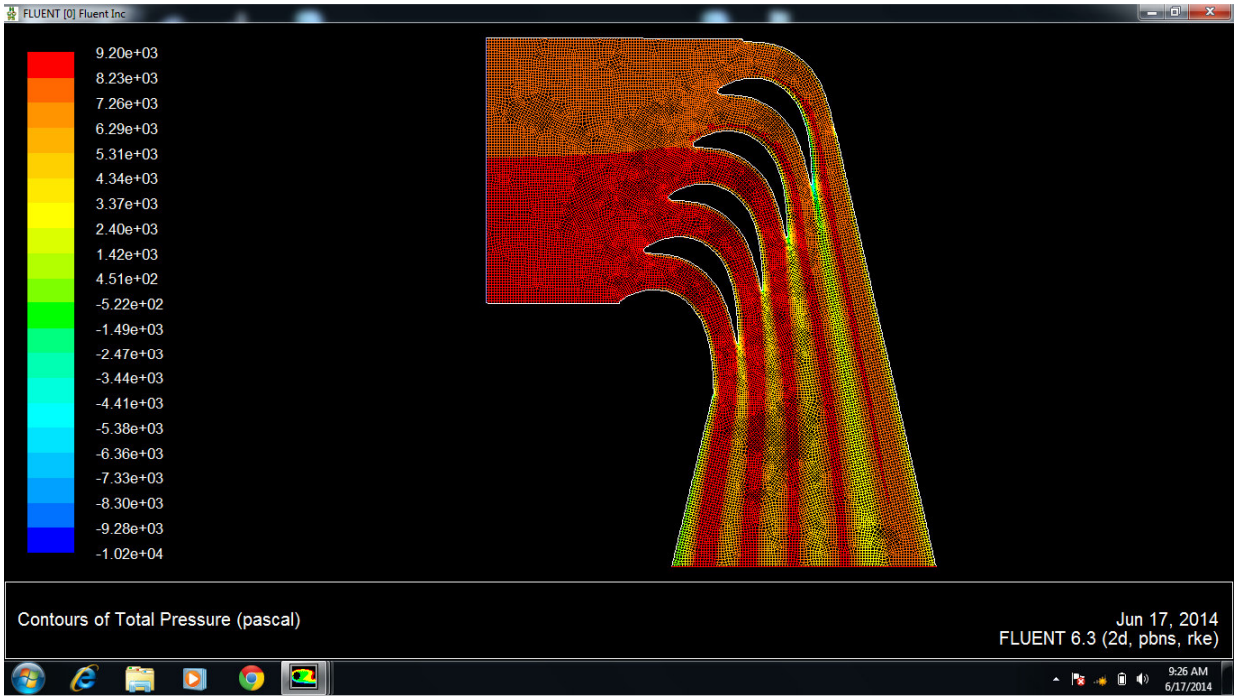

Figure 4.5: Contours of total pressure loss at velocity 100m/s with ash particles of 50µm

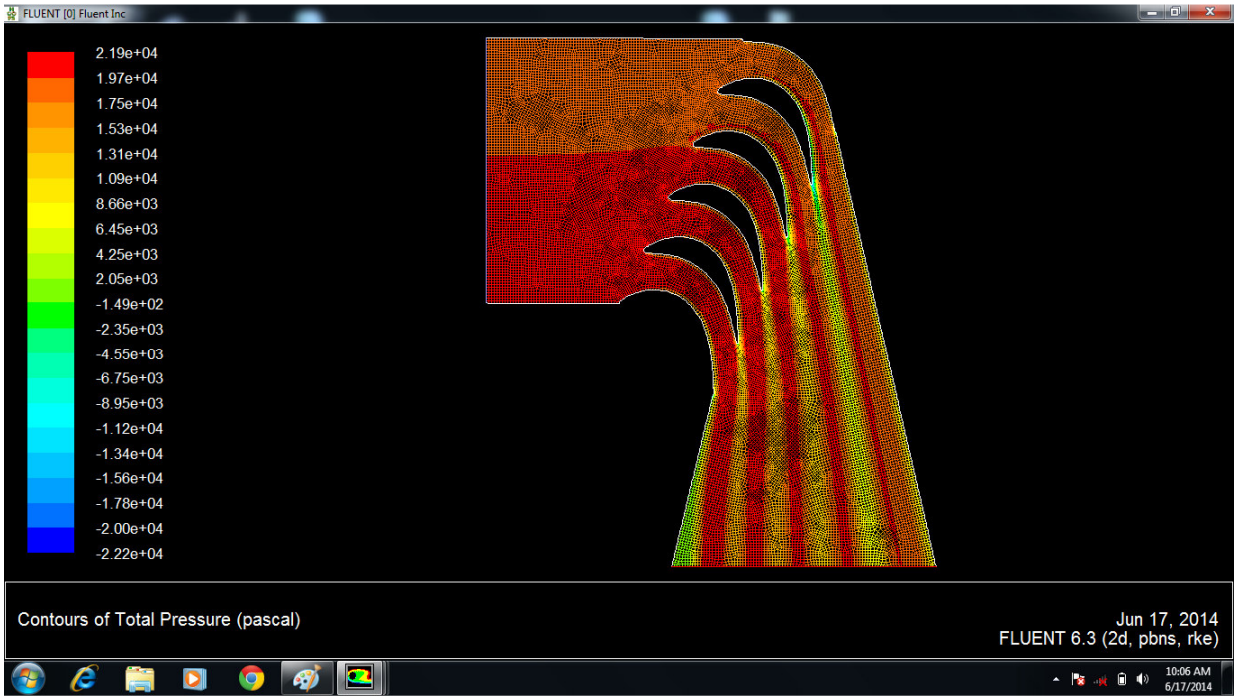

Figure 4.6: Contours of total pressure loss at velocity 150m/s with ash particles of 50µm

In above figures 4.4 to 4.6, percentage of profile loss coefficient is given for a blade span. Percentage of profile loss coefficient is decreasing due to increased velocity. The losses are decreased due to increase in particle diameter in case of ash particle. Some graphs of comparison of different µm particle size with same velocity and different velocities with same micron particle are given below. The graph given below is plotted from the values of table no. 1 provided in the appendix. The results are shown only for the middle blade and effect of side wall effect on flow pattern. The characteristics of wake that is width and height are taken as measurement of effect of particle injection on profile loss. The graphs for various combinations of particle injection are shown in figure 4.7 to 4.13.

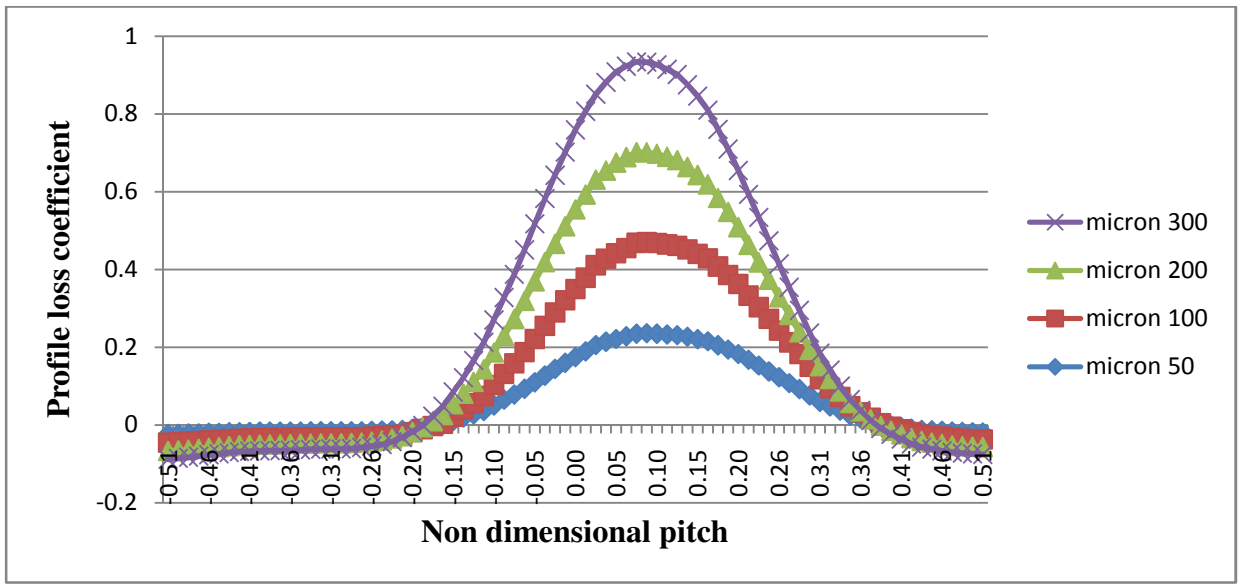

Figure 4.7: Pressure loss coefficient v/s non dimensional pitch for ash particle of different µm at velocity 50m/s

The graph given below is plotted from the values of table no. 2 provided in the appendix:

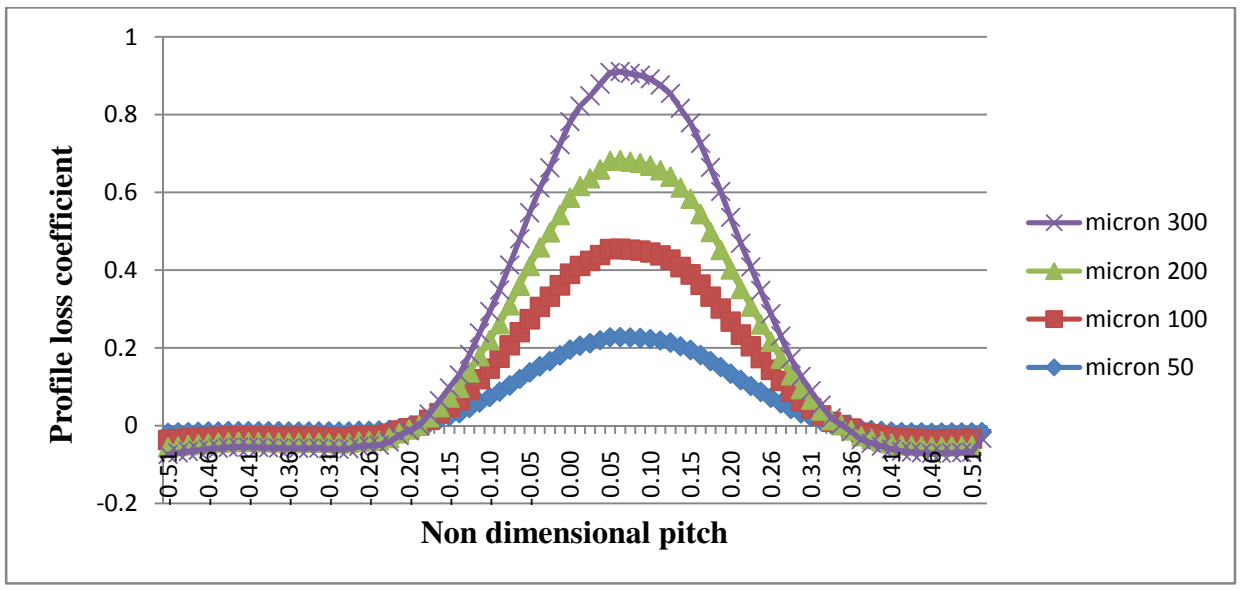

Figure 4.8: Pressure loss coefficient v/s non dimensional pitch for ash particle of different µm at velocity 100m/s

The graph given below is plotted from the values of table no. 3 provided in the appendix:

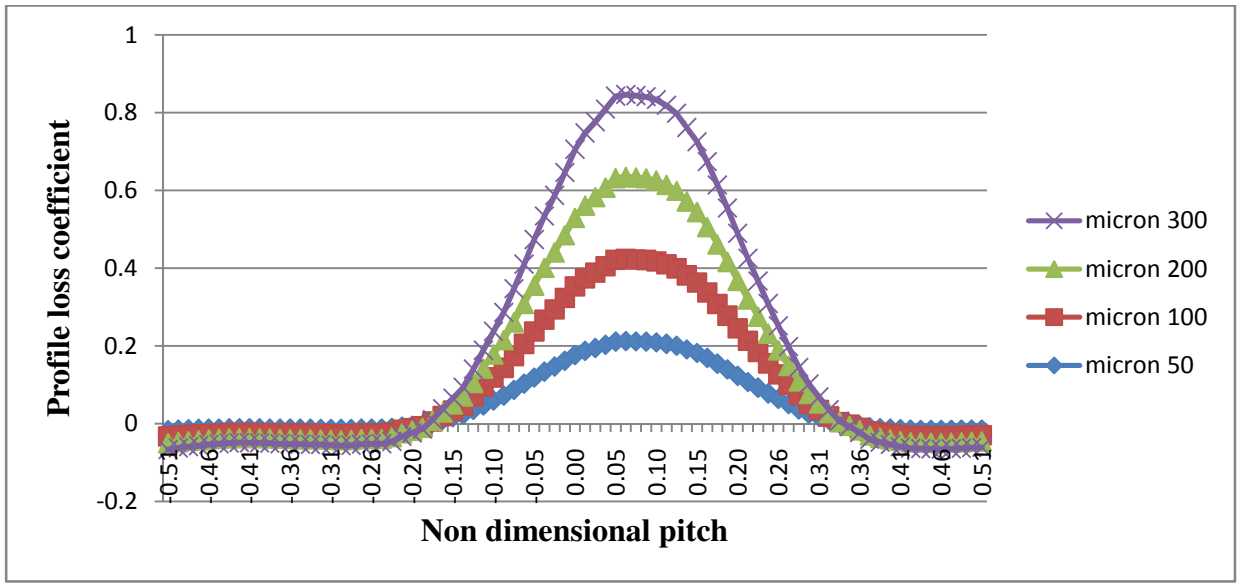

Figure 4.9: Pressure loss coefficient v/s non dimensional pitch for ash particle of different µm at velocity 150m/s

The graph given below is plotted from the values of table no. 1, 2 and 3 provided in the appendix:

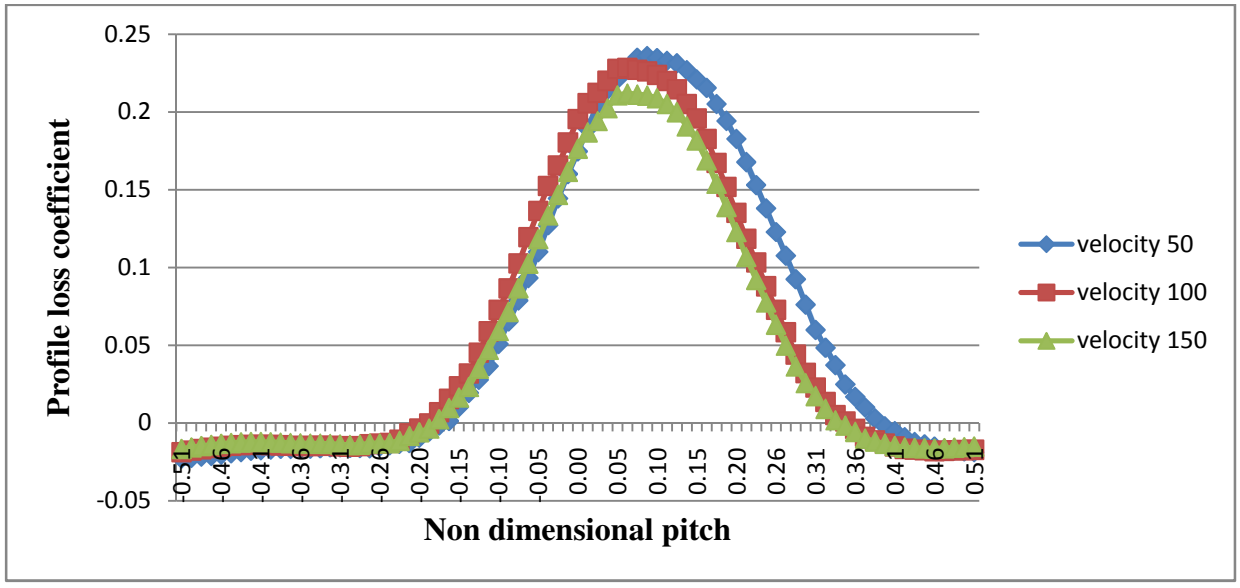

Figure 4.10: Pressure loss coefficient v/s non dimensional pitch at different velocities for ash particle of 50µm

The graph given below is plotted from the values of table no. 1, 2 and 3 provided in the appendix:

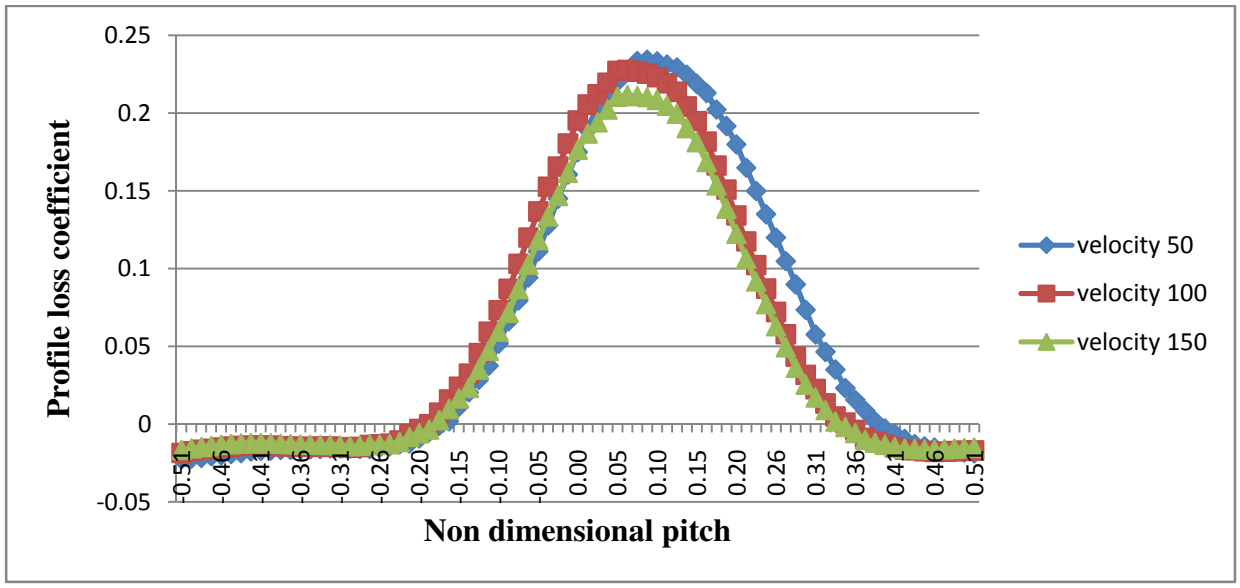

Figure 4.11: Pressure loss coefficient v/s non dimensional pitch at different velocities for ash particle of 100µm

The graph given below is plotted from the values of table no. 1, 2 and 3 provided in the appendix:

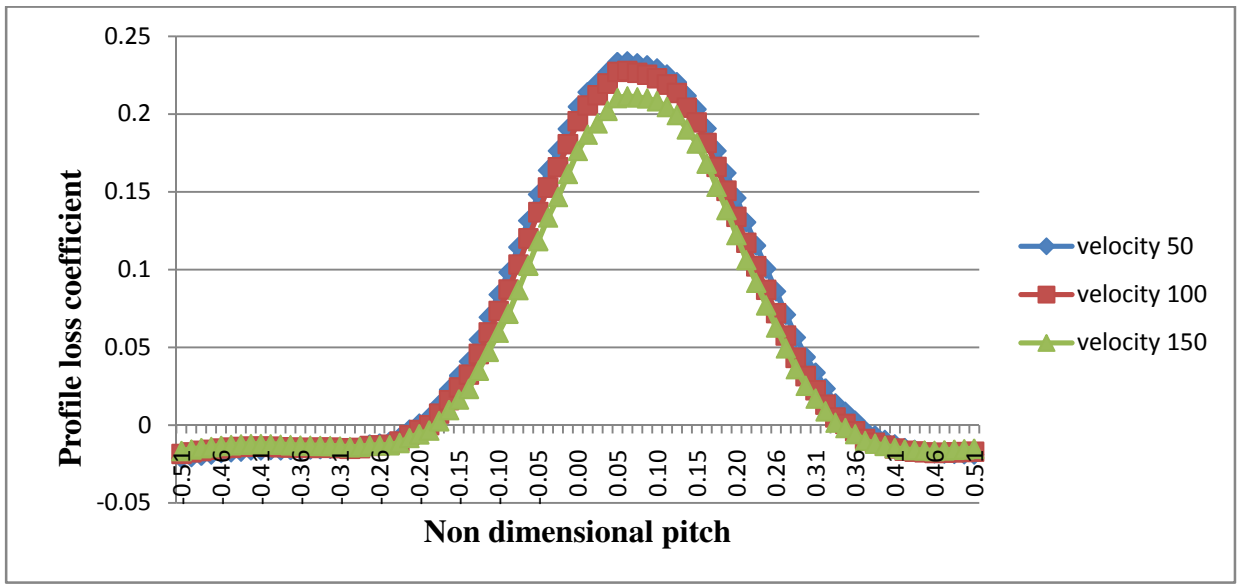

Figure 4.12: Pressure loss coefficient v/s non dimensional pitch at different velocities for ash particle of 200µm

The graph given below is plotted from the values of table no. 1, 2 and 3 provided in the appendix:

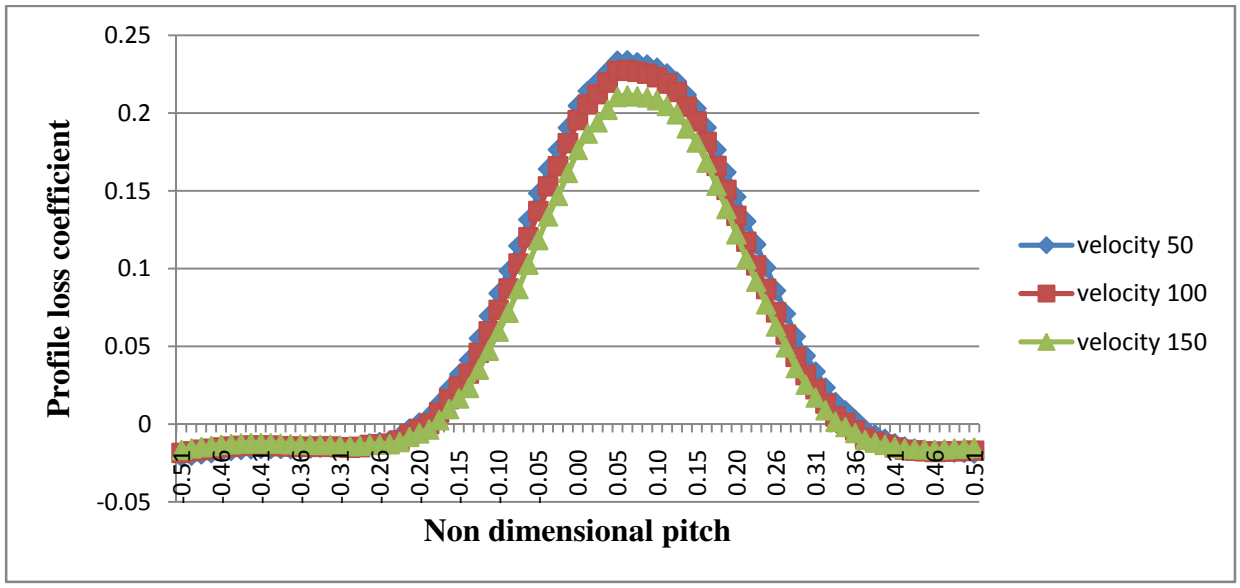

Figure 4.13: Pressure loss coefficient v/s non dimensional pitch at different velocities for ash particle of 300µm

After study of each case we found that the total pressure loss decreases with increase in velocity for a blade span and the wakes are shifted to suction side of blade surface due to increasing velocity. As per calculation, percentage of profile loss coefficient at velocity 50m/s with 50µm particle is 6.25 % and when we increase the µm size up to 300µm then the value of profile loss coefficient is 6.24% it shows that the profile loss is decreasing with increase in particle diameter in case of ash particles. At velocity 100m/s profile loss is 5.75% with 50µm particles of ash. At velocity 150m/s profile loss is 5.13% and 17.92% decrease due to increased velocity from 50m/s to 150m/s at 50µm particles. From this it can be concluded that the effect of ash particle is not significant on profile loss coefficient or on the performance of blade, however after sticking of these ash particle in this causing change in profile roughness effect significantly after a period of time.

4.2.2 For steel particles

From the total pressure contours we found that there is negligible difference as shown in 4.14 to 4.16, when we increase steel particle diameter from 50µm to 300µm at velocity 50m/s, 100m/s and 150m/s. The changes in losses are seen very minute in profile loss coefficient. As we discussed earlier, the value of profile loss coefficient is decrease by increasing velocity at the same µm particle. Flow patterns are shown in figure 4.14 to 4.16.

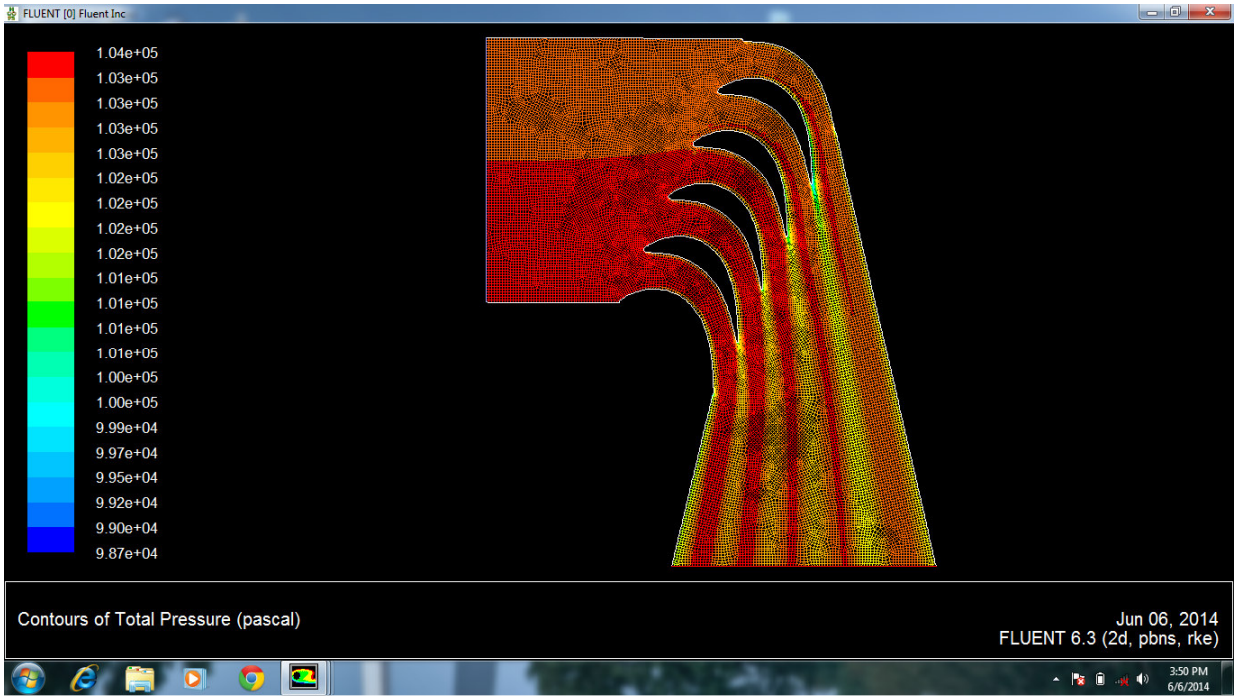

Figure 4.14: Contours of total pressure loss at velocity 50m/s with steel particles of 50µm

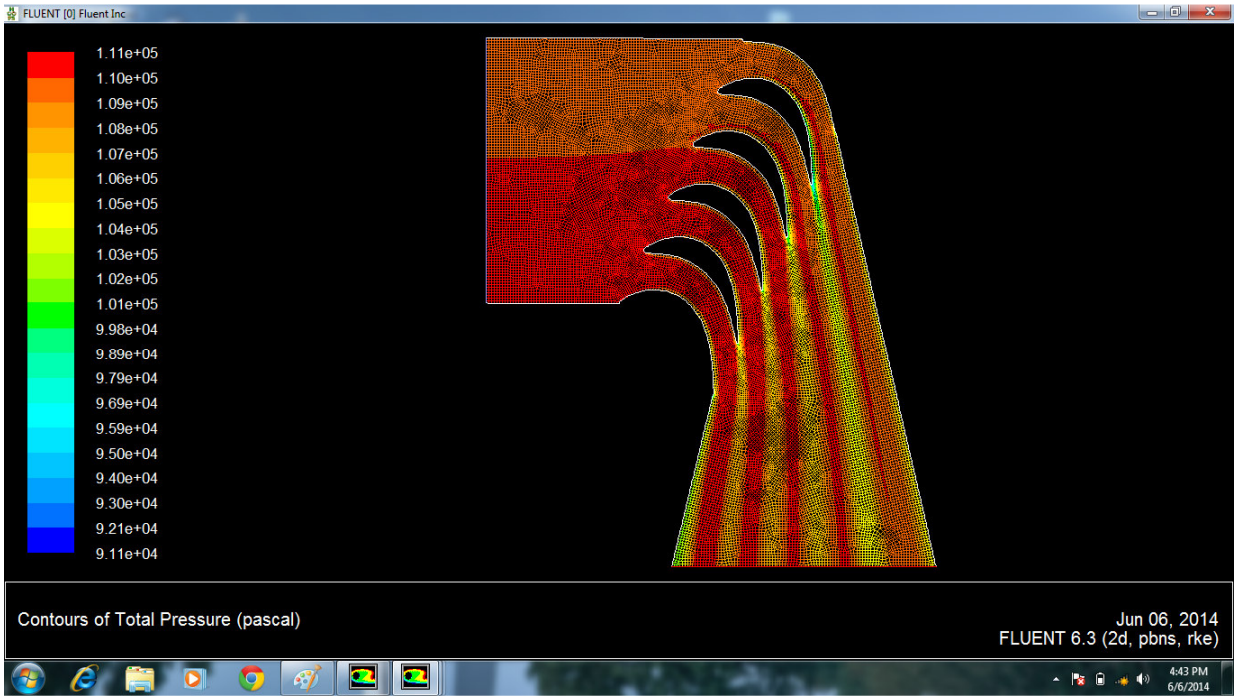

Figure 4.15: Contours of total pressure loss at velocity 100m/s with steel particles of 50µm

Figure 4.16: Contours of total pressure loss at velocity 150m/s with steel particles of 50µm

The graph given below is plotted from the values of table no. 4 provided in the appendix:

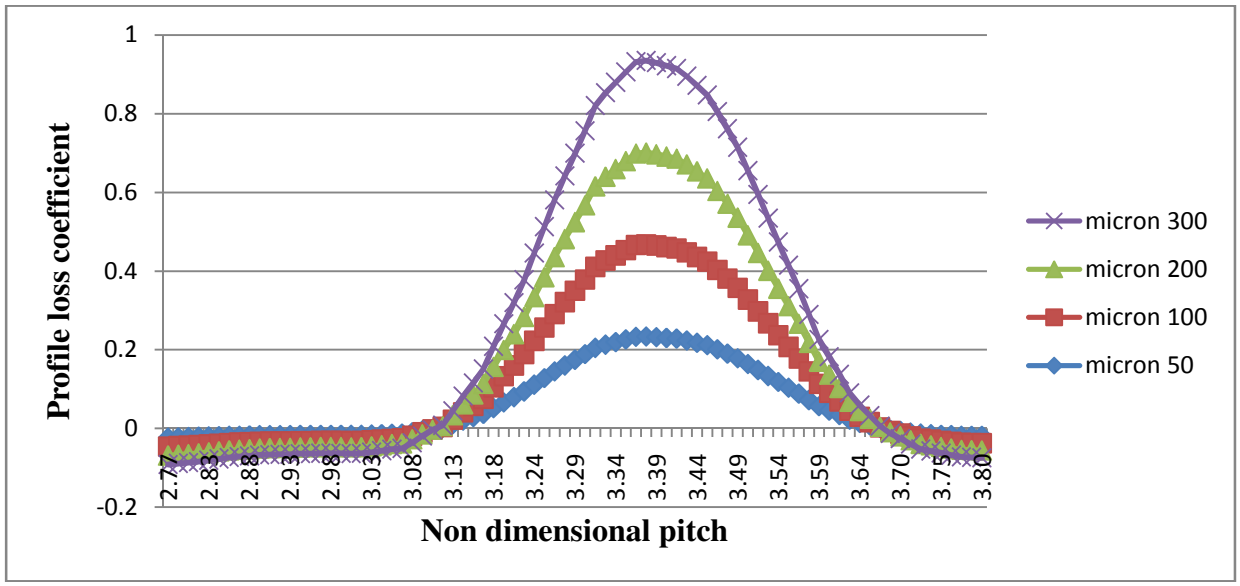

Figure 4.17: Profile loss coefficient v/s non dimensional pitch with steel particles of different µm at velocity 50m/s

The graph given below is plotted from the values of table no. 5 provided in the appendix:

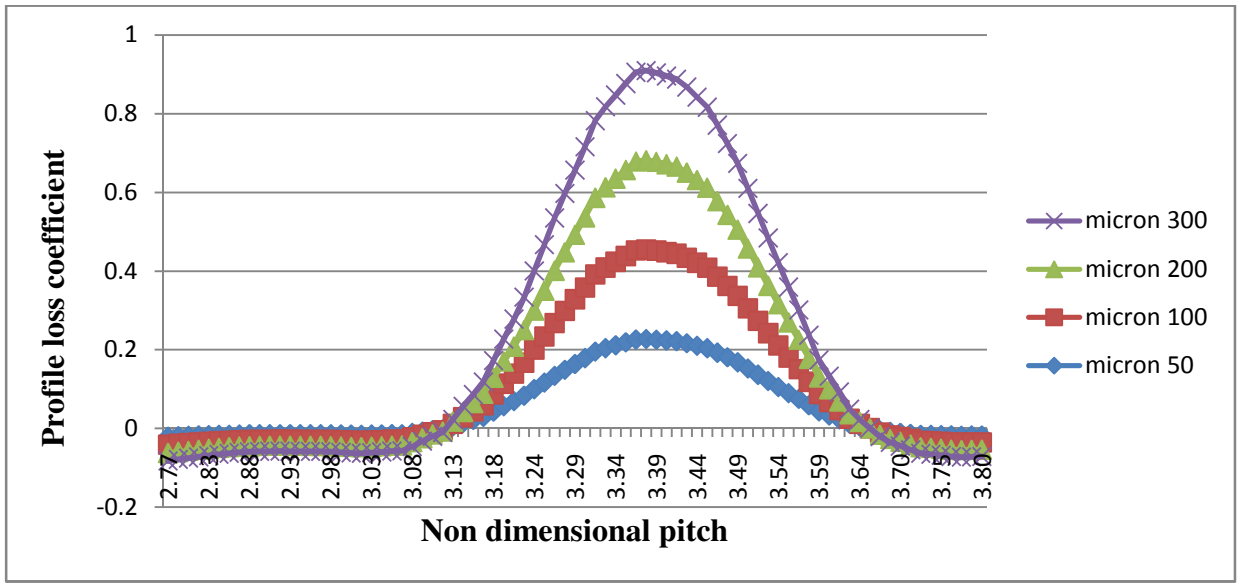

Figure 4.18: Profile loss coefficient v/s non dimensional pitch with steel particles of different µm at velocity 100m/s

The graph given below is plotted from the values of table no. 6 provided in the appendix:

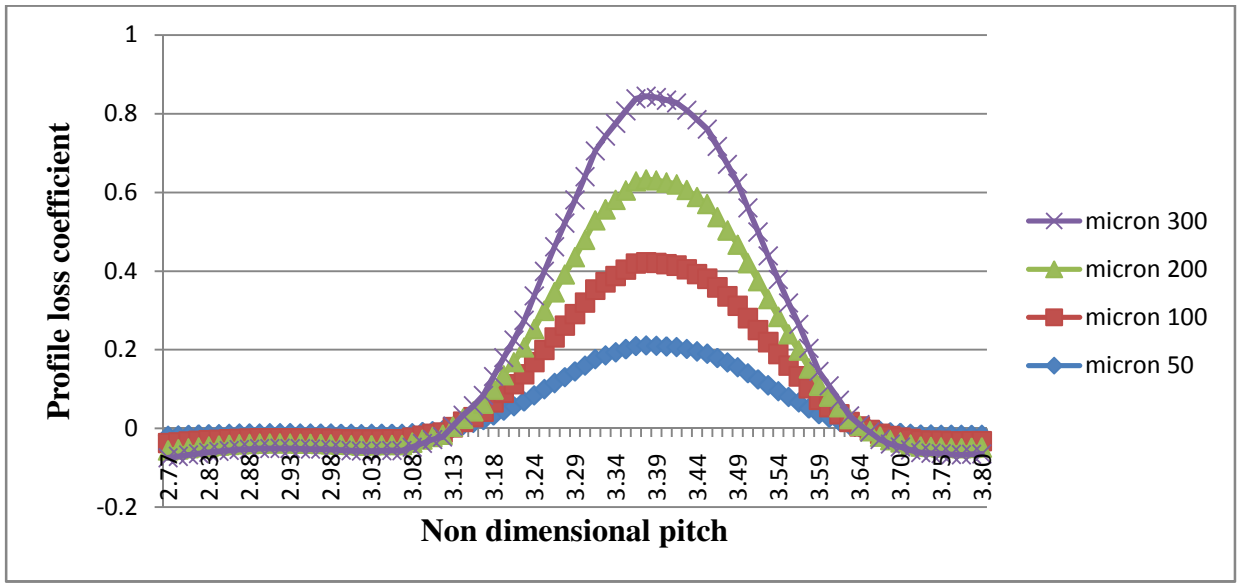

Figure 4.19: Profile loss coefficient v/s non dimensional pitch with steel particles of different µm at velocity 150m/s

The graph given below is plotted from the values of table no. 4,5and 6 provided in the appendix:

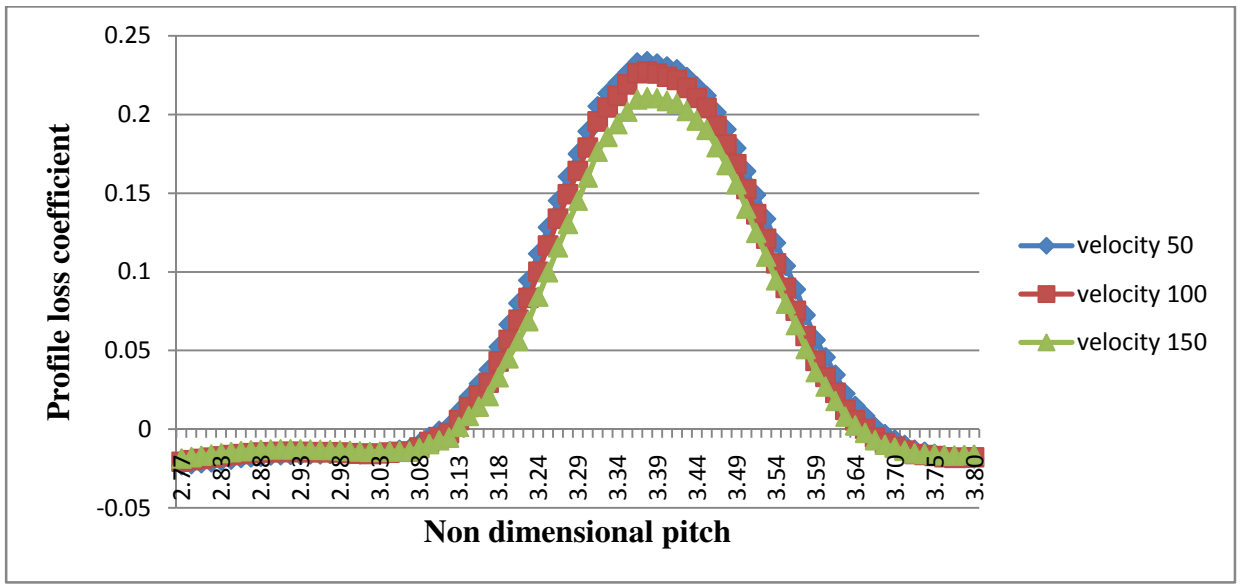

Figure 4.20: Profile loss coefficient v/s non dimensional pitch with 50µm steel particles at different velocities

The graph given below is plotted from the values of table no. 4,5 and 6 provided in the appendix:

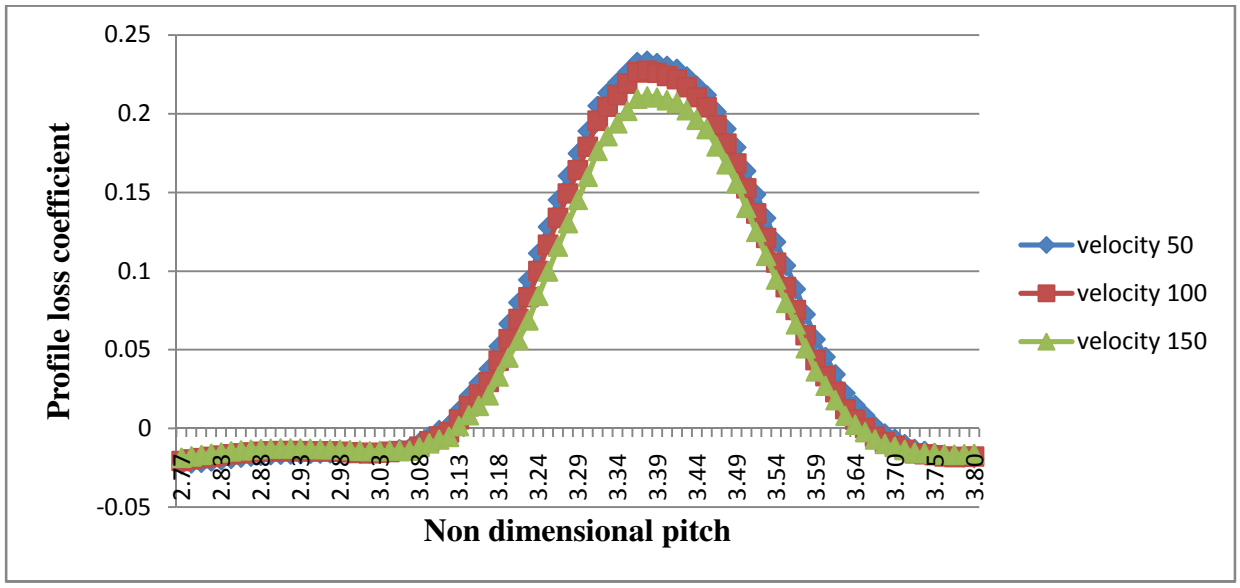

Figure 4.21: Profile loss coefficient v/s non dimensional pitch with 100µm steel particles at different velocities

The graph given below is plotted from the values of table no. 4,5 and 6 provided in the appendix:

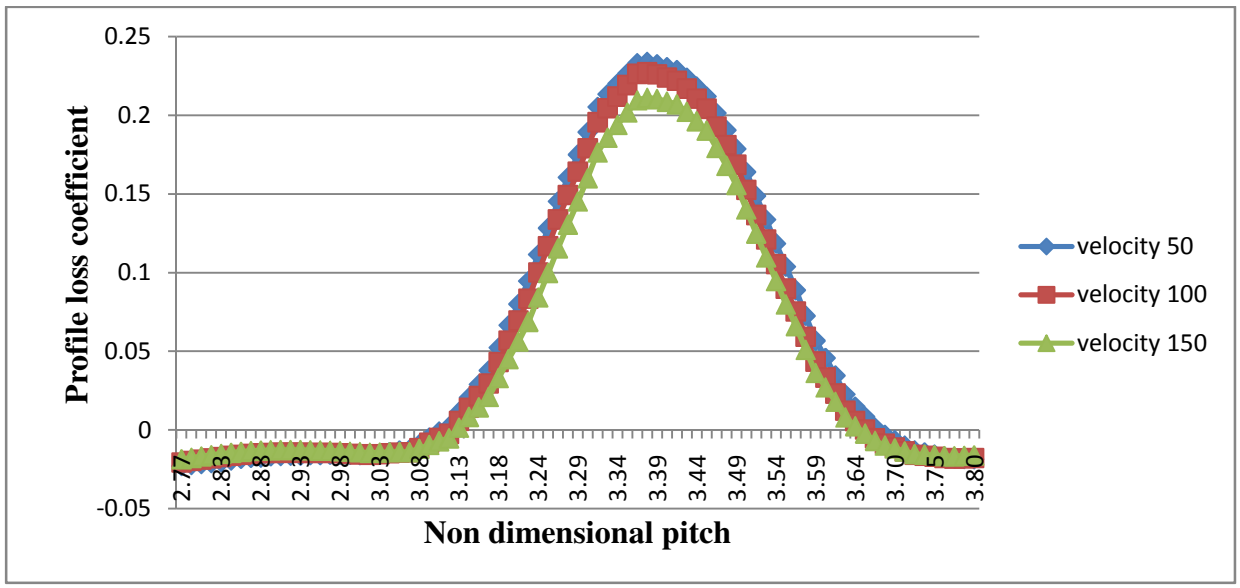

Figure 4.22: Profile loss coefficient v/s non dimensional pitch with 200µm steel particles at different velocities

The graph given below is plotted from the values of table no. 4,5and 6 provided in the appendix:

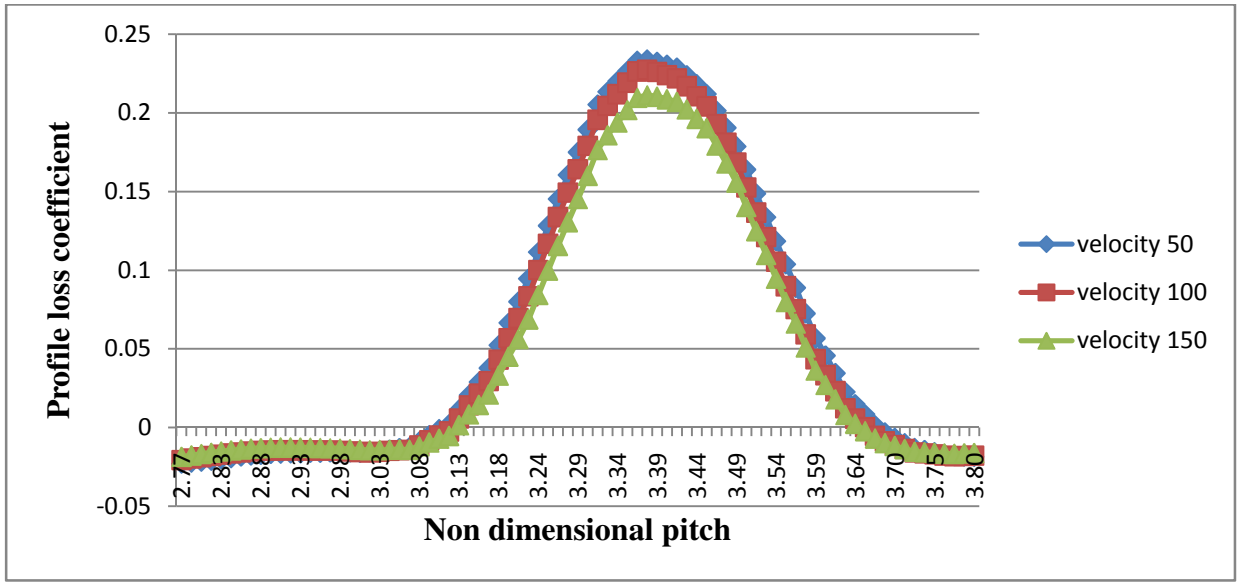

Figure 4.23: Profile loss coefficient v/s non dimensional pitch with 300µm steel particles at different velocities

From the calculations, It has been found that the value of profile loss coefficient is 6.23% at velocity 50m/s with steel particles of 50µm. The value of profile loss coefficient is increases when we increased the particle diameter from 50µm to 300µm at velocity 50m/s. At velocity 100m/s value of losses is 5.72% with 50µm particles and it increases when its particle size is increases from 50µm to 300µm. At velocity 150m/s losses are 5.12% with particle of 50µm and it increases by increasing particle size 50µm to 300µm. Due to injection of 50µm steel particles 17.89% losses are decrease by increasing the velocity from 50m/s to 150m/s.

4.2.3 For water particles:

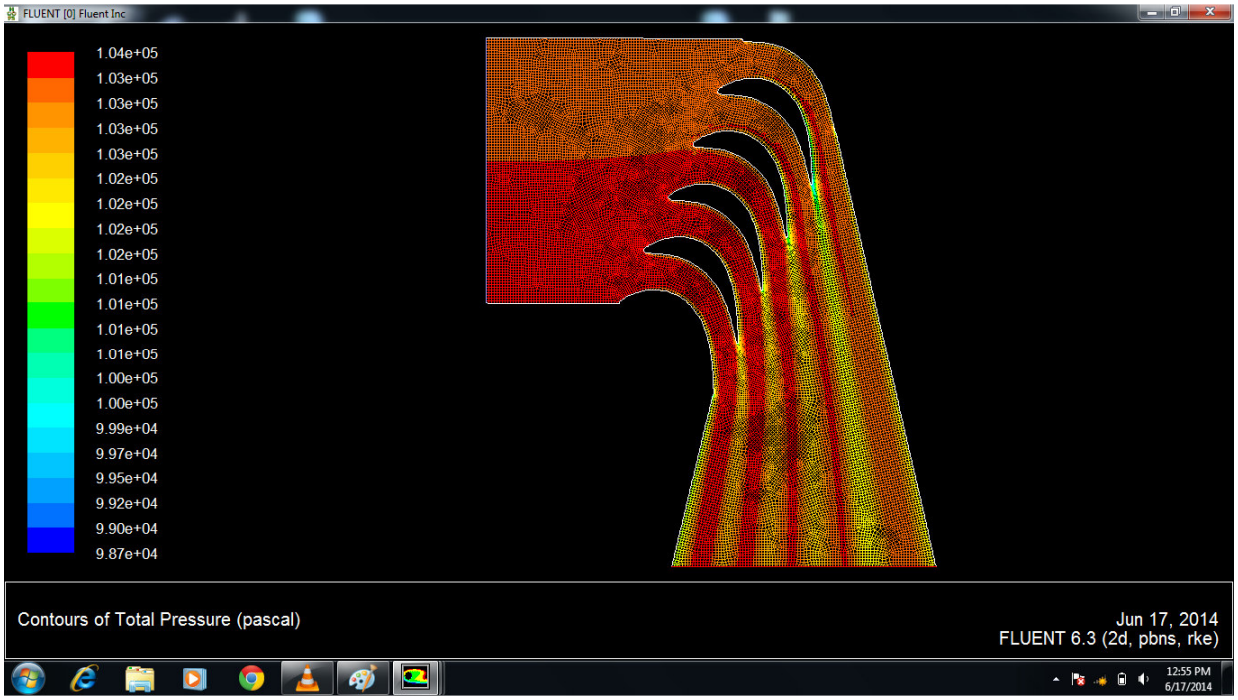

Figure 4.24: Contours of total pressure loss at velocity 50m/s with water particles of 50µm

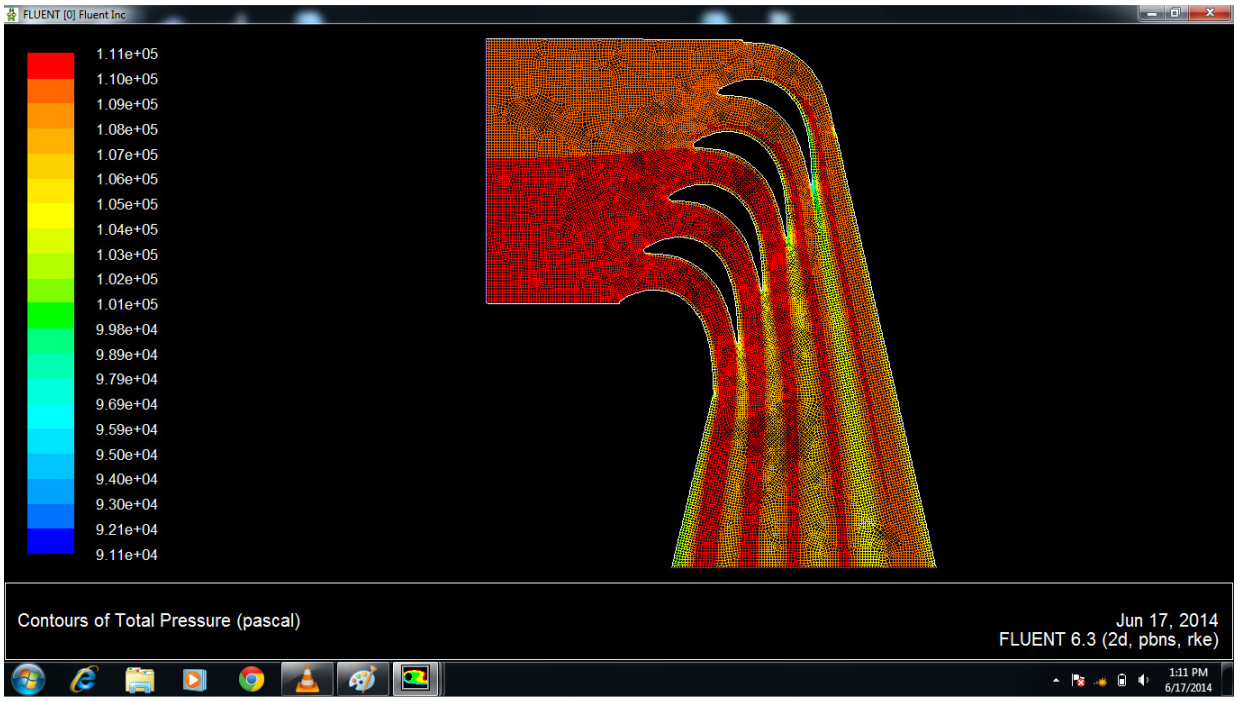

Figure 4.25: Contours of total pressure loss at velocity 100m/s with water particles of 50µm

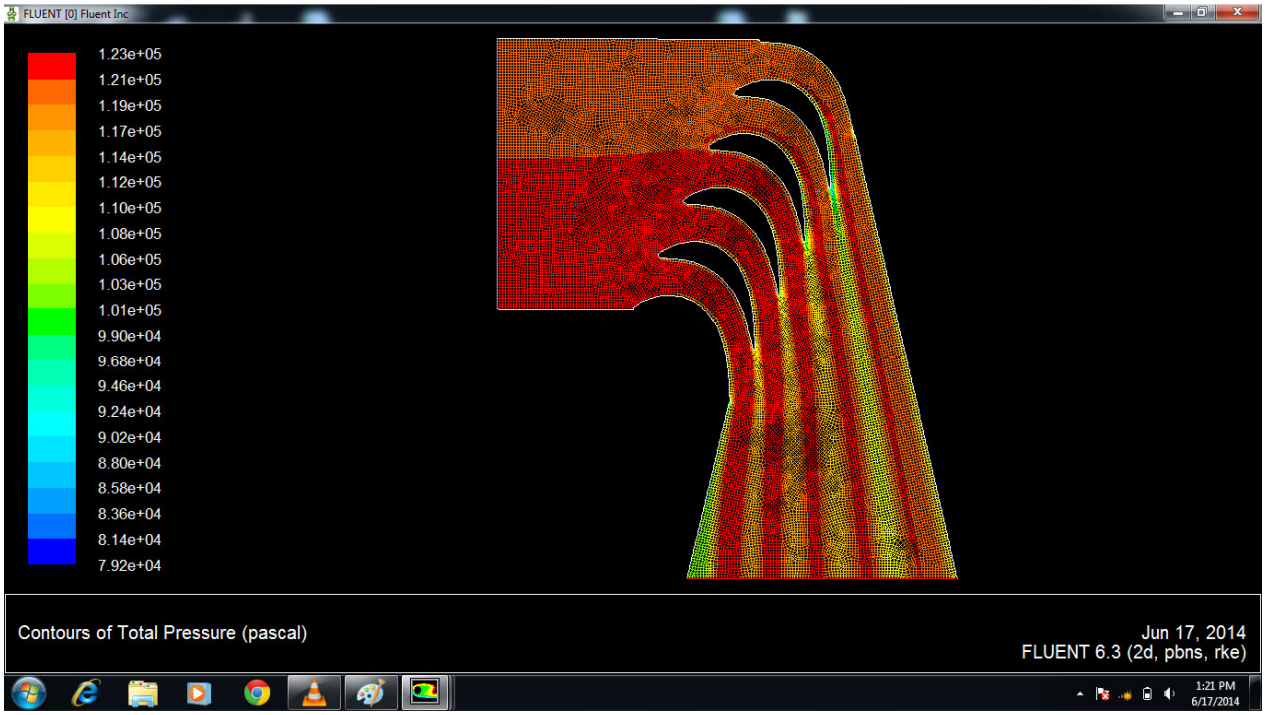

Figure 4.26: Contours of total pressure loss at velocity 150m/s with water particles of 50µm

The graph given below is plotted from the values of table no. 7 provided in the appendix:

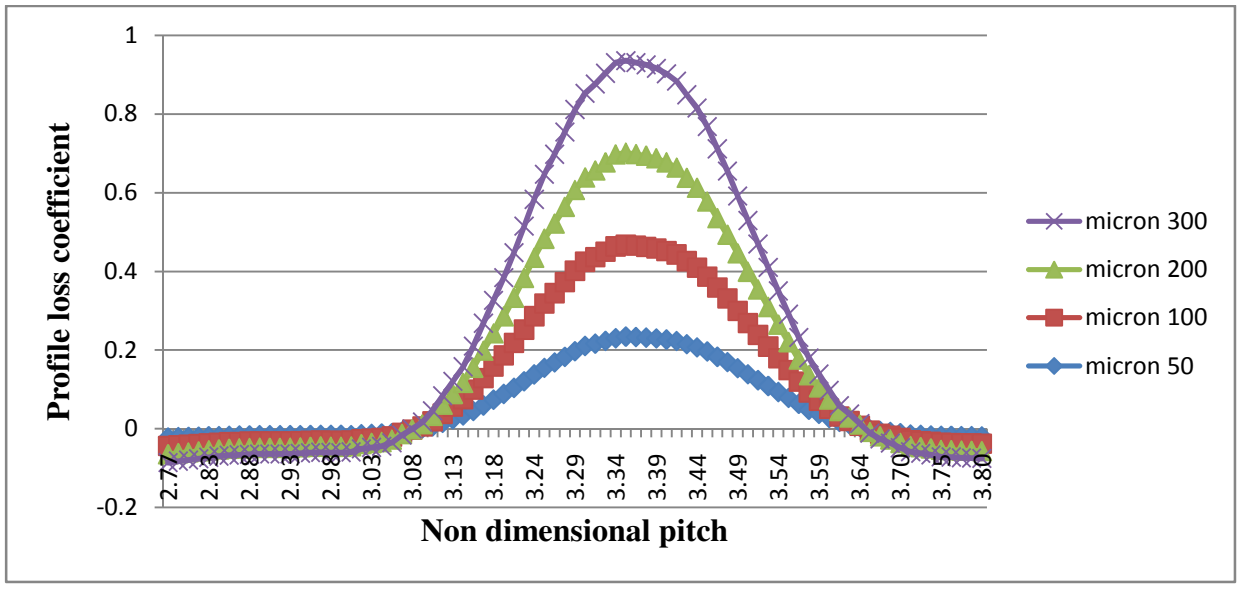

Figure 4.27 Profile loss coefficient v/s non dimensional pitch with water particles of different µm at velocity 50m/s

The graph given below is plotted from the values of table no. 8 provided in the appendix:

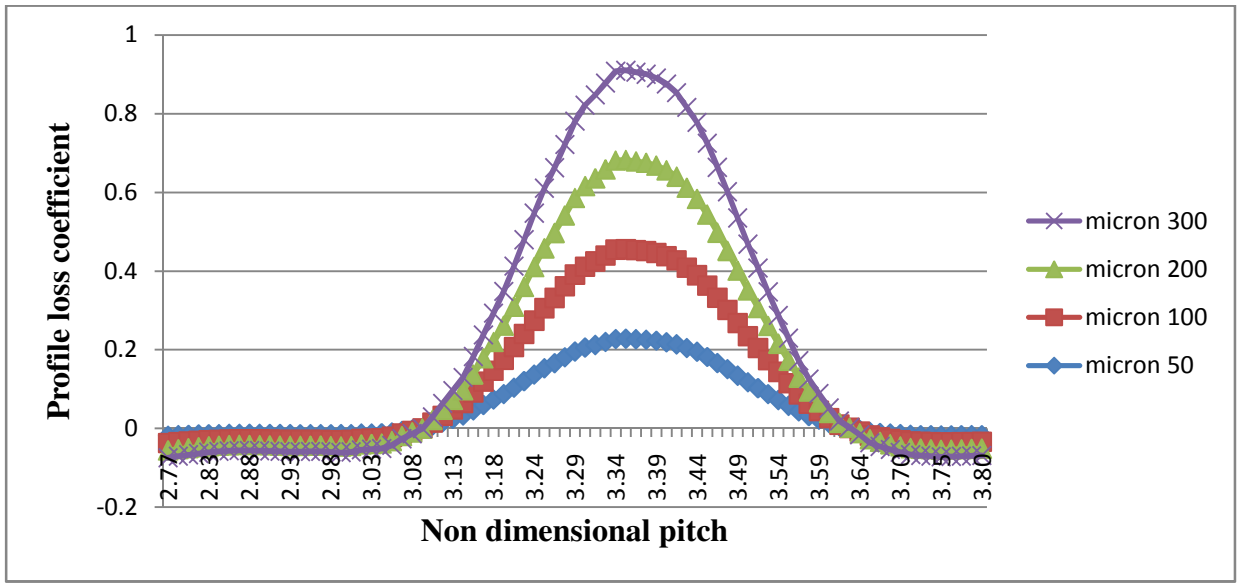

Figure 4.28: Profile loss coefficient v/s non dimensional pitch with water particles of different µm at velocity 100m/s

The graph given below is plotted from the values of table no. 9 provided in the appendix:

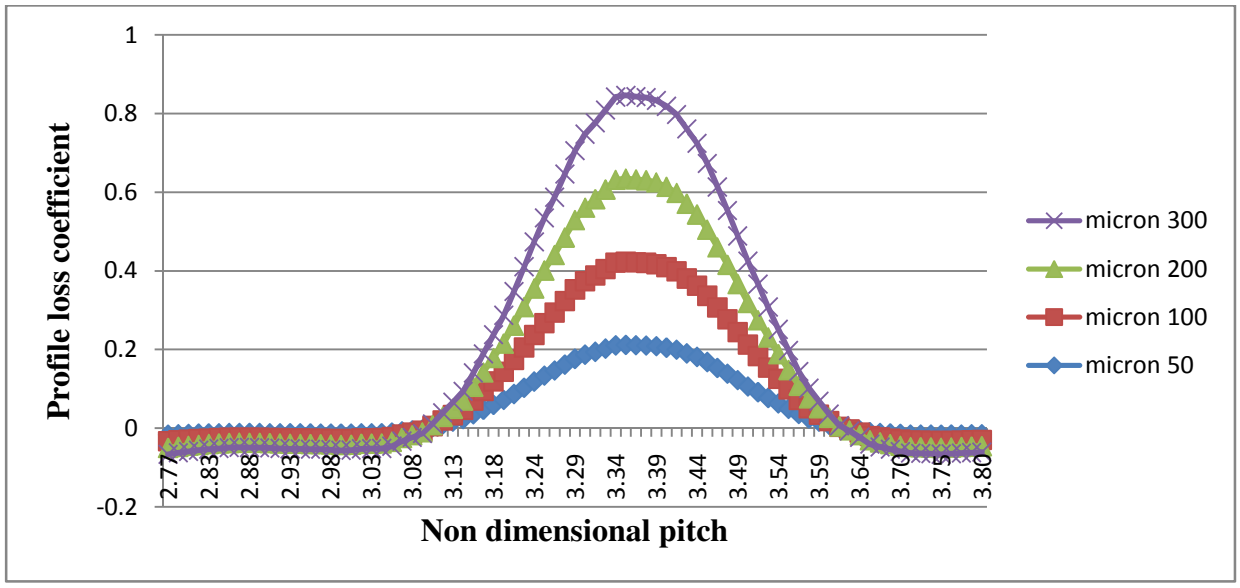

Figure 4.29: Profile loss coefficient v/s non dimensional pitch with water particles of different µm at velocity 150m/s

The graph given below is plotted from the values of table no. 7,8 and 9 provided in the appendix:

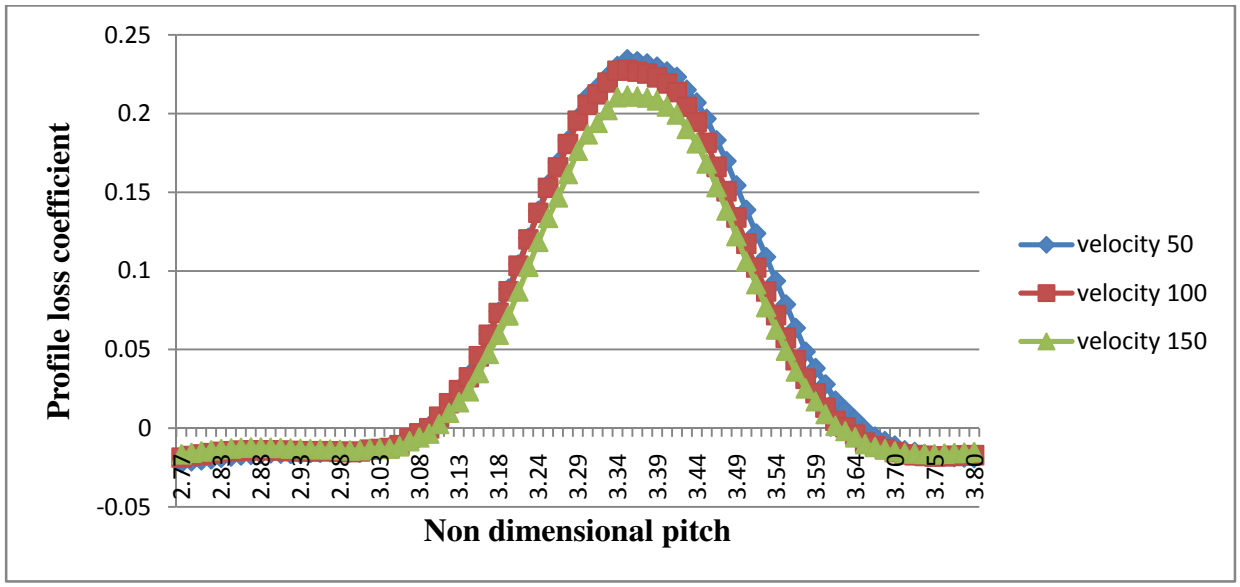

Figure 4.30: Profile loss coefficient v/s non dimensional pitch with 50µm water particles at different velocities

The graph given below is plotted from the values of table no. 7,8 and 9 provided in the appendix

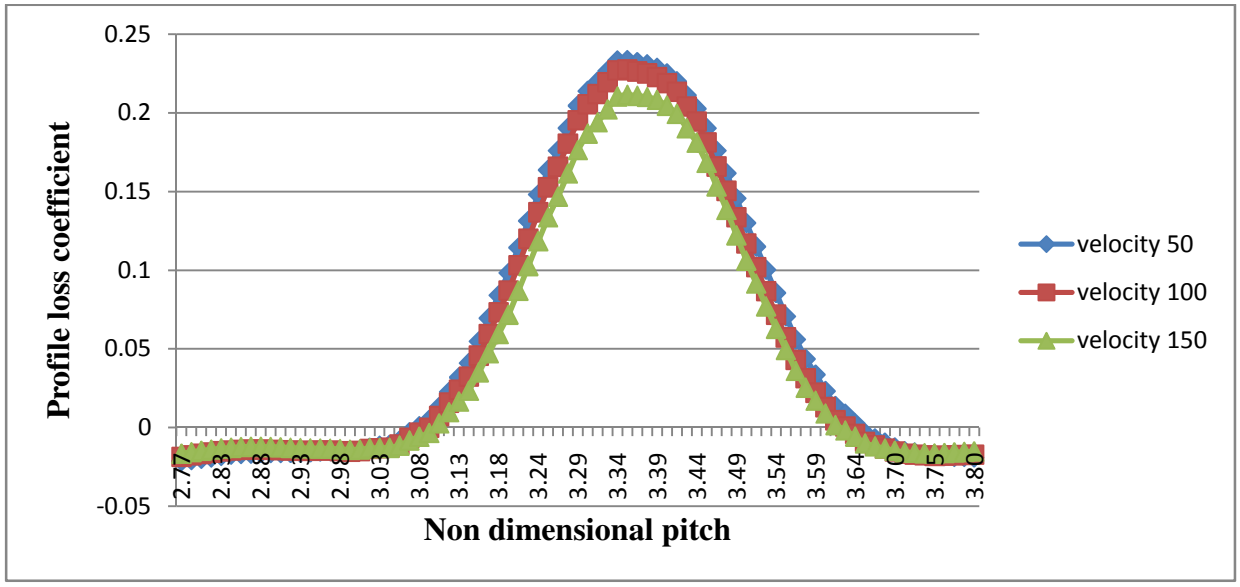

Figure 4.31: Profile loss coefficient v/s non dimensional pitch with 100µm water particles at different velocities

The graph given below is plotted from the values of table no. 7,8 and 9 provided in the appendix:

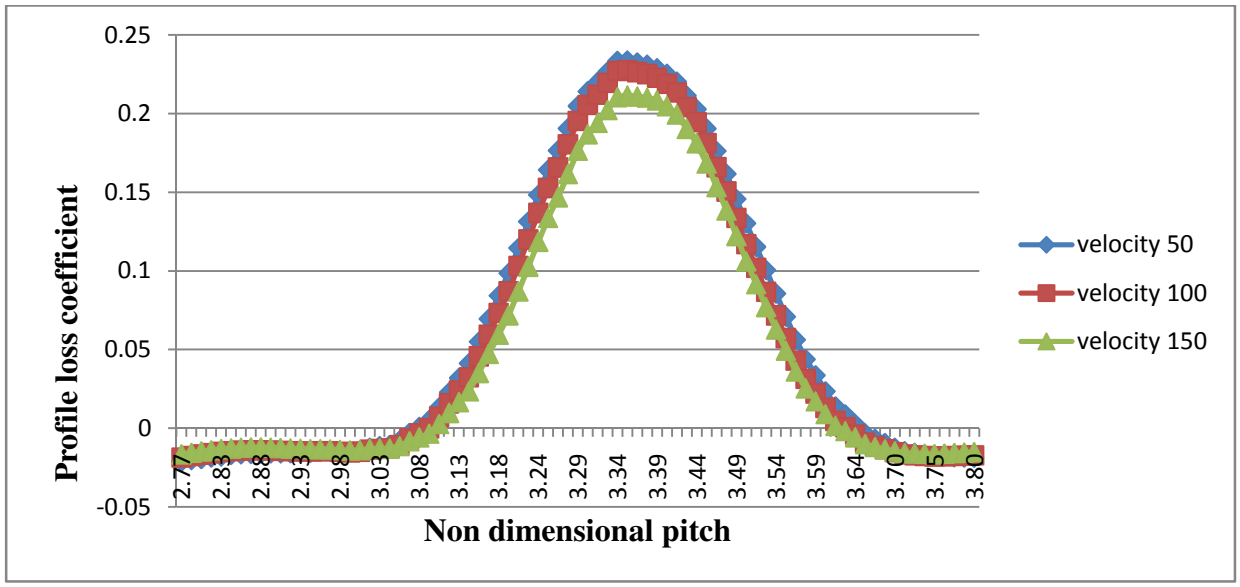

Figure 4.32: Profile loss coefficient v/s non dimensional pitch with 200µm water particles at different velocities

The graph given below is plotted from the values of table no. 7,8 and 9 provided in the appendix:

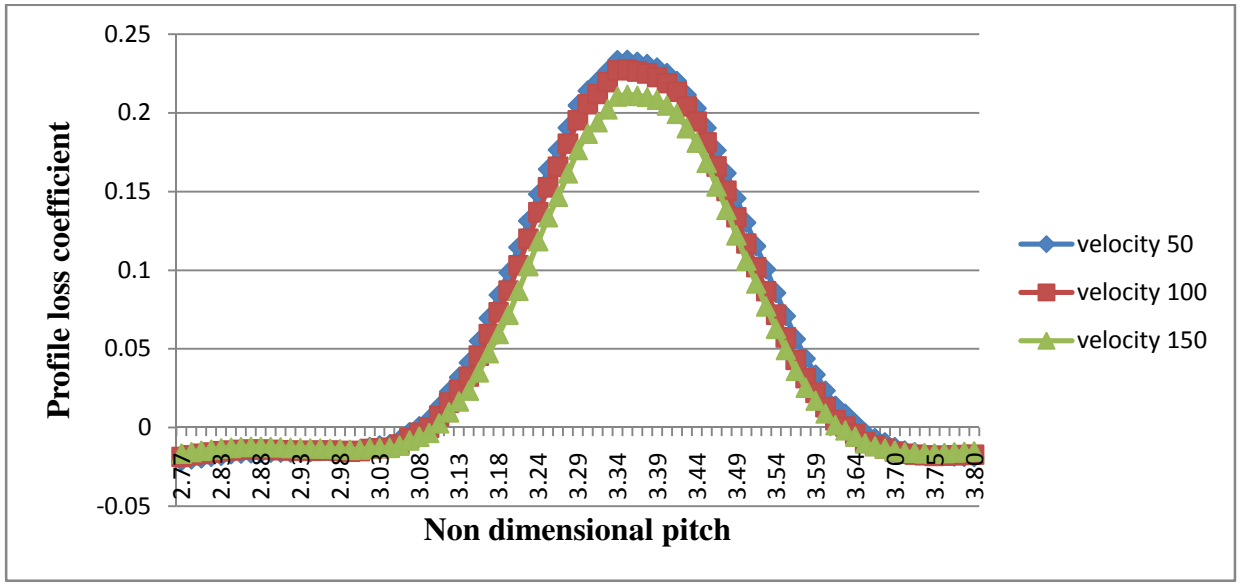

Figure 4.33: Profile loss coefficient v/s non dimensional pitch with 300µm water particles at different velocities

From the calculations, It is found that profile loss at 50m/s with water particles of 50µm is 6.18% and it increases when the particle size increases from 50µm to 300µm. At velocity 100m/s losses are 5.73% and with increase in diameter up to 300µm.When velocity increases from 50m/s to 150m/s with injection of water particles of 50µm losses are decreased by 17.15%. The effect of particle size of water is not significant on profile loss coefficient.

4.3 Analysis of effected length of blade due to hitting of particles:

4.3.1 Ash particles:

With the help of fluent, The effected length of blade due to particle injection is analyzed, basically during the flow of working fluid, the particles which are heavier and larger in diameter are hitting on the outer most part of the suction surface of the blade and the rest of the particle will strike on the pressure surface of the blade and almost full of the blade is effected by the particles, as this practically seen in the blade. The blade shape is also getting damaged because leading edge and trailing edge is fully affected by the particles. The lighter particle does not create the problem of erosion but they get stick with the blades and create the problem of fouling on the blades. The fouling effect can be removed by cleaning and polishing of the blade or some of the fouling losses are recoverable but the losses due to erosion are not recoverable. The strength of blade and overall efficiency of turbine get reduced due to these losses. Particle traces with the particle residence time describes the particle trajectories here the particles are hitting on the leading edge and after hitting it goes parallel to the blade length when its diameter increases, the effect of particles is increasing in the direction of suction surface. Then the chances of deposition are more in low velocity and in minimum diameter particle due to less effect of inertia. The effect of Reynolds number is same through the entire cascade but the Reynolds number goes increasing when it strikes on the pressure and suction surfaces. Particle trajectories for different simulation are shown in the figure 4.34 to 4.36 given below and some of them are not shown here, they are also following the same pattern:

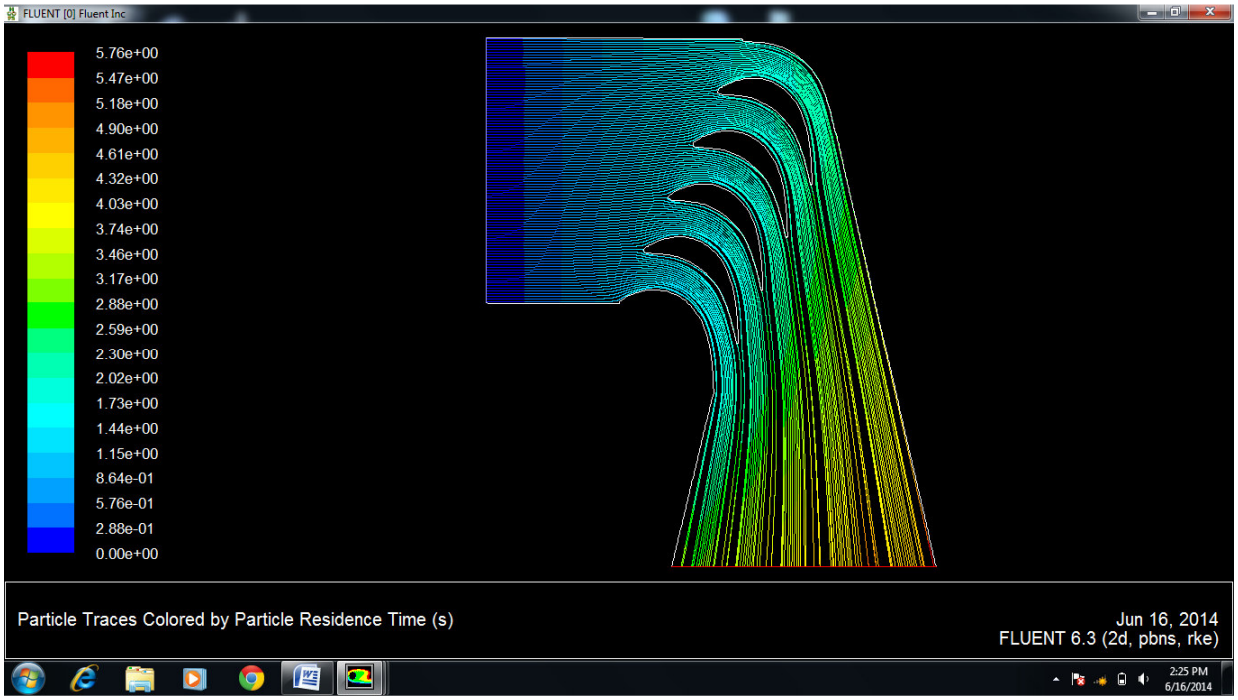

Figure 4.34: Trajectories of particle with residence time at velocity 50m/s with ash particles of 50µm

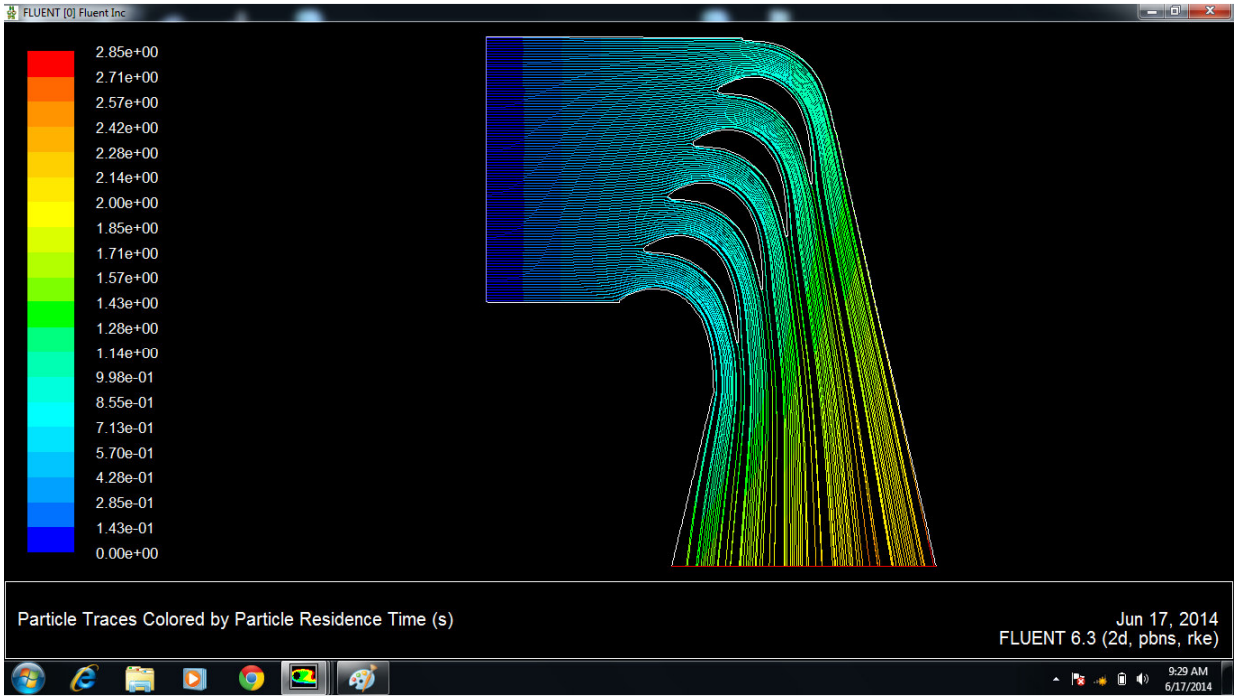

Figure 4.35: Trajectories of particle with particle residence time at velocity 100m/s with ash particles of 50µm

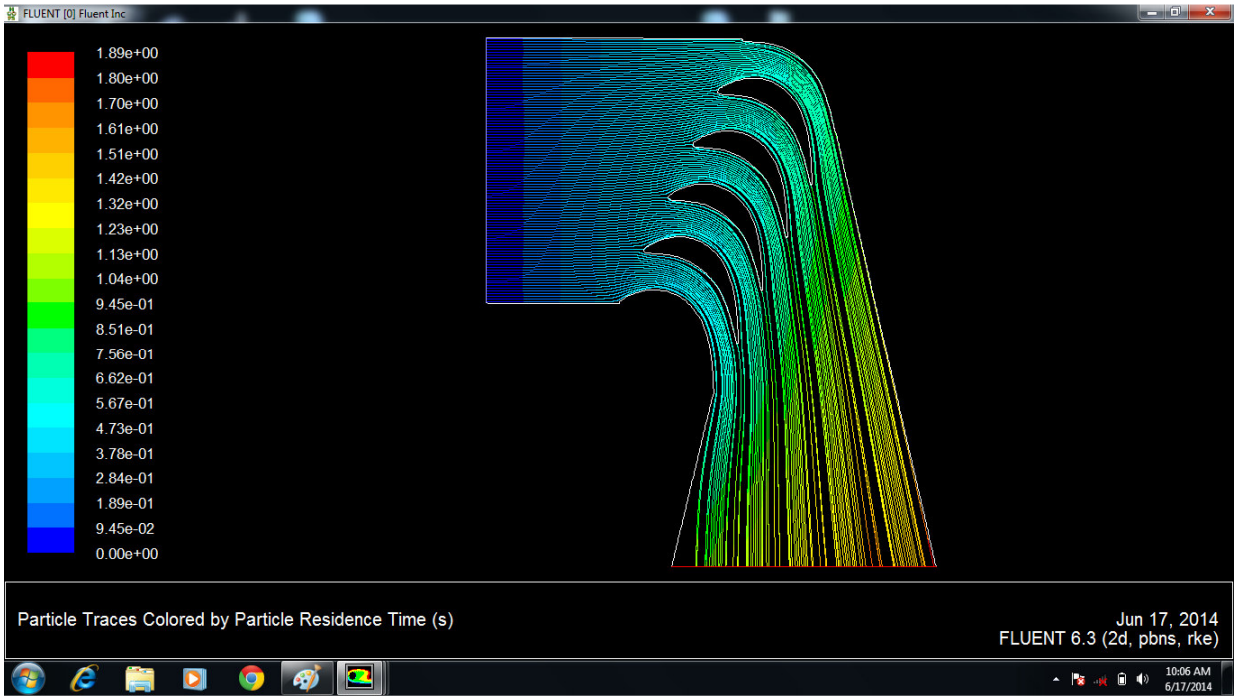

Figure 4.36: Trajectories of particle with particle residence time at velocity 150m/s with ash particles of 50µm

It is seen from the above figures (from 4.34 to 4.36) that the leading edge and trailing edge is being fully hit by the particles. Starting length of Suction surface is effected up to 10 to 12% of the blade length and pressure surface is affected up to 65 to 70% from mid to end. And the effected length is increasing by increasing particle diameter. The figure 4.34 and 4.36 given below shows the effected length of suction surface and pressure surface of blade with increase in particle diameter. The graph given below is plotted from the values of table no 10 provided in the appendix:

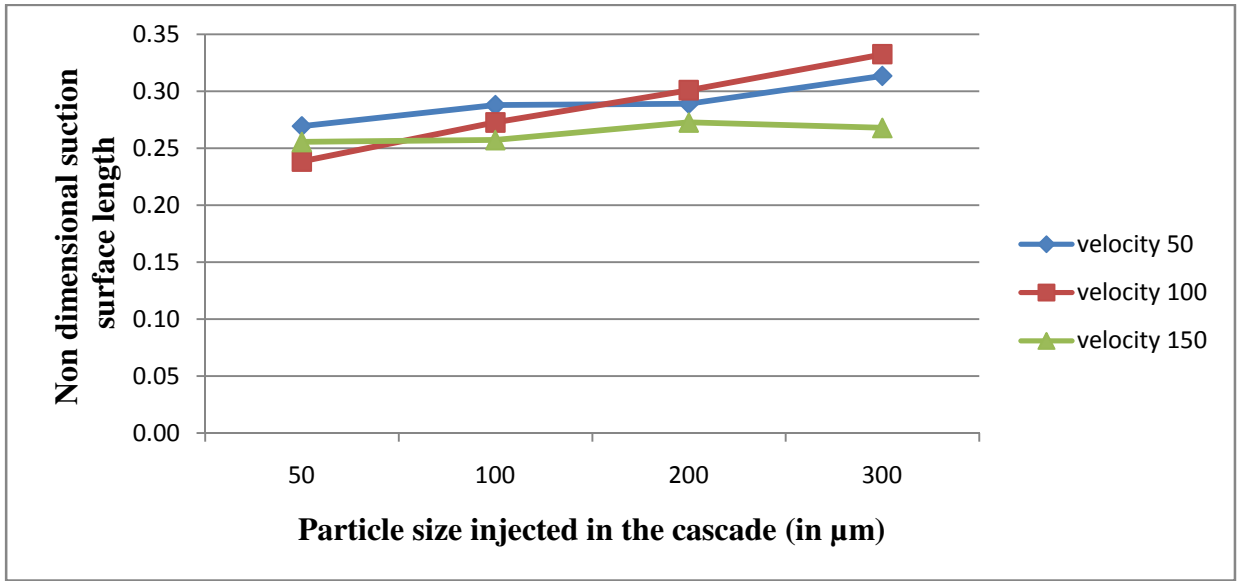

Figure 4.37: Affected suction surface of blade v/s particle size injected at different velocities of ash particles

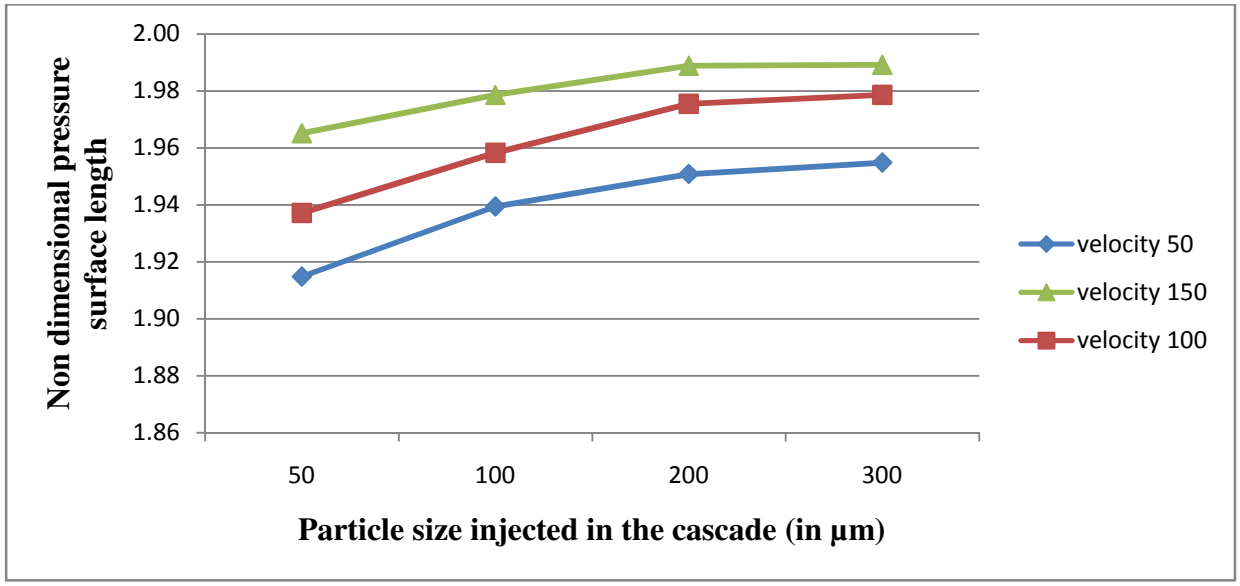

Figure 4.38: Affected pressure surface of blade v/s particle size injected at different velocities of ash particles

4.3.2 Steel particles:

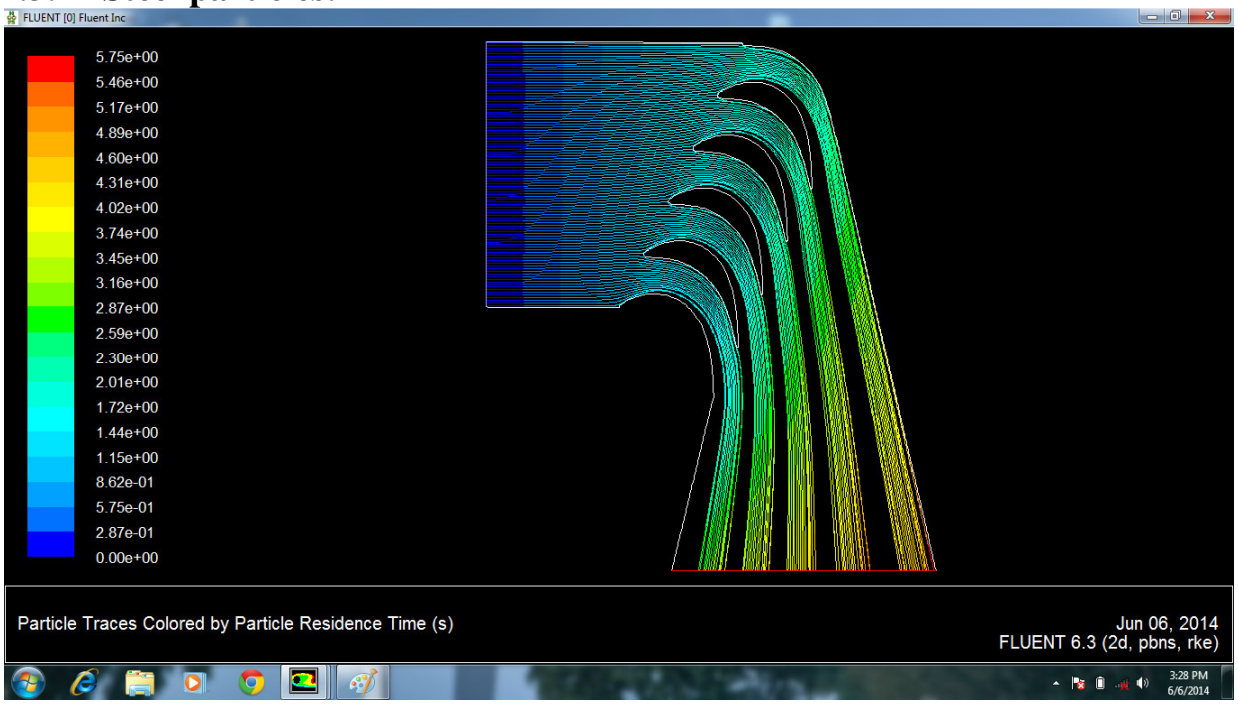

Figure 4.39: Trajectories of particle with particle residence time at velocity 50m/s with steel particles of 50µm

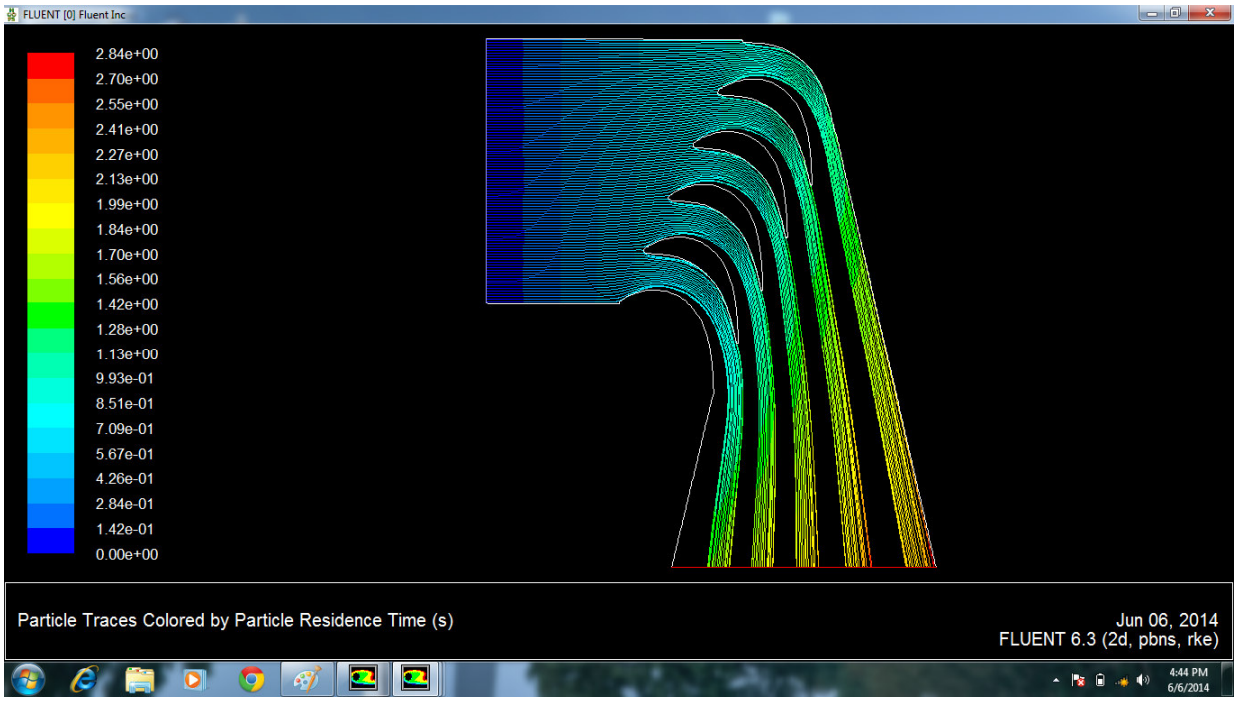

Figure 4.40: Trajectories of particle with particle residence time at velocity 100m/s with steel particles of 50µm

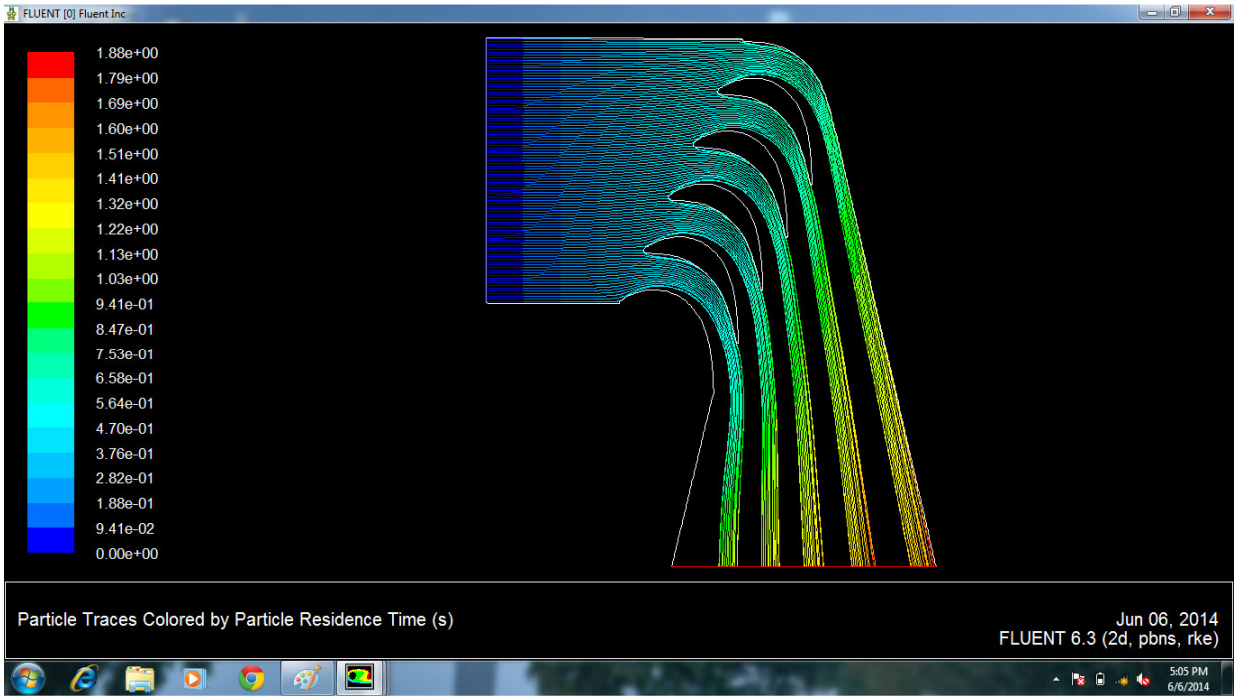

Figure 4.41: Trajectories of particle with particle residence time at velocity 150m/s with steel particles of 50µm

The graph given below is plotted from the values of table no 11 provided in the appendix:

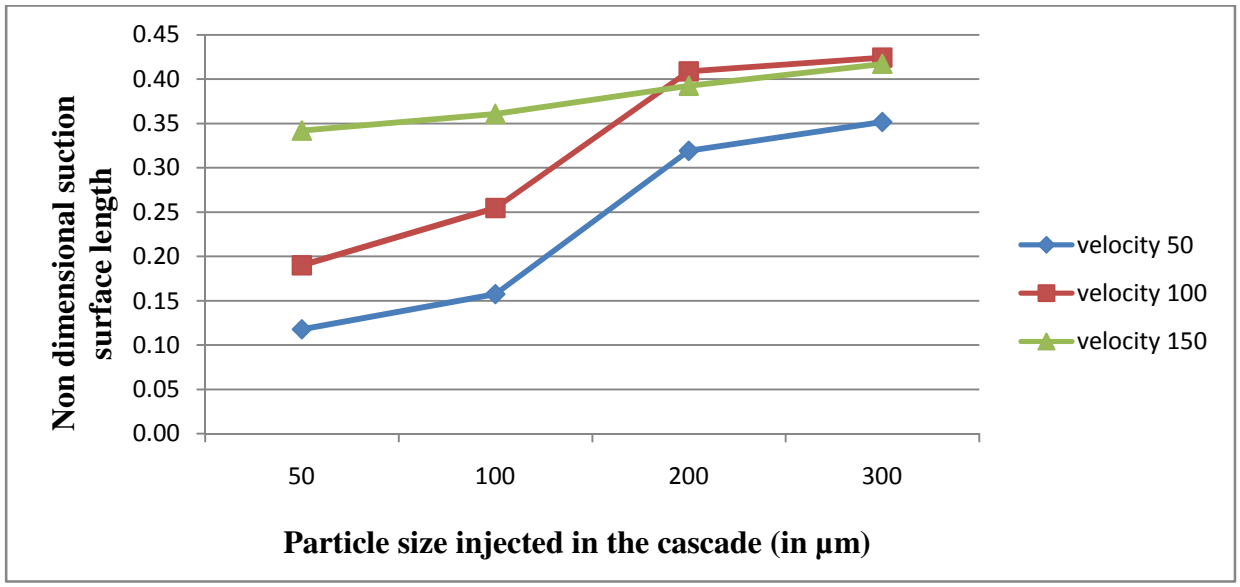

Figure 4.42: Affected suction surface of blade v/s particle size injected at different velocities of steel particles

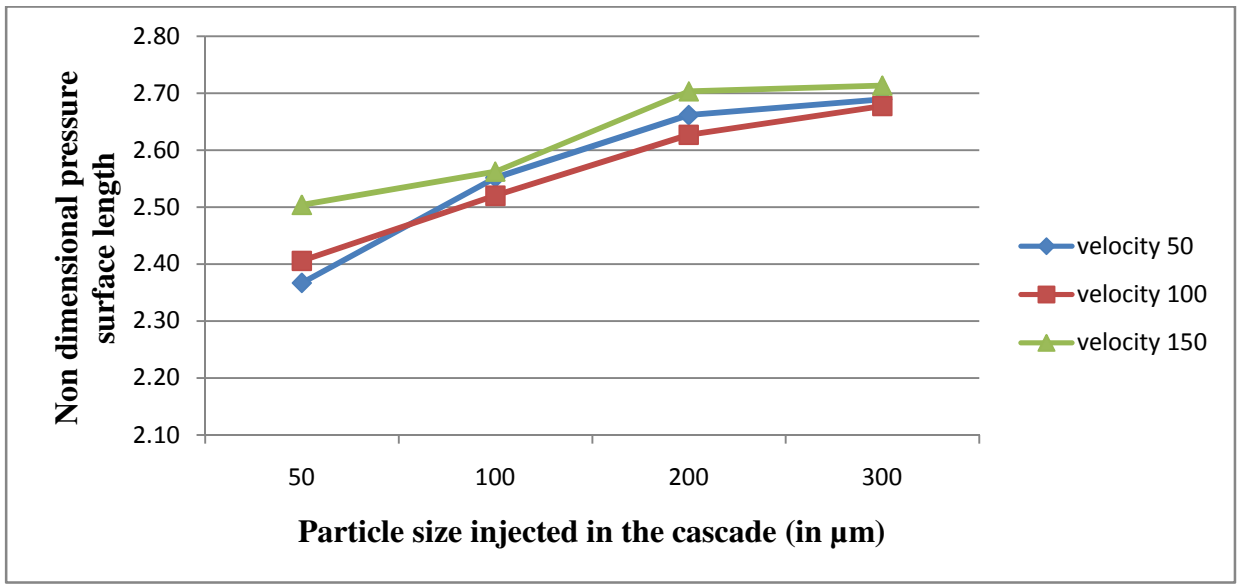

Figure 4.43: Affected pressure surface of blade v/s micron at different velocities with steel particles

From the figure 4.42 and 4.43, The effected length of blade is increased by increasing velocity and particle diameter. At velocity 50m/s, 4% to 15% length is affected on the suction side by the injection of 50µm to 300µm steel particles. 82 to 95% of pressure surface is affected by the particles at velocity 50m/s. More of the suction surface is getting affected and the pressure side is affected approx 84 to 95% when velocity increases from 50m/s to 150m/s.

4.3.3 Water particles

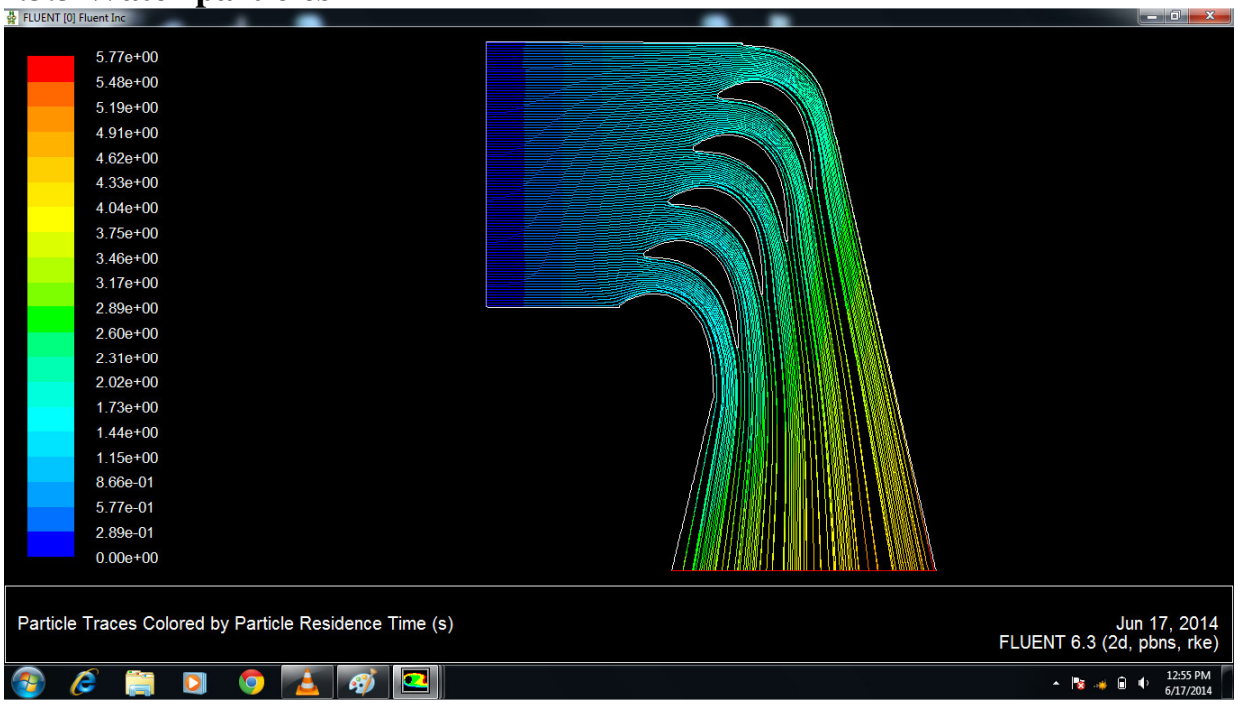

Figure 4.44: Trajectories of particle with particle residence time at velocity 50m/s with water particles of 50µm

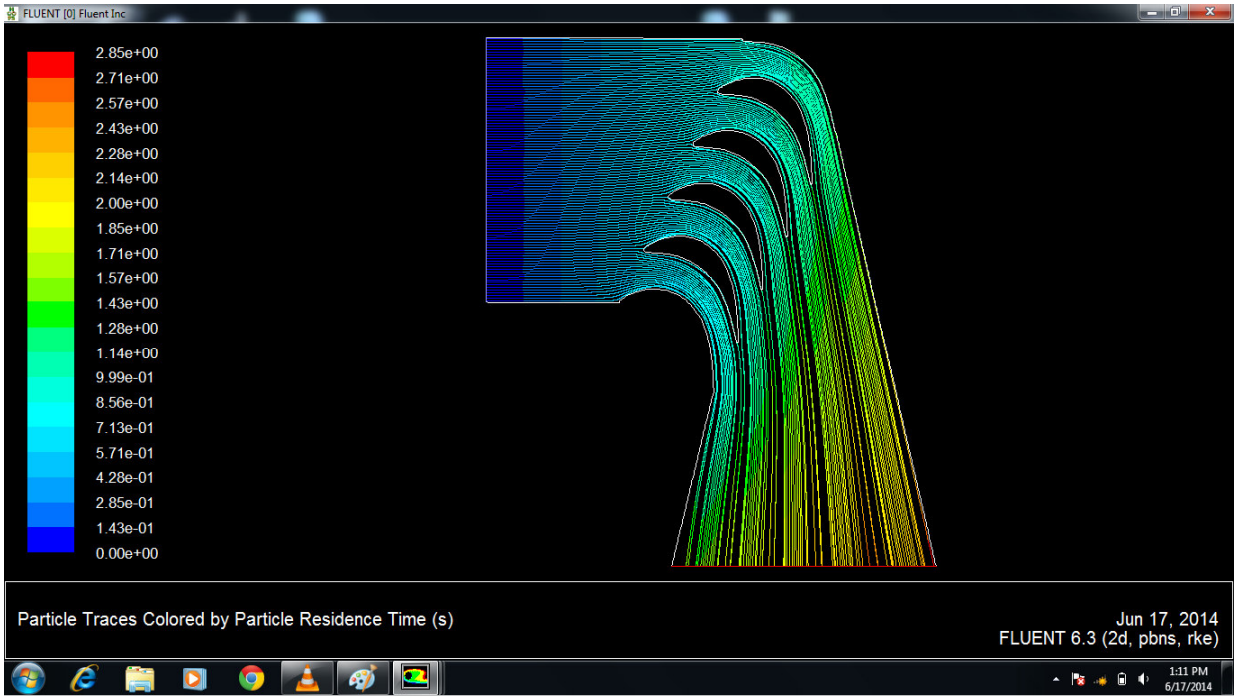

Figure 4.45: Trajectories of particle with particle residence time at velocity 100m/s with water particles of 50µm

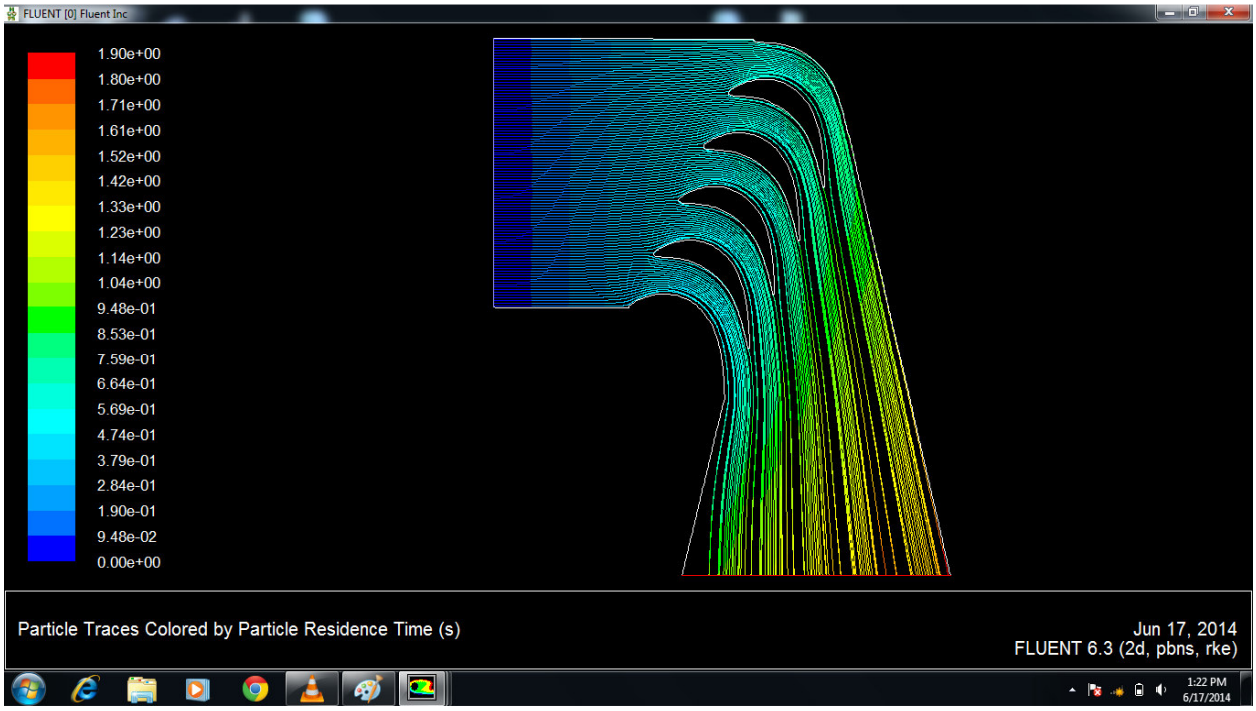

Figure 4.46: Trajectories of particle with particle residence time at velocity 150m/s with water particles of 50µm

The graph given below is plotted from the values of table no 12 provided in the appendix:

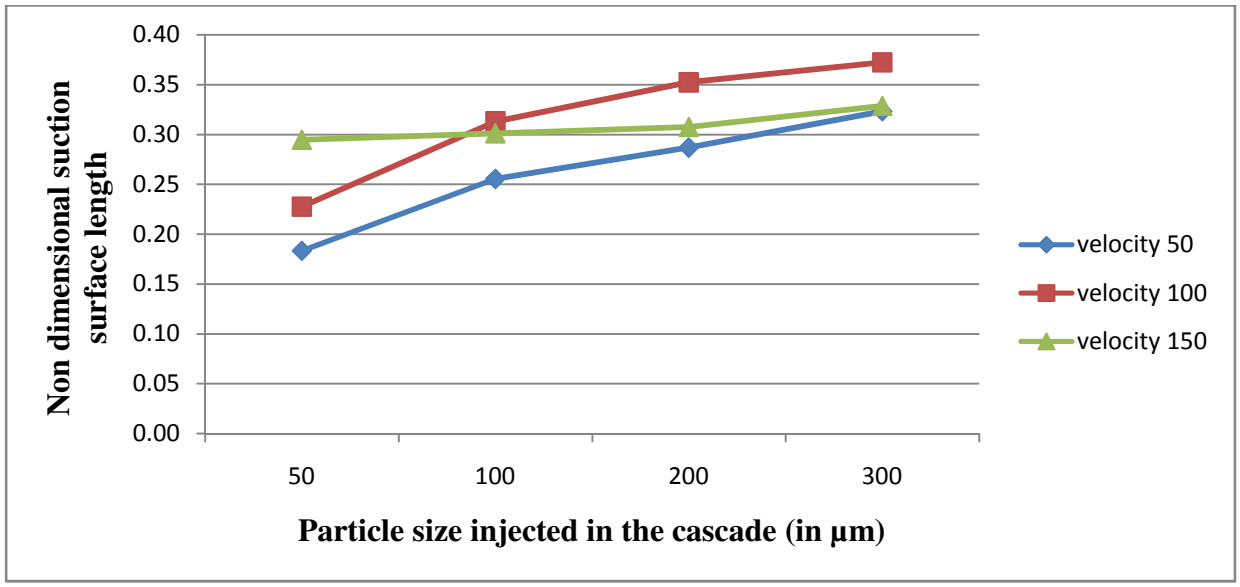

Figure 4.47: Affected suction surface of blade v/s particle size injected at different velocities of water particles

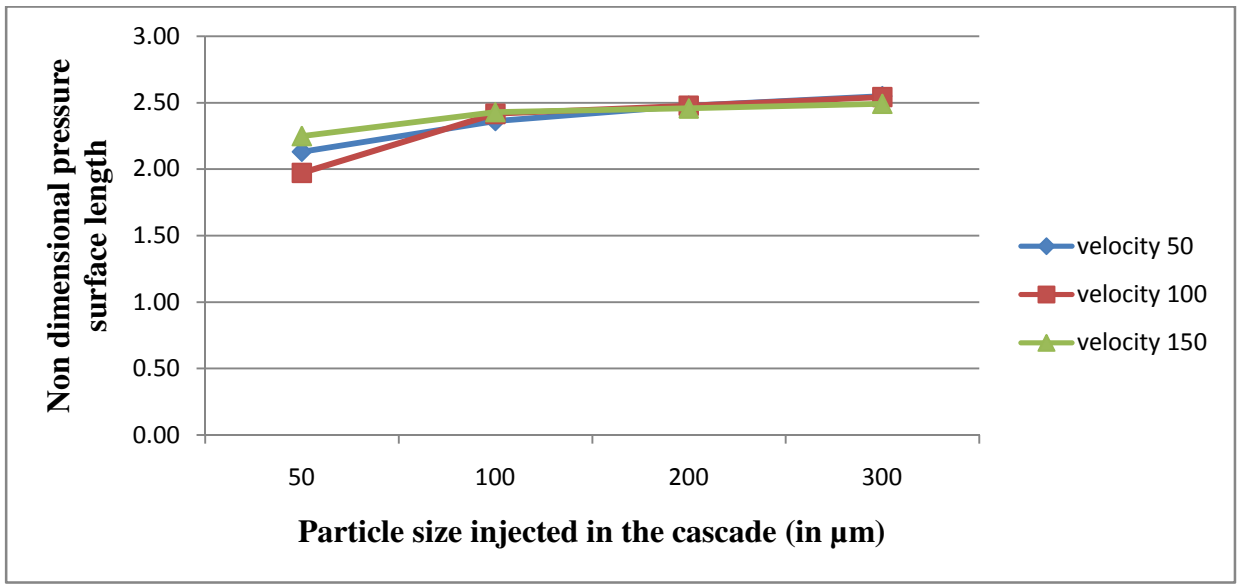

Figure 4.48: Affected pressure surface of blade v/s particle size injected at different velocities of water particles

From the analysis of figure 4.47 and 4.48, It is observed that 6 to 14% of suction surface and 74 to 89% of pressure surface is affected by particles of 50µm to 300µm at velocity 50m/s. 7 to 14% of suction and 68 to 90% of pressure surface at 100m/s velocity is affected particles by the particles of 50µm to 300µm. 10 to 14% of suction and 78 to 90% of pressure surface is affected by the particles of 50µm to 300µm at velocity 150m/s.

CHAPTER 5

CONCLUSIONS

The effect of increasing velocity on profile loss coefficient and also effected length of blade due to particle injection has been analysed in the present work. Air at velocity 50m/s, 100m/s and 150m/s with particles of ash, steel and water of 50µm, 100µm, 200µm and 300µm are passed through the cascade. The wakes are shifted to suction side due to increasing velocity. The profile loss decreases by increasing the velocity for a blade span at 50m/s to 150m/s velocity. If ash particles of 50µm to 300µm are injected then the losses decreases with the increase of diameter of particles, but in case of steel and water particles the losses increases by increasing the particle diameter from 50µm to 300µm. Profile loss is 17.92%, which decreases when the velocity is increased from 50m/s to 150m/s with the injection of ash particles of 50µm, 17.89% with steel particles,17.15% with water particles. Profile loss decreases if we increase particle diameter from 50µm to 300µm at velocity 50 m/s, increases in the case of steel particles and water particles. The effect of particles is not significant on profile loss coefficient. The blade length is affected approx 8 to 13 % at suction surface and 65 to 70% pressure surface is affected by the injection of ash particles of 50µm to 300µm at velocity 50m/s to 150m/s, up to 16 % suction surface and 80 to 95% of pressure surface in the case of steel particles, up to 15% suction surface and 70 to 90% of pressure surface is affected in the case of water particles. It concludes that the effected length on the suction and pressure side of the blade increases by increasing the velocity and diameter of injected particles.

CHAPTER 6

FUTURE SCOPE

The effect of particle injection on profile loss coefficient is analyzed by injection of ash, steel and water particles. During the present work, it has been observed that there are areas that require further investigations. Some of these are given below:

1) Investigation of the effect of particle injection on secondary flow and the losses can be studied further.
2) The effect of localized roughness on various surfaces on the secondary flow and losses can be studied further.
3) The effect of particle injection on secondary flow and various losses is also analyze using unsteady simulation that can give results closer to the real life situation.

REFERENCES

[1] Rainer kurz and Klaus brun, " Maintenance and operating practices effect on degradation and life" Proceedings of the thirty sixth turbomachinery symposium,2007

[2] Bolcs A, O Sari, "Influence of deposit on the flow in a turbine cascade" ASME vol.110, 1988

[3] HP Hodson and WN dawes, "On the interpretation of measured profile losses in unsteady wake-turbine blade interaction studies" ASME, 1998

[4] R.J. Boyle, "Measurements and predictions of surface roughness effects on turbine vane aerodynamics" proceedings of ASME TURBO EXPO, Atlanta, June 16-19, 2003.

[5] Li Weili, L Jinling, L Xingqui, L Yuan, "Research on the cavitation charactesitics of Kaplan turbine under sediment flow," IOP conf. series: Earth and environment science 12 012022(2012)

[6] Jain S, Saini R P & Kumar A, "CFD approach for prediction of efficiency of Francis turbine" oct. 21-23, AHEC, IIT Roorkee, India, IGHEM-2010

[7] Drtina, P and Sallaberger, M "Hydraulic turbines—basic principles and state-of-the art computational fluid dynamics applications" Proc Instn Mech Engrs Vol 213 Part C 1999

[8] Mishra alok, Saini R.P., Singhal M. K., "CFD based analysis of Kaplan turbine for micron hydro power" International conference on industrial and mechanical engineering, ISBN:978-93-81693-89-6

[9] Harsh vats, R.P. saini, "Investigation on combined effect of cavitation and silt erosion on francis turbine" International Journal of Mechanical and Production Engineering (IJMPE) ISSN 2315-4489, Vol-1, Iss-1, 2012

[10] Shuhong LIU, Qingguang CHEN, Yuliun WU "Unsteady cavitating turbulent flow simulation in a Kaplan turbine" Scientific Bulletin of the "Politehnica" University of Timisoara Transactions on Mechanics Tom 52(66), Fascicola 6, 2007

[11] L Poudel, B Thapa, B P Shrestha, B S Thapa, K P Shrestha and N K Shrestha, "Computational and experimental study of effects of sediment shape on erosion of hydraulic turbines" 26th IAHR Symposium on Hydraulic Machinery and Systems IOP Publishing IOP Conf. Series: Earth and Environmental Science 032054 doi:10.1088/1755-1315/15/3/032054, 2012

[12] Vinod Kumar Singoria, Deepika Sharma, Samsher "Effect of roughness on secondary flow in a rectilinear turbine cascade" Proceedings of the National Conference on Trends and Advances in Mechanical Engineering, YMCA University of Science & Technology, Faridabad, Haryana, Oct 19-20, 2012

[13] Singhal A.K, Li Hangyang, Athavale M.M. "Mathematical basis and validation of the full cavitation model" In: Proceeding of ASME FEDSM'01, Louisiana: ASME 2001

[14] Bhola Thapa, Pralhad Chaudhary, Ole G. Dahlhaug, Piyush Upadhyay, "Study of combined effect of sand erosion and cavitation in hydraulic turbines," International conference on small hydropower – Hydro Srilanka, 22-24 October 2007

[15] M. Mahendran, N. Sitaram "Computational Study of Mach Number Effects on Secondary Flows in a Linear Turbine Cascade" Proceedings of the 8th International Symposium on Experimental and Computational Aerothermodynamics of Internal Flows Lyon, Paper reference: ISAIF8 0084, July 2007

[16] Klaus brun, Marybeth nored, Rainer kurz, "Analysis of solid particle surface impact behaviour in turbo machines to assess blade erosion and fouling" proceedings of the forty-first turbomachinery symposium, houston, texas,September 24-27 , 2012

[17] Cyrus B. Meher Homji, Andrew Bromley, "Gas turbine axial compressor fouling and washing" Proceedings of the thirty-third turbomachinery symposium, 2004

[18] Hassan salem and aya diab, "A preliminary study on the performance degradation of wind turbine blade in dusty environments" Executive summary, mechanical power department, Ain shams university, Egypt,2013

[19] Vinod kumar singoria, Dr. Samsher, "A Review: techniques and processes for performance improvement of gas and steam turbine power plants", International journal of emerging technology and advance engineering, ISSN 2250-2459, ISO 9001:2008 Certified Journal, Volume 4, Issue 1, January 2014

[20] Deepika Sharma, "A Project report on Effect of roughness on secondary flow" M Tech thesis, Delhi Technological University, 2012

[21] Hao sun, jun li, Zhenping feng, "Investigations on aerodynamic performance of turbine cascade at different flow conditions" Engineering applications of computational fluid mechanics vol.6. No.2,pp. 214-223(2012)

[22] Sandeep Soni, " Analysis of liquid droplet erosion of steam turbine blades of turbine material, International journal of mechanical engineering and robotics research, ISSN 2278 – 0149, Vol. 1, No. 3, October 2012

[23] Yahya ,S.M, ”Turbine, Compressors & Fans”,chapter 8, 4TH ED. McGraw Hill,2011

[24] Lukas Motycak, Ales Skotak, Jiri Obrovsky “Conditions of kaplan turbine CFD analysis” ANSYS konference 2010 Frymburk 6. - 8. října 2010

APPENDIX-1

GLOSSORY OF TERMS

Aspect ratio - Ratio of blade height to chord. Reduction in aspect ratio increases the contribution of secondary losses in total aerodynamic losses.

Blade angle - Included angle between tangents drawn on the camber line at leading edge and trailing edge with the axial or tangential direction are the blade angles at inlet and exit, respectively.

Camber angle - The angle between tangent drawn on the camber line at leading edge and chord line at inlet, the angle between tangent drawn on the camber line at trailing edge and chord line is camber angle at exit. The sum of camber angle at inlet and exit is camber angle.

Camber line - A blade section of infinitesimal thickness is a curved line known as camber line. This forms the backbone line of a blade of finite thickness.

Cascade - An infinite row of equidistant similar blade is called a cascade. When blades are arranged in a straight line the cascade is called rectilinear cascade. In annular cascades, the blades are arranged in an annulus. In a radial cascade the blades are arranged radial inward or outward direction.

Chord - A straight line joining center of leading edge and center of trailing edge. The length of this line is blade chord.

Deviation - The difference between flow angle and blade angle at outlet is called deviation angle. It also may be positive or negative.

Flow inlet angle - Angle that the flow makes at inlet with the axial or tangential direction.

Flow outlet angle - Angle that the flow makes at outlet with the axial or tangential direction. It depends on pitch-chord ratio and stagger angle.

Incidence angle - The difference between flow angle and blade angle at inlet. It may be positive or negative.

Leading edge thickness - Edge of Blade where the flow enters.

Pitch-cord ratio - Ratio of pitch to the chord

Pressure and suction surface - The concave surface of the blade is called pressure surface, and convex surface is called suction surface.

Span - Height of the blade from hub to tip.

Stagger angle - Stagger angle is the inclination of chord line with the axial or tangential direction. The shape of the channel changes with change in stagger angle, which results in change in pressure distribution and boundary layer thickness and hence losses. Increase in stagger angle (axial) increases semi-vane-less region and reduces the throat. For the same stagger angle exit angle changes with pitch-chord ratio and for pitch-chord ratio exit angle increase with increase in stagger angle.

Trailing edge thickness - The edge of the blade at flow exit end.

APPENDIX - 2

Details of model used

A2.1 Meshing at glance

Number of cells	24629
Number of faces	49919
Number of nodes	25287
Number of face zones	4
Type of cell	Quadrilateral

A2.2 Fluent model at glance

Version 2d, realizable k-epsilon, discrete phase mode

Model	**Setting**
Space	2D
Time	Steady
Viscous	Realizable, k-ε turbulence model
Wall treatment	Standard wall functions
Domain motion	Stationary
Buoyancy	Non-buoyant
Heat transfer	Enabled
Solidification and melting	Disabled
Radiation	Disabled
Species transport	Disabled

Coupled dispersed phase	Disabled
Pollutants	Disabled
Soot	Disabled

A2.3 Solver Control

(a) Equation solved

Equations	**Solved**
Flow	Yes
Turbulence	Yes
Energy	No

(b) Numeric

Numeric	**Enabled**
Absolute velocity formulation	Yes

(c) Relaxation

Variable	**Relaxation factor**
Pressure	0.3
Density	1.0
Body force	1.0
Momentum	0.7
Turbulence Kinetic energy	0.8
Turbulence dissipation rate	0.8

Turbulence viscosity	1.0

(d) Linear solver

Variable	**Cycle type**	**Termination criteria**	**Residual reduction tolerance**
Pressure	V-cycle	0.1	
X-Momentum	Flexible	0.1	0.7
Y-Momentum	Flexible	0.1	0.7
Turbulence kinetic energy	Flexible	0.1	0.7
Turbulence dissipation rate	Flexible	0.1	0.7

(e) Discretization scheme

Variable	**Scheme**
Pressure	Standard
Pressure velocity compounding	Simple
Turbulence kinetic energy	Second order upwind
Turbulence dissipation rate	Second order upwind

(f) Solution limits

Quantity	**Limit**
Minimum absolute pressure	1
Maximum absolute pressure	5000000
Minimum turbulence kinetic energy	$1 \times e^{-14}$

Minimum turbulence dissipation rate	$1\times e^{-20}$
Maximum turbulence viscosity rate	100000

A2.4 Material Property

(a) Material air (fluid)

Property	**Units**	**Method**	**Value**
Density	Kg/m^3	Ideal gas	1.225
Thermal conductivity	W/m-K	Constant	0.0242
Viscosity	Kg/m-s	Constant	1.789×10^{-5}
Reference temperature	k	Constant	298.15

(b) Material aluminum (solid)

Property	**Units**	**Method**	**Value**
Density	Kg/m^3	Constant	2719
Specific heat (C_p)	J/kg-K	Constant	871
Thermal conductivity	W/m-K	Constant	202.4

A2.5 Convergence criteria

Continuity	$1\times e^{-06}$
X-velocity	$1\times e^{-06}$
Y-velocity	$1\times e^{-06}$
Turbulence kinetic energy (k)	$1\times e^{-06}$
Turbulence dissipation rate (ε)	$1\times e^{-06}$

A2.6 Operating conditions

Operating pressure (Pascal)	101325.00
Reference pressure location –X(m)	0.00
Reference pressure location –Y(m)	0.00

A2.7 Solution Initialization

Gauge pressure (Pascal)	0
X velocity (m/s)	50,100,150,200
Y velocity (m/s)	0.0
Turbulence K.E. (m2/s2)	1
Turbulence Dissipation rate (m2/s3)	1

APPENDIX – 3

Table no. 1: Percentage of profile loss coefficient at velocity 50m/s with ash particles of 50µm, 100µm, 200µm and 300µm.

S. No.	y/s	50µm	100µm	200µm	300µm
1.	2.77	-2.291	-2.268	-2.108	-2.123
2.	2.79	-2.245	-2.222	-2.038	-2.043
3.	2.80	-2.175	-2.176	-1.968	-1.962
4.	2.81	-2.129	-2.082	-1.873	-1.878
5.	2.84	-1.965	-1.942	-1.732	-1.729
6.	2.85	-1.871	-1.872	-1.686	-1.666
7.	2.86	-1.801	-1.778	-1.615	-1.625
8.	2.88	-1.755	-1.732	-1.617	-1.612
9.	2.89	-1.709	-1.710	-1.594	-1.601
10.	2.90	-1.662	-1.664	-1.620	-1.603
11.	2.92	-1.664	-1.665	-1.597	-1.606
12.	2.93	-1.642	-1.618	-1.599	-1.603
13.	2.94	-1.643	-1.620	-1.552	-1.564
14.	2.95	-1.621	-1.597	-1.529	-1.525
15.	2.97	-1.574	-1.575	-1.506	-1.483
16.	2.98	-1.575	-1.576	-1.483	-1.495
17.	2.99	-1.601	-1.577	-1.509	-1.511
18.	3.00	-1.602	-1.603	-1.412	-1.435
19.	3.02	-1.627	-1.604	-1.242	-1.249
20.	3.03	-1.531	-1.532	-1.170	-1.156
21.	3.04	-1.435	-1.436	-1.073	-1.068
22.	3.06	-1.339	-1.315	-0.805	-0.804
23.	3.07	-1.291	-1.267	-0.293	-0.306
24.	3.08	-0.951	-0.927	0.098	0.092
25.	3.09	-0.561	-0.512	0.489	0.493
26.	3.11	-0.171	-0.122	1.297	1.314
27.	3.12	0.122	0.171	2.277	2.266
28.	3.13	1.026	1.100	3.185	3.185
29.	3.15	1.932	2.030	4.094	4.105
30.	3.16	2.764	2.839	5.495	5.499
31.	3.17	3.646	3.746	6.944	6.947
32.	3.18	5.068	5.168	8.396	8.397
33.	3.20	6.514	6.593	9.825	9.847
34.	3.21	7.865	7.944	11.449	11.453
35.	3.22	9.315	9.418	13.151	13.139

36.	3.24	10.988	11.091	14.829	14.825
37.	3.25	12.707	12.765	16.386	16.395
38.	3.26	14.430	14.489	17.640	17.635
39.	3.27	16.004	16.035	19.044	19.049
40.	3.29	17.454	17.486	20.473	20.464
41.	3.30	18.924	18.912	21.406	21.408
42.	3.31	20.547	20.511	22.013	21.993
43.	3.32	21.407	21.342	22.679	22.669
44.	3.34	22.115	22.006	23.345	23.347
45.	3.35	22.805	22.672	23.388	23.379
46.	3.36	23.480	23.341	23.271	23.248
47.	3.38	23.580	23.422	23.129	23.117
48.	3.39	23.460	23.321	22.926	22.895
49.	3.40	23.279	23.114	22.547	22.530
50.	3.41	23.116	22.932	22.042	22.028
51.	3.43	22.676	22.462	21.173	21.154
52.	3.44	22.084	21.870	20.312	20.280
53.	3.45	21.537	21.280	19.070	19.051
54.	3.47	20.499	20.218	17.640	17.617
55.	3.48	19.414	19.152	16.207	16.178
56.	3.49	18.258	17.971	14.614	14.600
57.	3.50	16.762	16.475	13.047	13.026
58.	3.52	15.289	14.980	11.546	11.541
59.	3.53	13.790	13.481	10.072	10.057
60.	3.54	12.269	11.981	8.600	8.564
61.	3.55	10.752	10.463	7.109	7.092
62.	3.57	9.235	8.973	5.645	5.622
63.	3.58	7.603	7.340	4.377	4.385
64.	3.59	5.972	5.755	3.378	3.359
65.	3.61	4.829	4.636	2.356	2.334
66.	3.62	3.710	3.494	1.409	1.396
67.	3.63	2.472	2.304	0.874	0.873
68.	3.64	1.672	1.551	0.291	0.284
69.	3.66	0.993	0.848	-0.340	-0.348
70.	3.67	0.291	0.170	-0.655	-0.675
71.	3.68	-0.218	-0.291	-0.946	-0.957
72.	3.70	-0.532	-0.629	-1.236	-1.238
73.	3.71	-0.919	-0.968	-1.454	-1.462
74.	3.72	-1.233	-1.282	-1.575	-1.570
75.	3.73	-1.378	-1.427	-1.696	-1.679
76.	3.75	-1.523	-1.523	-1.792	-1.788
77.	3.76	-1.667	-1.693	-1.816	-1.810
78.	3.77	-1.764	-1.813	-1.840	-1.831

79.	3.78	-1.836	-1.837	-1.864	-1.860
80.	3.80	-1.884	-1.885	-1.888	-1.888

Table no. 2: Percentage of profile loss coefficient at velocity 100m/s with ash particles of 50µm, 100µm, 200µm and 300µm.

S. No.	y/s	50µm	100µm	200µm	300µm
1.	2.77	-1.865	-1.86	-1.857	-1.857
2.	2.79	-1.767	-1.76	-1.758	-1.758
3.	2.80	-1.674	-1.67	-1.666	-1.665
4.	2.81	-1.594	-1.59	-1.587	-1.586
5.	2.84	-1.514	-1.51	-1.507	-1.507
6.	2.85	-1.464	-1.46	-1.458	-1.458
7.	2.86	-1.417	-1.41	-1.412	-1.412
8.	2.88	-1.391	-1.39	-1.388	-1.387
9.	2.89	-1.397	-1.39	-1.394	-1.394
10.	2.90	-1.403	-1.40	-1.400	-1.400
11.	2.92	-1.427	-1.43	-1.424	-1.424
12.	2.93	-1.451	-1.45	-1.449	-1.449
13.	2.94	-1.472	-1.47	-1.470	-1.470
14.	2.95	-1.468	-1.47	-1.465	-1.465
15.	2.97	-1.464	-1.46	-1.460	-1.460
16.	2.98	-1.457	-1.45	-1.453	-1.453
17.	2.99	-1.489	-1.49	-1.485	-1.485
18.	3.00	-1.523	-1.52	-1.520	-1.520
19.	3.02	-1.485	-1.48	-1.480	-1.480
20.	3.03	-1.360	-1.35	-1.352	-1.352
21.	3.04	-1.316	-1.31	-1.307	-1.306
22.	3.06	-1.277	-1.27	-1.266	-1.265
23.	3.07	-1.078	-1.07	-1.064	-1.063
24.	3.08	-0.667	-0.65	-0.648	-0.647
25.	3.09	-0.351	-0.33	-0.327	-0.325
26.	3.11	-0.032	-0.01	-0.003	-0.001
27.	3.12	0.698	0.72	0.732	0.733
28.	3.13	1.552	1.58	1.591	1.592
29.	3.15	2.371	2.41	2.415	2.417
30.	3.16	3.194	3.23	3.243	3.245
31.	3.17	4.521	4.56	4.570	4.573
32.	3.18	5.895	5.94	5.947	5.949
33.	3.20	7.273	7.32	7.326	7.329

34.	3.21	8.655	8.70	8.710	8.713
35.	3.22	10.271	10.31	10.319	10.322
36.	3.24	11.954	11.99	11.997	11.999
37.	3.25	13.642	13.67	13.680	13.682
38.	3.26	15.235	15.26	15.265	15.267
39.	3.27	16.554	16.57	16.572	16.573
40.	3.29	18.044	18.05	18.048	18.049
41.	3.30	19.537	19.53	19.529	19.529
42.	3.31	20.560	20.54	20.540	20.539
43.	3.32	21.229	21.20	21.197	21.196
44.	3.34	21.995	21.96	21.950	21.948
45.	3.35	22.763	22.72	22.705	22.703
46.	3.36	22.827	22.77	22.760	22.757
47.	3.38	22.713	22.65	22.637	22.633
48.	3.39	22.598	22.53	22.513	22.509
49.	3.40	22.378	22.31	22.285	22.281
50.	3.41	21.987	21.91	21.889	21.884
51.	3.43	21.448	21.37	21.344	21.339
52.	3.44	20.511	20.42	20.400	20.394
53.	3.45	19.576	19.48	19.458	19.452
54.	3.47	18.259	18.16	18.136	18.130
55.	3.48	16.723	16.62	16.596	16.590
56.	3.49	15.187	15.08	15.056	15.050
57.	3.50	13.513	13.41	13.384	13.378
58.	3.52	11.848	11.75	11.720	11.714
59.	3.53	10.320	10.23	10.201	10.196
60.	3.54	8.798	8.71	8.687	8.682
61.	3.55	7.287	7.21	7.185	7.181
62.	3.57	5.839	5.77	5.749	5.744
63.	3.58	4.398	4.33	4.318	4.314
64.	3.59	3.219	3.16	3.150	3.146
65.	3.61	2.288	2.24	2.229	2.226
66.	3.62	1.359	1.32	1.310	1.308
67.	3.63	0.521	0.49	0.481	0.479
68.	3.64	0.108	0.08	0.074	0.072
69.	3.66	-0.367	-0.39	-0.395	-0.396
70.	3.67	-0.883	-0.90	-0.904	-0.905
71.	3.68	-1.119	-1.13	-1.136	-1.137
72.	3.70	-1.311	-1.32	-1.325	-1.326
73.	3.71	-1.504	-1.51	-1.514	-1.515
74.	3.72	-1.651	-1.66	-1.659	-1.659
75.	3.73	-1.699	-1.70	-1.705	-1.705
76.	3.75	-1.748	-1.75	-1.753	-1.753

77.	3.76	-1.798	-1.80	-1.801	-1.801
78.	3.77	-1.776	-1.78	-1.777	-1.777
79.	3.78	-1.751	-1.75	-1.751	-1.751
80.	3.80	-1.732	-1.73	-1.731	-1.731

Table no. 3: Percentage of profile loss coefficient at velocity 150m/s with ash particles of 50µm, 100µm, 200µm and 300µm.

S. No.	y/s	50µm	100µm	200µm	300µm
1.	2.77	-1.661	-1.659	-1.658	-1.658
2.	2.79	-1.567	-1.564	-1.563	-1.563
3.	2.80	-1.479	-1.476	-1.475	-1.475
4.	2.81	-1.405	-1.402	-1.401	-1.401
5.	2.84	-1.331	-1.328	-1.327	-1.327
6.	2.85	-1.284	-1.283	-1.282	-1.282
7.	2.86	-1.241	-1.239	-1.239	-1.239
8.	2.88	-1.218	-1.216	-1.216	-1.216
9.	2.89	-1.224	-1.223	-1.222	-1.222
10.	2.90	-1.230	-1.229	-1.229	-1.229
11.	2.92	-1.256	-1.255	-1.255	-1.255
12.	2.93	-1.283	-1.282	-1.282	-1.282
13.	2.94	-1.308	-1.307	-1.307	-1.307
14.	2.95	-1.318	-1.318	-1.318	-1.318
15.	2.97	-1.329	-1.328	-1.328	-1.328
16.	2.98	-1.337	-1.337	-1.336	-1.336
17.	2.99	-1.371	-1.370	-1.370	-1.370
18.	3.00	-1.406	-1.406	-1.405	-1.405
19.	3.02	-1.389	-1.388	-1.388	-1.388
20.	3.03	-1.310	-1.308	-1.308	-1.308
21.	3.04	-1.296	-1.294	-1.293	-1.293
22.	3.06	-1.286	-1.283	-1.282	-1.282
23.	3.07	-1.144	-1.140	-1.139	-1.139
24.	3.08	-0.827	-0.822	-0.821	-0.820
25.	3.09	-0.591	-0.584	-0.582	-0.582
26.	3.11	-0.351	-0.343	-0.341	-0.340
27.	3.12	0.252	0.261	0.264	0.265
28.	3.13	0.961	0.972	0.976	0.976
29.	3.15	1.639	1.652	1.656	1.657
30.	3.16	2.321	2.336	2.340	2.341
31.	3.17	3.493	3.508	3.513	3.514

32.	3.18	4.704	4.720	4.725	4.726
33.	3.20	5.921	5.939	5.943	5.945
34.	3.21	7.145	7.163	7.168	7.170
35.	3.22	8.666	8.682	8.686	8.687
36.	3.24	10.239	10.253	10.257	10.258
37.	3.25	11.822	11.835	11.838	11.839
38.	3.26	13.340	13.350	13.353	13.354
39.	3.27	14.663	14.669	14.671	14.672
40.	3.29	16.142	16.145	16.145	16.146
41.	3.30	17.631	17.629	17.629	17.629
42.	3.31	18.682	18.677	18.675	18.675
43.	3.32	19.407	19.397	19.394	19.394
44.	3.34	20.231	20.216	20.212	20.211
45.	3.35	21.058	21.039	21.033	21.032
46.	3.36	21.175	21.151	21.144	21.143
47.	3.38	21.110	21.082	21.074	21.073
48.	3.39	21.045	21.014	21.005	21.003
49.	3.40	20.864	20.830	20.819	20.817
50.	3.41	20.496	20.459	20.449	20.446
51.	3.43	19.978	19.939	19.928	19.926
52.	3.44	19.065	19.025	19.014	19.011
53.	3.45	18.158	18.116	18.104	18.101
54.	3.47	16.876	16.832	16.820	16.817
55.	3.48	15.382	15.338	15.325	15.323
56.	3.49	13.893	13.849	13.836	13.833
57.	3.50	12.272	12.229	12.216	12.213
58.	3.52	10.666	10.624	10.612	10.609
59.	3.53	9.204	9.165	9.153	9.150
60.	3.54	7.751	7.715	7.705	7.702
61.	3.55	6.325	6.292	6.283	6.280
62.	3.57	4.978	4.949	4.941	4.938
63.	3.58	3.641	3.616	3.609	3.607
64.	3.59	2.566	2.544	2.538	2.536
65.	3.61	1.739	1.721	1.716	1.714
66.	3.62	0.917	0.901	0.897	0.896

67.	3.63	0.179	0.166	0.163	0.162
68.	3.64	-0.164	-0.175	-0.178	-0.179
69.	3.66	-0.562	-0.571	-0.574	-0.574
70.	3.67	-0.995	-1.003	-1.005	-1.005
71.	3.68	-1.179	-1.185	-1.186	-1.187
72.	3.70	-1.323	-1.328	-1.329	-1.330
73.	3.71	-1.468	-1.472	-1.473	-1.473
74.	3.72	-1.575	-1.578	-1.579	-1.579
75.	3.73	-1.598	-1.601	-1.601	-1.602
76.	3.75	-1.622	-1.624	-1.624	-1.625
77.	3.76	-1.647	-1.648	-1.649	-1.649
78.	3.77	-1.613	-1.614	-1.614	-1.615
79.	3.78	-1.577	-1.578	-1.577	-1.578
80.	3.80	-1.545	-1.545	-1.545	-1.545

Table no. 4: Percentage of profile loss coefficient at velocity 50m/s with Steel particles of 50µm, 100µm, 200µm and 300µm.

S. No.	y/s	50µm	100µm	200µm	300µm
1.	2.77	-2.123	-2.123	-2.123	-2.123
2.	2.79	-2.043	-2.043	-2.043	-2.043
3.	2.80	-1.962	-1.961	-1.961	-1.961
4.	2.81	-1.877	-1.877	-1.877	-1.877
5.	2.84	-1.793	-1.792	-1.792	-1.792
6.	2.85	-1.728	-1.728	-1.728	-1.728
7.	2.86	-1.665	-1.665	-1.665	-1.665
8.	2.88	-1.624	-1.624	-1.624	-1.624
9.	2.89	-1.612	-1.612	-1.612	-1.612
10.	2.90	-1.600	-1.600	-1.600	-1.600
11.	2.92	-1.602	-1.602	-1.602	-1.602
12.	2.93	-1.605	-1.605	-1.605	-1.605
13.	2.94	-1.602	-1.602	-1.602	-1.602
14.	2.95	-1.563	-1.563	-1.563	-1.563
15.	2.97	-1.524	-1.524	-1.524	-1.524
16.	2.98	-1.482	-1.482	-1.482	-1.482
17.	2.99	-1.494	-1.494	-1.494	-1.494
18.	3.00	-1.510	-1.509	-1.510	-1.509
19.	3.02	-1.433	-1.433	-1.433	-1.433

20.	3.03	-1.247	-1.247	-1.247	-1.247
21.	3.04	-1.154	-1.154	-1.153	-1.154
22.	3.06	-1.065	-1.065	-1.065	-1.065
23.	3.07	-0.801	-0.801	-0.801	-0.801
24.	3.08	-0.303	-0.302	-0.302	-0.302
25.	3.09	0.096	0.096	0.097	0.096
26.	3.11	0.497	0.497	0.498	0.497
27.	3.12	1.318	1.318	1.319	1.318
28.	3.13	2.271	2.272	2.273	2.272
29.	3.15	3.190	3.190	3.191	3.190
30.	3.16	4.111	4.111	4.112	4.111
31.	3.17	5.504	5.505	5.506	5.505
32.	3.18	6.953	6.953	6.954	6.953
33.	3.20	8.402	8.403	8.404	8.402
34.	3.21	9.853	9.853	9.854	9.853
35.	3.22	11.458	11.458	11.459	11.458
36.	3.24	13.142	13.142	13.144	13.143
37.	3.25	14.828	14.828	14.829	14.828
38.	3.26	16.397	16.397	16.399	16.397
39.	3.27	17.635	17.635	17.636	17.635
40.	3.29	19.048	19.049	19.049	19.049
41.	3.30	20.462	20.462	20.463	20.462
42.	3.31	21.404	21.404	21.405	21.404
43.	3.32	21.988	21.988	21.989	21.988
44.	3.34	22.663	22.663	22.664	22.664
45.	3.35	23.340	23.340	23.340	23.340
46.	3.36	23.371	23.371	23.371	23.371
47.	3.38	23.239	23.239	23.239	23.239
48.	3.39	23.107	23.107	23.107	23.107
49.	3.40	22.885	22.885	22.885	22.885
50.	3.41	22.519	22.519	22.519	22.519
51.	3.43	22.016	22.016	22.016	22.016
52.	3.44	21.141	21.141	21.141	21.141
53.	3.45	20.266	20.266	20.266	20.266
54.	3.47	19.037	19.037	19.037	19.037
55.	3.48	17.602	17.602	17.602	17.602
56.	3.49	16.162	16.162	16.162	16.163
57.	3.50	14.585	14.585	14.584	14.585
58.	3.52	13.010	13.010	13.010	13.011
59.	3.53	11.526	11.525	11.525	11.526
60.	3.54	10.042	10.042	10.042	10.043
61.	3.55	8.550	8.550	8.550	8.550
62.	3.57	7.079	7.079	7.078	7.079

63.	3.58	5.610	5.610	5.610	5.610
64.	3.59	4.374	4.374	4.374	4.374
65.	3.61	3.349	3.349	3.349	3.349
66.	3.62	2.326	2.325	2.325	2.326
67.	3.63	1.388	1.388	1.388	1.389
68.	3.64	0.867	0.866	0.866	0.867
69.	3.66	0.279	0.278	0.278	0.279
70.	3.67	-0.352	-0.352	-0.352	-0.352
71.	3.68	-0.679	-0.679	-0.679	-0.679
72.	3.70	-0.960	-0.960	-0.960	-0.960
73.	3.71	-1.241	-1.241	-1.241	-1.240
74.	3.72	-1.464	-1.464	-1.464	-1.464
75.	3.73	-1.571	-1.571	-1.571	-1.571
76.	3.75	-1.680	-1.680	-1.680	-1.679
77.	3.76	-1.789	-1.789	-1.789	-1.789
78.	3.77	-1.810	-1.810	-1.810	-1.810
79.	3.78	-1.831	-1.831	-1.831	-1.831
80.	3.80	-1.860	-1.860	-1.860	-1.860

Table no. 5: Percentage of profile loss coefficient at velocity 100m/s with Steel particles of 50µm, 100µm, 200µm and 300µm.

S. No.	y/s	50µm	100µm	200µm	300µm
1.	2.77	-1.856	-1.856	-1.857	-1.857
2.	2.79	-1.757	-1.757	-1.758	-1.758
3.	2.80	-1.665	-1.665	-1.665	-1.665
4.	2.81	-1.586	-1.586	-1.586	-1.586
5.	2.84	-1.507	-1.507	-1.507	-1.507
6.	2.85	-1.458	-1.458	-1.458	-1.458
7.	2.86	-1.412	-1.411	-1.412	-1.412
8.	2.88	-1.387	-1.387	-1.387	-1.387
9.	2.89	-1.393	-1.393	-1.393	-1.393
10.	2.90	-1.400	-1.400	-1.400	-1.400
11.	2.92	-1.424	-1.424	-1.424	-1.424
12.	2.93	-1.449	-1.449	-1.449	-1.449
13.	2.94	-1.469	-1.469	-1.470	-1.469
14.	2.95	-1.465	-1.465	-1.465	-1.465
15.	2.97	-1.460	-1.460	-1.460	-1.460
16.	2.98	-1.452	-1.452	-1.452	-1.452
17.	2.99	-1.485	-1.484	-1.485	-1.484

18.	3.00	-1.519	-1.519	-1.520	-1.519
19.	3.02	-1.480	-1.479	-1.480	-1.479
20.	3.03	-1.352	-1.351	-1.351	-1.351
21.	3.04	-1.306	-1.306	-1.306	-1.306
22.	3.06	-1.264	-1.264	-1.264	-1.264
23.	3.07	-1.062	-1.062	-1.062	-1.062
24.	3.08	-0.646	-0.646	-0.646	-0.645
25.	3.09	-0.324	-0.324	-0.324	-0.324
26.	3.11	0.000	0.000	0.001	0.001
27.	3.12	0.735	0.735	0.735	0.735
28.	3.13	1.594	1.595	1.595	1.595
29.	3.15	2.419	2.420	2.420	2.420
30.	3.16	3.248	3.248	3.248	3.248
31.	3.17	4.575	4.575	4.576	4.576
32.	3.18	5.952	5.952	5.952	5.952
33.	3.20	7.332	7.332	7.332	7.332
34.	3.21	8.716	8.716	8.716	8.716
35.	3.22	10.324	10.324	10.325	10.325
36.	3.24	12.001	12.001	12.002	12.002
37.	3.25	13.683	13.684	13.684	13.684
38.	3.26	15.268	15.269	15.269	15.269
39.	3.27	16.573	16.574	16.574	16.574
40.	3.29	18.049	18.049	18.049	18.049
41.	3.30	19.528	19.529	19.529	19.529
42.	3.31	20.538	20.539	20.539	20.539
43.	3.32	21.195	21.195	21.195	21.195
44.	3.34	21.947	21.947	21.947	21.947
45.	3.35	22.700	22.700	22.701	22.700
46.	3.36	22.754	22.754	22.754	22.754
47.	3.38	22.630	22.630	22.630	22.630
48.	3.39	22.506	22.506	22.506	22.506
49.	3.40	22.277	22.277	22.277	22.277
50.	3.41	21.880	21.880	21.880	21.880
51.	3.43	21.335	21.335	21.335	21.335
52.	3.44	20.390	20.390	20.390	20.390
53.	3.45	19.447	19.447	19.447	19.447
54.	3.47	18.125	18.125	18.125	18.125
55.	3.48	16.585	16.585	16.585	16.585
56.	3.49	15.045	15.045	15.045	15.045
57.	3.50	13.372	13.372	13.372	13.372
58.	3.52	11.708	11.708	11.708	11.708
59.	3.53	10.191	10.191	10.191	10.191

60.	3.54	8.678	8.678	8.677	8.677
61.	3.55	7.176	7.176	7.176	7.176
62.	3.57	5.741	5.741	5.740	5.740
63.	3.58	4.311	4.311	4.310	4.310
64.	3.59	3.144	3.144	3.143	3.143
65.	3.61	2.224	2.224	2.223	2.223
66.	3.62	1.306	1.306	1.306	1.306
67.	3.63	0.478	0.477	0.477	0.477
68.	3.64	0.071	0.071	0.071	0.071
69.	3.66	-0.398	-0.398	-0.398	-0.398
70.	3.67	-0.906	-0.906	-0.906	-0.907
71.	3.68	-1.137	-1.138	-1.138	-1.138
72.	3.70	-1.326	-1.326	-1.326	-1.327
73.	3.71	-1.515	-1.515	-1.515	-1.515
74.	3.72	-1.659	-1.659	-1.659	-1.660
75.	3.73	-1.706	-1.706	-1.706	-1.706
76.	3.75	-1.753	-1.753	-1.753	-1.753
77.	3.76	-1.801	-1.801	-1.801	-1.801
78.	3.77	-1.777	-1.778	-1.778	-1.778
79.	3.78	-1.751	-1.752	-1.752	-1.752
80.	3.80	-1.731	-1.731	-1.731	-1.731

Table no. 6: Percentage of profile loss coefficient at velocity 150m/s with Steel particles of 50µm, 100µm, 200µm and 300µm.

S. No.	y/s	50µm	100µm	200µm	300µm
1.	2.77	-1.657	-1.657	-1.657	-1.657
2.	2.79	-1.563	-1.563	-1.563	-1.563
3.	2.80	-1.474	-1.474	-1.474	-1.475
4.	2.81	-1.401	-1.401	-1.401	-1.401
5.	2.84	-1.327	-1.327	-1.327	-1.327
6.	2.85	-1.282	-1.282	-1.282	-1.282
7.	2.86	-1.238	-1.239	-1.239	-1.239
8.	2.88	-1.216	-1.216	-1.216	-1.216
9.	2.89	-1.222	-1.222	-1.222	-1.222
10.	2.90	-1.229	-1.228	-1.229	-1.229
11.	2.92	-1.255	-1.255	-1.255	-1.255
12.	2.93	-1.282	-1.282	-1.282	-1.282
13.	2.94	-1.306	-1.307	-1.307	-1.307
14.	2.95	-1.317	-1.317	-1.317	-1.317

15.	2.97	-1.328	-1.328	-1.328	-1.328
16.	2.98	-1.336	-1.336	-1.336	-1.336
17.	2.99	-1.370	-1.370	-1.370	-1.370
18.	3.00	-1.405	-1.405	-1.405	-1.405
19.	3.02	-1.388	-1.387	-1.387	-1.388
20.	3.03	-1.307	-1.307	-1.307	-1.308
21.	3.04	-1.293	-1.292	-1.293	-1.293
22.	3.06	-1.282	-1.281	-1.282	-1.282
23.	3.07	-1.138	-1.138	-1.138	-1.138
24.	3.08	-0.820	-0.820	-0.820	-0.820
25.	3.09	-0.581	-0.581	-0.581	-0.581
26.	3.11	-0.340	-0.340	-0.340	-0.340
27.	3.12	0.265	0.266	0.266	0.266
28.	3.13	0.977	0.977	0.977	0.977
29.	3.15	1.658	1.658	1.658	1.658
30.	3.16	2.342	2.342	2.343	2.343
31.	3.17	3.515	3.515	3.515	3.515
32.	3.18	4.727	4.727	4.728	4.728
33.	3.20	5.945	5.946	5.946	5.946
34.	3.21	7.170	7.171	7.171	7.171
35.	3.22	8.688	8.689	8.689	8.689
36.	3.24	10.259	10.259	10.259	10.259
37.	3.25	11.840	11.840	11.840	11.840
38.	3.26	13.355	13.355	13.355	13.355
39.	3.27	14.672	14.672	14.673	14.672
40.	3.29	16.146	16.146	16.146	16.146
41.	3.30	17.629	17.629	17.629	17.629
42.	3.31	18.674	18.674	18.675	18.674
43.	3.32	19.393	19.393	19.393	19.393
44.	3.34	20.210	20.210	20.210	20.210
45.	3.35	21.031	21.031	21.031	21.031
46.	3.36	21.141	21.141	21.142	21.141
47.	3.38	21.071	21.071	21.071	21.071
48.	3.39	21.001	21.001	21.001	21.001
49.	3.40	20.815	20.816	20.815	20.815
50.	3.41	20.445	20.445	20.445	20.445
51.	3.43	19.924	19.924	19.924	19.924
52.	3.44	19.009	19.009	19.009	19.009
53.	3.45	18.099	18.099	18.099	18.099
54.	3.47	16.815	16.815	16.815	16.815
55.	3.48	15.320	15.320	15.320	15.320
56.	3.49	13.831	13.831	13.831	13.831

57.	3.50	12.211	12.211	12.211	12.211
58.	3.52	10.607	10.607	10.607	10.607
59.	3.53	9.149	9.149	9.149	9.149
60.	3.54	7.701	7.701	7.701	7.700
61.	3.55	6.279	6.279	6.279	6.279
62.	3.57	4.937	4.937	4.937	4.937
63.	3.58	3.606	3.606	3.606	3.606
64.	3.59	2.535	2.536	2.535	2.535
65.	3.61	1.713	1.713	1.713	1.713
66.	3.62	0.895	0.895	0.895	0.895
67.	3.63	0.162	0.162	0.162	0.162
68.	3.64	-0.179	-0.179	-0.179	-0.179
69.	3.66	-0.575	-0.575	-0.575	-0.575
70.	3.67	-1.005	-1.005	-1.006	-1.005
71.	3.68	-1.187	-1.187	-1.187	-1.187
72.	3.70	-1.330	-1.330	-1.330	-1.330
73.	3.71	-1.473	-1.473	-1.473	-1.473
74.	3.72	-1.579	-1.579	-1.579	-1.579
75.	3.73	-1.602	-1.602	-1.602	-1.602
76.	3.75	-1.625	-1.625	-1.625	-1.625
77.	3.76	-1.649	-1.649	-1.649	-1.649
78.	3.77	-1.614	-1.614	-1.614	-1.614
79.	3.78	-1.577	-1.577	-1.578	-1.578
80.	3.80	-1.545	-1.545	-1.545	-1.545

Table no. 7: Percentage of profile loss coefficient at velocity 50m/s with Water particles of 50µm, 100µm, 200µm and 300µm.

S. No.	y/s	50µm	100µm	200µm	300µm
1.	2.77	-2.202	-2.132	-2.132	-2.132
2.	2.79	-2.107	-2.062	-2.038	-2.038
3.	2.80	-2.038	-1.992	-1.968	-1.968
4.	2.81	-1.967	-1.898	-1.873	-1.873
5.	2.84	-1.873	-1.803	-1.803	-1.803
6.	2.85	-1.802	-1.733	-1.708	-1.708
7.	2.86	-1.732	-1.686	-1.662	-1.662
8.	2.88	-1.686	-1.664	-1.639	-1.639
9.	2.89	-1.640	-1.617	-1.617	-1.617
10.	2.90	-1.593	-1.619	-1.594	-1.594
11.	2.92	-1.619	-1.621	-1.596	-1.596
12.	2.93	-1.620	-1.622	-1.598	-1.598

13.	2.94	-1.622	-1.599	-1.599	-1.599
14.	2.95	-1.575	-1.577	-1.552	-1.552
15.	2.97	-1.552	-1.530	-1.505	-1.505
16.	2.98	-1.505	-1.507	-1.482	-1.482
17.	2.99	-1.531	-1.508	-1.508	-1.508
18.	3.00	-1.532	-1.533	-1.509	-1.509
19.	3.02	-1.557	-1.461	-1.437	-1.437
20.	3.03	-1.363	-1.292	-1.242	-1.242
21.	3.04	-1.291	-1.170	-1.146	-1.146
22.	3.06	-1.194	-1.098	-1.073	-1.073
23.	3.07	-1.122	-0.830	-0.806	-0.806
24.	3.08	-0.684	-0.318	-0.318	-0.318
25.	3.09	-0.293	0.073	0.073	0.073
26.	3.11	0.147	0.489	0.514	0.514
27.	3.12	0.636	1.298	1.322	1.322
28.	3.13	1.566	2.254	2.278	2.278
29.	3.15	2.473	3.186	3.186	3.186
30.	3.16	3.405	4.095	4.118	4.118
31.	3.17	4.510	5.471	5.495	5.495
32.	3.18	5.960	6.946	6.946	6.946
33.	3.20	7.409	8.398	8.421	8.421
34.	3.21	8.861	9.828	9.850	9.850
35.	3.22	10.413	11.430	11.452	11.452
36.	3.24	12.089	13.129	13.129	13.129
37.	3.25	13.812	14.808	14.829	14.829
38.	3.26	15.491	16.365	16.410	16.410
39.	3.27	16.872	17.598	17.643	17.643
40.	3.29	18.276	19.028	19.048	19.048
41.	3.30	19.724	20.453	20.472	20.472
42.	3.31	21.054	21.386	21.406	21.406
43.	3.32	21.642	21.975	21.994	21.994
44.	3.34	22.332	22.660	22.660	22.660
45.	3.35	23.017	23.325	23.344	23.344
46.	3.36	23.436	23.350	23.368	23.368
47.	3.38	23.313	23.226	23.245	23.245
48.	3.39	23.171	23.085	23.104	23.104
49.	3.40	22.975	22.863	22.882	22.882
50.	3.41	22.664	22.503	22.522	22.522
51.	3.43	22.309	21.998	22.017	22.017
52.	3.44	21.495	21.109	21.129	21.129
53.	3.45	20.682	20.267	20.267	20.286
54.	3.47	19.653	19.025	19.045	19.045
55.	3.48	18.297	17.594	17.614	17.614

56.	3.49	16.966	16.162	16.162	16.162
57.	3.50	15.421	14.568	14.568	14.568
58.	3.52	13.873	13.000	13.022	13.022
59.	3.53	12.374	11.499	11.520	11.521
60.	3.54	10.875	10.025	10.047	10.047
61.	3.55	9.356	8.553	8.553	8.553
62.	3.57	7.863	7.062	7.085	7.085
63.	3.58	6.374	5.598	5.621	5.621
64.	3.59	4.863	4.354	4.377	4.377
65.	3.61	3.816	3.355	3.355	3.355
66.	3.62	2.793	2.308	2.332	2.332
67.	3.63	1.748	1.360	1.384	1.384
68.	3.64	1.141	0.874	0.874	0.874
69.	3.66	0.534	0.267	0.267	0.267
70.	3.67	-0.097	-0.364	-0.340	-0.340
71.	3.68	-0.533	-0.704	-0.679	-0.679
72.	3.70	-0.800	-0.970	-0.945	-0.945
73.	3.71	-1.090	-1.261	-1.236	-1.236
74.	3.72	-1.405	-1.503	-1.478	-1.478
75.	3.73	-1.502	-1.599	-1.575	-1.575
76.	3.75	-1.647	-1.696	-1.671	-1.671
77.	3.76	-1.768	-1.792	-1.792	-1.792
78.	3.77	-1.791	-1.816	-1.792	-1.792
79.	3.78	-1.839	-1.865	-1.840	-1.840
80.	3.80	-1.863	-1.864	-1.864	-1.864

Table no. 8: Percentage of profile loss coefficient at velocity 100m/s with Water particles of 50µm, 100µm, 200µm and 300µm.

S. No.	y/s	50µm	100µm	200µm	300µm
1.	2.77	-1.859	-1.853	-1.853	-1.853
2.	2.79	-1.760	-1.755	-1.755	-1.755
3.	2.80	-1.667	-1.662	-1.662	-1.662
4.	2.81	-1.590	-1.585	-1.585	-1.585
5.	2.84	-1.508	-1.502	-1.502	-1.502
6.	2.85	-1.459	-1.454	-1.454	-1.454
7.	2.86	-1.416	-1.410	-1.410	-1.410
8.	2.88	-1.390	-1.384	-1.384	-1.384
9.	2.89	-1.397	-1.391	-1.391	-1.391

10.	2.90	-1.398	-1.404	-1.404	-1.404
11.	2.92	-1.422	-1.428	-1.428	-1.428
12.	2.93	-1.446	-1.452	-1.452	-1.452
13.	2.94	-1.470	-1.470	-1.470	-1.470
14.	2.95	-1.466	-1.466	-1.466	-1.466
15.	2.97	-1.461	-1.456	-1.456	-1.456
16.	2.98	-1.451	-1.451	-1.451	-1.451
17.	2.99	-1.486	-1.486	-1.486	-1.481
18.	3.00	-1.521	-1.521	-1.521	-1.521
19.	3.02	-1.477	-1.483	-1.483	-1.483
20.	3.03	-1.353	-1.353	-1.353	-1.348
21.	3.04	-1.309	-1.309	-1.309	-1.309
22.	3.06	-1.264	-1.264	-1.264	-1.264
23.	3.07	-1.067	-1.061	-1.061	-1.061
24.	3.08	-0.648	-0.648	-0.648	-0.648
25.	3.09	-0.330	-0.324	-0.324	-0.324
26.	3.11	-0.006	-0.006	0.000	0.000
27.	3.12	0.729	0.735	0.735	0.735
28.	3.13	1.592	1.592	1.592	1.592
29.	3.15	2.416	2.416	2.416	2.416
30.	3.16	3.242	3.242	3.242	3.242
31.	3.17	4.570	4.575	4.575	4.575
32.	3.18	5.941	5.953	5.953	5.953
33.	3.20	7.328	7.328	7.328	7.328
34.	3.21	8.708	8.714	8.714	8.714
35.	3.22	10.318	10.318	10.318	10.318
36.	3.24	11.997	11.997	11.997	11.997
37.	3.25	13.676	13.682	13.682	13.682
38.	3.26	15.266	15.267	15.267	15.267
39.	3.27	16.569	16.570	16.570	16.570
40.	3.29	18.050	18.045	18.045	18.051
41.	3.30	19.528	19.529	19.528	19.528
42.	3.31	20.539	20.539	20.539	20.539
43.	3.32	21.196	21.197	21.197	21.197
44.	3.34	21.953	21.948	21.948	21.948
45.	3.35	22.705	22.704	22.704	22.704
46.	3.36	22.762	22.756	22.756	22.756
47.	3.38	22.637	22.631	22.631	22.631
48.	3.39	22.517	22.506	22.506	22.506
49.	3.40	22.285	22.274	22.274	22.274
50.	3.41	21.888	21.881	21.881	21.881
51.	3.43	21.344	21.333	21.333	21.333

52.	3.44	20.402	20.395	20.395	20.395
53.	3.45	19.458	19.451	19.447	19.451
54.	3.47	18.137	18.126	18.126	18.126
55.	3.48	16.599	16.588	16.588	16.588
56.	3.49	15.056	15.045	15.045	15.045
57.	3.50	13.385	13.374	13.374	13.374
58.	3.52	11.724	11.708	11.708	11.708
59.	3.53	10.206	10.195	10.195	10.195
60.	3.54	8.684	8.678	8.678	8.678
61.	3.55	7.187	7.181	7.181	7.181
62.	3.57	5.748	5.737	5.737	5.737
63.	3.58	4.320	4.309	4.309	4.309
64.	3.59	3.147	3.142	3.142	3.142
65.	3.61	2.228	2.222	2.222	2.222
66.	3.62	1.310	1.304	1.304	1.304
67.	3.63	0.479	0.474	0.474	0.474
68.	3.64	0.073	0.073	0.073	0.073
69.	3.66	-0.394	-0.400	-0.400	-0.400
70.	3.67	-0.906	-0.906	-0.906	-0.906
71.	3.68	-1.136	-1.136	-1.136	-1.136
72.	3.70	-1.327	-1.327	-1.327	-1.327
73.	3.71	-1.512	-1.518	-1.518	-1.518
74.	3.72	-1.663	-1.658	-1.658	-1.658
75.	3.73	-1.708	-1.708	-1.708	-1.708
76.	3.75	-1.752	-1.752	-1.752	-1.752
77.	3.76	-1.797	-1.802	-1.802	-1.802
78.	3.77	-1.779	-1.779	-1.779	-1.779
79.	3.78	-1.751	-1.757	-1.757	-1.757
80.	3.80	-1.734	-1.728	-1.728	-1.728

Table no. 9: Percentage of profile loss coefficient at velocity 150m/s with Water particles of 50µm, 100µm, 200µm and 300µm.

S. No.	y/s	50µm	100µm	200µm	300µm
1.	2.77	-1.656	-1.656	-1.656	-1.656
2.	2.79	-1.563	-1.563	-1.563	-1.563
3.	2.80	-1.476	-1.476	-1.476	-1.476
4.	2.81	-1.400	-1.400	-1.400	-1.400
5.	2.84	-1.326	-1.326	-1.326	-1.326

6.	2.85	-1.281	-1.281	-1.281	-1.281
7.	2.86	-1.238	-1.238	-1.238	-1.238
8.	2.88	-1.217	-1.217	-1.217	-1.217
9.	2.89	-1.222	-1.222	-1.222	-1.222
10.	2.90	-1.228	-1.228	-1.228	-1.228
11.	2.92	-1.254	-1.254	-1.254	-1.254
12.	2.93	-1.282	-1.282	-1.282	-1.282
13.	2.94	-1.305	-1.305	-1.305	-1.305
14.	2.95	-1.315	-1.315	-1.317	-1.317
15.	2.97	-1.330	-1.330	-1.327	-1.327
16.	2.98	-1.337	-1.337	-1.337	-1.337
17.	2.99	-1.367	-1.367	-1.370	-1.370
18.	3.00	-1.404	-1.404	-1.406	-1.406
19.	3.02	-1.387	-1.387	-1.387	-1.387
20.	3.03	-1.307	-1.307	-1.307	-1.307
21.	3.04	-1.294	-1.294	-1.292	-1.292
22.	3.06	-1.282	-1.282	-1.282	-1.282
23.	3.07	-1.139	-1.139	-1.137	-1.139
24.	3.08	-0.819	-0.819	-0.819	-0.819
25.	3.09	-0.581	-0.581	-0.581	-0.581
26.	3.11	-0.340	-0.340	-0.340	-0.340
27.	3.12	0.266	0.266	0.266	0.266
28.	3.13	0.977	0.977	0.975	0.975
29.	3.15	1.657	1.657	1.659	1.659
30.	3.16	2.341	2.341	2.341	2.341
31.	3.17	3.513	3.513	3.515	3.515
32.	3.18	4.726	4.726	4.726	4.726
33.	3.20	5.943	5.943	5.943	5.943
34.	3.21	7.170	7.170	7.170	7.170
35.	3.22	8.687	8.687	8.687	8.687
36.	3.24	10.259	10.259	10.258	10.258
37.	3.25	11.839	11.839	11.839	11.839
38.	3.26	13.354	13.354	13.354	13.354
39.	3.27	14.671	14.671	14.673	14.673
40.	3.29	16.144	16.144	16.147	16.147
41.	3.30	17.627	17.627	17.629	17.629
42.	3.31	18.674	18.674	18.674	18.674
43.	3.32	19.395	19.395	19.393	19.393
44.	3.34	20.211	20.211	20.210	20.210
45.	3.35	21.031	21.031	21.031	21.031
46.	3.36	21.142	21.142	21.142	21.142
47.	3.38	21.071	21.071	21.070	21.071
48.	3.39	21.002	21.002	21.002	21.002

49.	3.40	20.816	20.816	20.814	20.815
50.	3.41	20.445	20.445	20.447	20.447
51.	3.43	19.925	19.925	19.925	19.925
52.	3.44	19.011	19.011	19.011	19.011
53.	3.45	18.100	18.100	18.100	18.100
54.	3.47	16.815	16.817	16.817	16.817
55.	3.48	15.321	15.321	15.321	15.321
56.	3.49	13.833	13.833	13.833	13.833
57.	3.50	12.213	12.213	12.213	12.213
58.	3.52	10.608	10.608	10.608	10.608
59.	3.53	9.149	9.149	9.149	9.149
60.	3.54	7.700	7.700	7.700	7.700
61.	3.55	6.279	6.279	6.279	6.279
62.	3.57	4.938	4.938	4.938	4.938
63.	3.58	3.605	3.605	3.607	3.605
64.	3.59	2.535	2.535	2.535	2.535
65.	3.61	1.712	1.712	1.712	1.712
66.	3.62	0.895	0.895	0.895	0.895
67.	3.63	0.162	0.162	0.162	0.162
68.	3.64	-0.180	-0.180	-0.180	-0.180
69.	3.66	-0.574	-0.574	-0.574	-0.574
70.	3.67	-1.005	-1.005	-1.005	-1.005
71.	3.68	-1.188	-1.188	-1.188	-1.188
72.	3.70	-1.329	-1.329	-1.331	-1.331
73.	3.71	-1.474	-1.474	-1.474	-1.474
74.	3.72	-1.581	-1.581	-1.581	-1.581
75.	3.73	-1.602	-1.602	-1.602	-1.602
76.	3.75	-1.626	-1.626	-1.624	-1.626
77.	3.76	-1.650	-1.648	-1.648	-1.648
78.	3.77	-1.616	-1.616	-1.616	-1.616
79.	3.78	-1.578	-1.578	-1.578	-1.578
80.	3.80	-1.545	-1.545	-1.545	-1.545

Table no. 10: Non dimensional effected surface length of blade due to Ash particles at different velocities:

	Velocity 50		Velocity 100		Velocity 150	
	S	**P**	**S**	**P**	**S**	**P**
Micron 50	0.27	1.91	0.24	1.94	0.26	1.97
Micron 100	0.29	1.94	0.27	1.96	0.26	1.98
Micron 200	0.29	1.95	0.30	1.98	0.27	1.99
Micron 300	0.31	1.95	0.33	1.98	0.27	1.99

Table no. 11: Non dimensional effected surface length of blade due to Steel particles at different velocities:

	Velocity 50		Velocity 100		Velocity 150	
	S	**P**	**S**	**P**	**S**	**P**
Micron 50	0.12	2.37	0.19	2.41	0.34	2.50
Micron 100	0.16	2.55	0.25	2.52	0.36	2.56
Micron 200	0.32	2.66	0.41	2.63	0.39	2.70
Micron 300	0.35	2.69	0.42	2.68	0.42	2.71

Table no. 12: Non dimensional effected surface length of blade due to Water particles at different velocities:

	Velocity 50		**Velocity 100**		**Velocity 150**	
	S	**P**	**S**	**P**	**S**	**P**
Micron 50	0.18	2.13	0.23	1.97	0.29	2.25
Micron 100	0.26	2.36	0.31	2.41	0.30	2.43
Micron 200	0.29	2.48	0.35	2.48	0.31	2.46
Micron 300	0.32	2.55	0.37	2.54	0.33	2.49